Unravelling the sediment transport mechanisms in an artificial lagoon

Multi-modal sand transport analysis at the hard flood defence of Maasvlakte 2

M. (Mathijs) Mann

May 2019

Delft University of Technology

TU Delft

Van Oord
Marine ingenuity

Unravelling the sediment transport mechanisms in an artificial lagoon

Multi-modal sand transport analysis at the hard flood defence of Maasvlakte 2

by

M. (Mathijs) Mann

in partial fulfillment of the requirements for the degree of

Master of Science
in Civil Engineering

at the Delft University of Technology,

to be presented publicly on May 16, 2019, at 10:30 AM.

Student number:	4224434	
Project duration:	September 11, 2018 - May 16, 2019	
Thesis committee:	Dr. ir. S. de Vries	TU Delft, chair
	Prof. dr. ir. S. G. J. Aarninkhof	TU Delft
	Dr. ir. B. Hofland	TU Delft
	Dr. ir. B. Hoonhout	Van Oord, daily supervisor

TU Delft

Van Oord
Marine ingenuity

Acknowledgements

It feels strange to think about the fact that this will be my very last text that I will write as a student. This thesis finalises my Master of Science program 'Hydraulic Engineering' at the Delft University of Technology. I have carried out this thesis in cooperation with Van Oord in Rotterdam.

First, I would like to thank my thesis committee for their time invested in me. Many thanks to my daily supervisor Bas Hoonhout for the endless optimism and feedback during my thesis. Getting structure in my report was difficult, but after a few discussions we managed to find a solution. Moreover, thanks for the helpful advice in representing my results and the support in order to perform the field experiments. Furthermore, many thanks to Sierd de Vries, Bas Hofland and Stefan Aarninkhof for the constructive and enthusiastic meetings we always had. The meetings were always quite intense and luckily I was able to record the meetings and listen them again. I really enjoyed the enthusiasm and the endless amount of ideas that you always came up with!

Second, I would also like to express my gratitude to Van Oord for their hospitality and all the helpful colleagues who have shared their experiences about Maasvlakte 2 and helped me with their expertise in hydraulic engineering. And not to forget, I want to thank Maurice de Kok for the unexpected visit to the dredging project in Lithuania. As a result, this suddenly gave me the opportunity to experience a dredging project at first hand. For hours I was able to walk around on the enormous trailing suction hopper dredgers. It was an inspiring experience!

Third, thanks to Wouter Sonnema and Jaap Resink for your help during the field experiments. We managed to make it one of the most memorable days of my academic career. Luckily, I had made a risk assessment to make sure that everything went smoothly during this measurement. Furthermore, I would like to thank Jan van den Oever for his flexibility in renting his boat during my thesis. I was able to store his boat for almost the entire winter period at my house in Rotterdam. And of course, many thanks to all other graduate students at Van Oord for our lunch and coffee breaks at the Rivium building. Everyone's enthusiasm during the many riddles and puzzles was a nice distraction from the work that we actually had to do.

Finally, thanks go out to my family, friends and girlfriend for the support they gave me during this research project. Testing a floating device in the lagoon of Maasvlakte 2 together with my girlfriend, is something I could only dream of!

Mathijs Mann
Delft, May 2019

Abstract

The port of Rotterdam was full and new mooring locations were required to host the largest ships in the world. And if there's no space to expand on land, why not create land in the sea? That is exactly what The Netherlands did by creating Maasvlakte 2. The construction of Maasvlakte 2 started in 2008 and was officially completed on May 22^{nd}, 2013. The seaside protection of Maasvlakte 2 consists of a hard and soft protection, whereby the soft protection is built as a 7.5km long sandy beach with one dune-row. The hard flood defence of Maasvlakte 2 is 3.5km long and consists of a cobble beach with a cube reef in front. This research focused on the morphodynamics in the domain between the cube reef and cobble beach at the hard flood defence, which is named "the lagoon". Over the past 5 years a large sand volume propagated into the lagoon. The current sand volume (after 5 years) in the given domain is about four times larger than the predicted value by PUMA. The processes behind the sand layer formation were not fully understood.

This research started by creating a conceptual model with all processes that could contribute to the formation of the sand layer. All processes are divided into hydrodynamic or aeolian transport, whereby hydrodynamic transport is divided into overtopping over the cube reef and transport through the cube reef due to tidal currents. We performed field experiments at Maasvlakte 2 to measure the flow velocity in the lagoon and to measure the aeolian transport capacity. From a sediment budget analysis we observed a sand layer increase during winter periods. This increase is justified with the fact that sand transport towards the lagoon depends on extreme events, which happen mostly during winter periods. Based on the estimated transport volumes we concluded that the main mechanisms that contribute in the formation of the sand layer are overtopping over the cube reef and aeolian transport, whereby overtopping is the largest mechanism.
Our estimates indicate a total maximum sand layer volume of 51,000 m^3 (whereby transport by overtopping = 25,000 m^3, tidal currents = 8,700 m^3 and aeolian transport = 17,300 m^3). Which leaves 20,000 m^3 of sand unaccounted for compared with our estimated 71,000 m^3 volume of sand in the lagoon. The accuracy of each calculation is analysed in order to explain the missing volume compared with the total sand layer volume. Based on this analysis we concluded that only the uncertainty in the overtopping calculation can explain the missing volume of 20,000 m^3.

High wind speeds and high waves will cause for sand transport towards the lagoon. Aeolian transport will always happen if there is a supply of granular material and atmospheric winds of sufficient strength. Moreover, the source for aeolian and hydrodynamic transport is the, southern located, soft protection. Since nourishments are necessary to secure the safety of the soft protection, the supply of sediment will remain. Sand is transported in northern direction along the hard protection by longshore transport. Currently, the water depth northwards of KP2700 is too deep to stir the sediment up and transport it into the lagoon by overtopping. Depending on the foreshore migration in the northern direction, the sand layer will also increase in northern direction.

There are many discussions about whether the formation of the sand layer volume is an advantage or disadvantage for the safety of Maasvlakte 2. It is unknown if the current situation still meets the overtopping requirement during a design storm. In 2023 the maintenance responsibility of Maasvlakte 2 will be transferred to Rijkswaterstaat. Before the responsibility transfers, all contract details will be discussed between PUMA and Rijkswaterstaat. Based on these negotiations the sand layer volume will be removed or not. If the sand volume in the lagoon is not removed manually, we concluded that the sand layer volume will increase indefinitely until the lagoon is filled. Before removing the sand volume based on contractual details, it is suggested to conduct more research into the effect of wave dissipation through this sand volume. Why should we remove the sand volume if the safety requirement still holds with the sand volume in the lagoon?

Contents

Nomenclature

Symbol	Unit	Value	Description
a	m		Reference level
β	$degrees$		Angle of wave incidence
C_a	kg/m^3		Reference concentration
C	-		Dimensionless constant of order unity
D	m	0.00025	Nearly uniform grain size originally used in Bagnold's experiments
D_*	m		Dimensionless particle diameter
d_{50}	m	0.00033	50% representative of the grain diameter
d_{90}	m	0.00050	90% representative of the grain diameter
g	m/s^2	9.81	Gravitational acceleration
h	m		Water depth
H_{m0}	m		Mean wave height
κ	-	0.41	Von Karmann coefficient
k	-		Wave number
L	m		Wave length
p_s	-	0.4	Porosity of sand
p_c	-	0.379	Porosity of cobble beach
ρ_{air}	kg/m^3	1.25	Density of air
ρ_s	kg/m^3	2,650	Density sediment
ρ_w	kg/m^3	1,025	Density sea-water
q_h	$m^3/m/s$		Overtoppings volume
q_a	$m^3/m/s$		Aeolian transport
Q	m^3		Aeolian transport
R_c	m		Free-board
s	-	2.59	Relative density
T	-		Dimensionless bed-shear parameter
T_m	s		Mean wave period
T_p	s		Peak period
u^*	m/s		Bed-shear velocity
u_*	m/s		Friction velocity
u_{*th}	m/s		Shear velocity threshold
U	m/s		Current velocity
U_{dir}	$degrees$		Wind direction
U_w	m/s		Wind speed at 10 meters above the surface
V	m^3		Volume
v	m^2/s	10^{-6}	Viscosity
w_s	m^2/s	0.02	Particle fall velocity
γ_f	-		Parameter to account for oblique waves
γ_β	-		Roughness factor
z_a	m		Reference height

Definition	Description
Cobble beach	The constructed dike from cobble stones at the hard flood defence
Cube reef	Offshore breakwater, constructed parallel to the coastline at the hard flood defence
Lagoon	The water volume between the cube reef and cobble beach
Sand layer	The volume of sand between the cube reef and cobble beach
Lateral dam	Small breakwater perpendicular to the coast at the hard flood defence

Acronym	Full name
BIP	Beheer Instel Periode = Maintainance period (2013-2018)
DCM	Design, construct and maintenance
GPS	Global Positioning System
PUMA	Projectorganisatie Uitbreiding Maasvlakte = consortium between Boskalis and Van Oord
UTM	Universal Transverse Mercator projection

1 Introduction

This chapter provides an introduction of the investigated topic of this research. First, background information of the project Maasvlakte 2 is given together with the final flood defence design. Secondly, in section 1.3 we describe the problem definition of this research. Followed by the research questions in section 1.4. During brainstorm sessions we created a conceptual model to identify all possible transport mechanisms, as is shown in section 1.5. Finally the scope and research outline are given.

1.1. Background Maasvlakte 2

The two most up-to-date, automatic container terminals in the world, the largest sea-going vessels on earth, giant foundation piles for wind turbines at sea: Maasvlakte 2's short existence seems characterised by superlatives (Havenbedrijf Rotterdam NV, 2018). Over 15 years ago it was forecasted that, by now, the Port of Rotterdam would reach its maximum capacity (Havenbedrijf Rotterdam NV, 2013a). The port of Rotterdam was full and new mooring locations were necessary to host the largest ships in the world. Wanting to maintain its position as the biggest port in Europe, the Port of Rotterdam Authority decided to think outside the box (Havenbedrijf Rotterdam NV, 2013a). If there's no space to expand on land, why not create land in the sea? Long discussions were necessary before the construction of Maasvlakte 2 got a green light (Ter Brugge, 2006). Finally, the port authorities reached consensus with the nature and environmental organizations. "Space for growth" was the phrase where the Port of Rotterdam Authority attracted clients to the 2,000 hectares of newly sprayed land (Havenbedrijf Rotterdam NV, 2018). Trailing suction hopper dredgers extracted sand from the North Sea floor, 10 kilometres off the coast. This is illustrated in figure 1.1: new land for port expansion was created. (Havenbedrijf Rotterdam NV, 2018).

Figure 1.1: Contractor PUMA completes first part of Maasvlakte 2 (Van Oord, 2013)

Early 2008, the DCM (design, construct and maintenance) contract of the first phase of the Maasvlakte 2 project was awarded to PUMA (Projectorganisatie Uitbreiding Maasvlakte). PUMA is a joint venture of the companies Boskalis and Van Oord (Loman, 2009). The total costs of the port extension were estimated in 2010 to 2.9 billion euros. This expansion will raise the annual handling capacity of the Port of Rotterdam from circa 11 million TEU to circa 18 million TEU (Loman, 2009). After construction of Maasvlakte 1 in the 1970's, Maasvlakte 2 was built between 2008 and 2013 (Loman, 2009). Building Maasvlakte 2 was a mega reclamation, it extends the Port of Rotterdam with 2000 hectares up to the 18 meter depth contour. This results in a port expansion by about 20% (Loman, 2009). In May 22nd 2013, the construction was officially finished and followed by five years of monitoring (Havenbedrijf Rotterdam NV, 2018). This period is the so-called adaptation period, in which the morphological behaviour of Maasvlakte 2 is observed. The knowledge of the adaptation period is used during the maintenance period, which will run from April 2018 until April 2023. PUMA is responsible for both the adaptation and maintenance periods. Rijkswaterstaat will be responsible for Maasvlakte 2 after April 2023.

In figure 1.2 the location of Maasvlakte 2 is indicated within the Netherlands. The protection of Maasvlakte 2 consist of a hard- and soft-flood defence. The hard flood defence is 3.5km long and consists of a cobble beach with a cube reef in front. In figure 1.3 a 3D-plot is shown of the hard protection, elevations of the area are indicated with the colorbar on the right (elevations are with respect to NAP). Moreover, some used definitions within this research are highlighted in this figure. The soft protection is built as a 7.5km long sandy beach with one dune-row. Between the hard and soft protection a transition zone is present. Transition zones are often vulnerable and unpredictable components of a coastal defence system. Not only the hard-soft transition, but also the curved coastline and tidal currents create a complex domain for coastal dynamics around the Maasvlakte.

Figure 1.2: Maasvlakte 2 located in The Netherlands, figures are obtained and adjusted from Google Maps and Aeroview b.v.

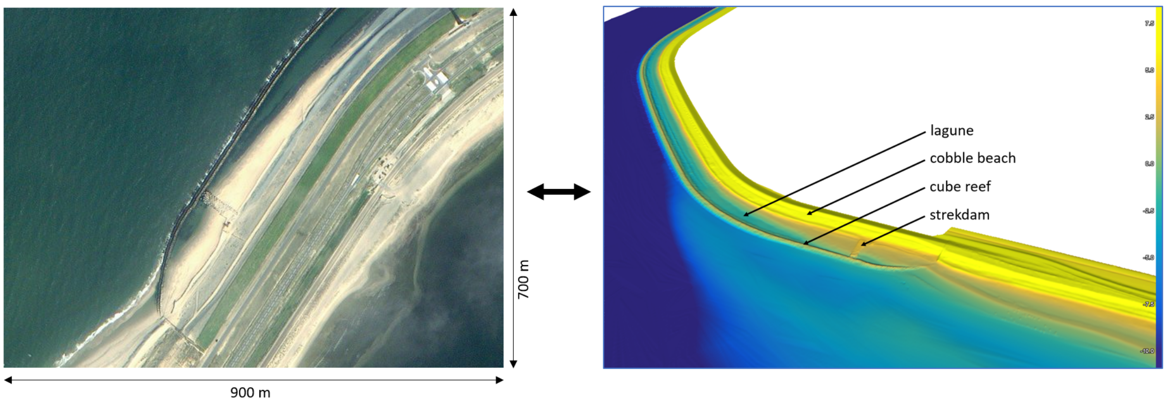

Figure 1.3: Zoomed figures of the transition zone at Maasvlakte 2. The right figure shows elevations of the area (with respect to NAP) combined with used definitions during this research.

1.2. Design hard flood defence of Maasvlakte 2

Due to the shipping traffic at the northern side of the flood defence the available space was not sufficient for a soft flood defence. Therefore a hard flood defence is constructed over a length of 3.5 km. The hard flood defence consists of a cobble beach (dike) combined with a cube reef. This cube reef consists of about 20,000 cubic blocks, whereof each block has a weigh of 43,000kg (Havenbedrijf Rotterdam NV, 2013b). In figures 1.4 and 1.5 a topview and cross-section of the design are shown. The hard flood defence is designed for a once in 10,000 years storm. A 1:10,000 year storm corresponds with a waterlevel of NAP +5.0m and wave height of 8m. Model investigations are performed with a waterlevel of 5.3m, this includes a predicted 0.3m sea level until 2060 (Havenbedrijf Rotterdam NV, 2010).

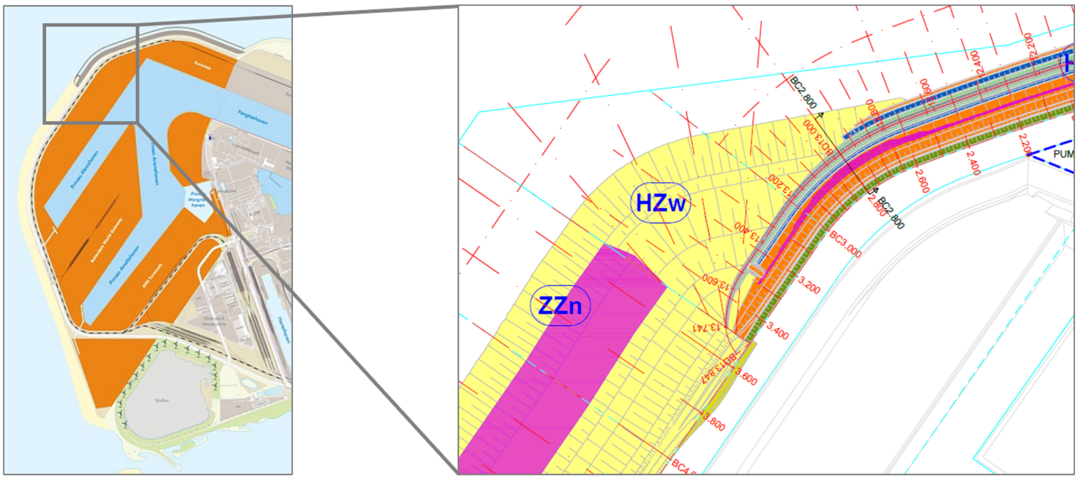

Figure 1.4: Left: top-view of Maasvlakte 2 (Havenbedrijf Rotterdam NV, 2013b). Right: zoomed figure of transition zone (PUMA, 2008a)

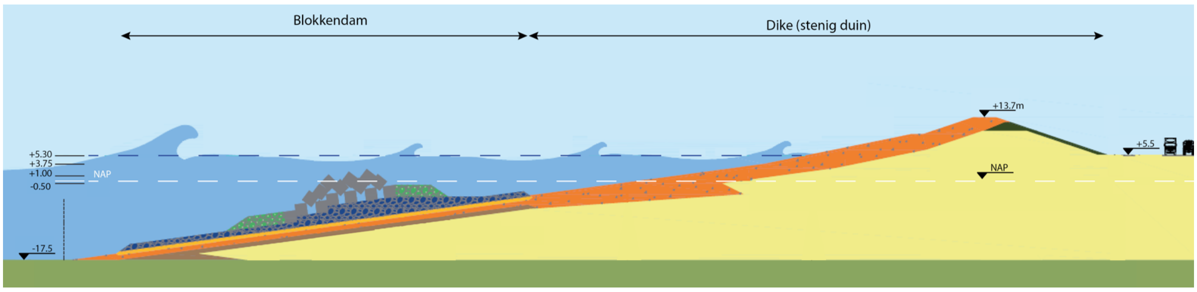

Figure 1.5: Typical cross-section of the hard flood defence at Maasvlakte 2

Despite the fact that hard-soft transitions are used worldwide, no generic assessment method is available. In the design by puma a cube reef is constructed in front of the shore. The cube reef consists of large, cubic blocks that must absorb the incoming waves. The biggest part of the wave-energy is absorbed and small waves are approaching the cobble shore behind. Moreover, in the design a small breakwater is constructed perpendicular to the coast. This small breakwater is named a "lateral dam" (see figure 1.6). This dam is incorporated into the design for different reasons, mainly:

- to prevent that sand particles from the soft protection are moving in northern direction
- waves from a northern direction create a southern directed current behind the cube reef. The lateral dam prevent this current from damaging the area around the transition zone.

As is visible from figure 1.6, water is present between the cube reef and cobble beach. This artificially created water volume between these two structures is named "the lagoon". Most of the mentioned definitions are shown in figure 1.6a.

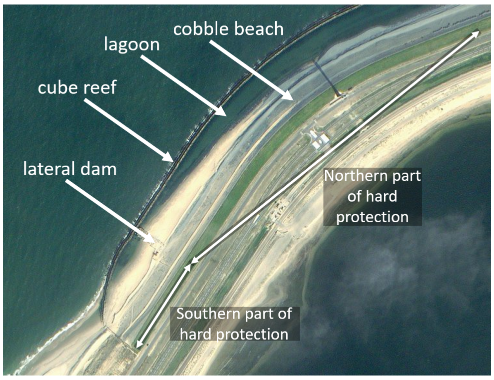

(a) Used definitions around the hard protection of Maasvlakte 2

(b) Overtopping over the cube reef at Maasvlakte 2. The picture is made in northern direction from the lateral dam.

Figure 1.6: Used definitions around the hard protection of Maasvlakte 2

1.3. Problem definition

This research will focus on the morphodynamics in the domain between the cube reef and cobble beach at Maasvlakte 2. Over the last years a large sand volume entered the lagoon. The formation of this sand layer is visible by analysing the differences between the satellite images of 2014 and 2018, as shown in figure 1.7. The sand volume is indicated within the yellow circle. As shown in figure 1.8, the volume increase is also visible at a cross-section along the hard protection (KP3300). This transported sand volume will be named the "sand layer" during this research. PUMA knew on beforehand that sand would move from the soft protection in the lagoon. They predicted a sand volume increase in the lagoon of about 20,000 m^3 within the first 10 years after construction. The current sand volume (after 5 years) is about four times larger than this predicted value by PUMA. We will present detailed volume calculations later this research. The mechanisms and respective contributions leading to sediment transport towards the lagoon were not fully understood.

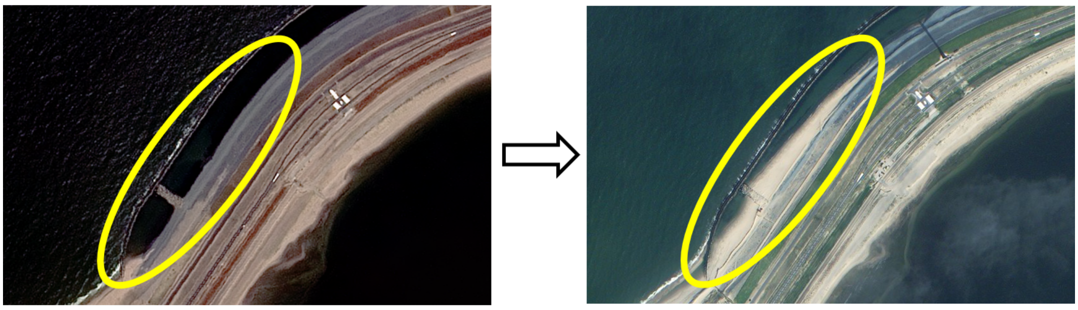

Figure 1.7: Development of the sand layer between July 2014 and September 2018.

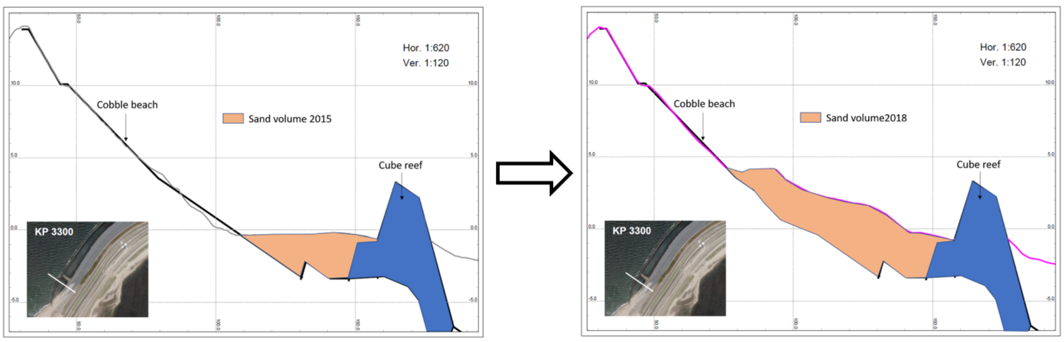

Figure 1.8: Sand volume increase for the cross-section at KP3300 (satellite images are from April 2015 and April 2018). Section KP3300 is indicated with the white line in the lower left corner

Current knowledge on the origin or future of the sand layer is rather limited. The problem of a sand layer formation was not foreseen and so far, no attention has been paid to this problem. The responsible processes in the formation of the sand layer are unknown. Studies of Arcadis and PUMA provide more insight into the morphological processes around the soft protection, but not around the hard protection. Thorough understanding of the system requires more research into the transport mechanisms around the hard protection of Maasvlakte 2.

Sand volumes between the cobbles could increase the amount of run-up on the cobble beach, which could induce for more wave overtopping. At the same time, the sand volume in the lagoon could dissipate incoming wave energy and decrease the run-up on the cobble beach. The relation between cobble revetments, sand and overtopping is currently investigated by Zaalberg (2019). In 2023 the maintenance responsibility for Maasvlakte 2 will be transferred from PUMA towards Rijkswaterstaat. Before the responsibility transfers, all contract details will be discussed between PUMA and Rijkswaterstaat. The safety standard of the hard flood defence is discussed, whereby more knowledge is needed regarding the formation and future of the sand layer in the lagoon.

In sum, the current knowledge about the formation of the sand layer is limited, resulting in a poor understanding of the transport mechanisms around Maasvlakte 2. This research will focus on the formation of the sand layer in the lagoon. It will help to increase our scientific knowledge on processes that are responsible for the formation of the sand layer. Moreover, it is investigated how the sand layer will develop in the coming years. It is unknown if the current size of the sand layer is an equilibrium or that the sand layer volume will increase in the coming years.

The **sand layer** is defined as the propagated sand volume between the cube reef and cobble beach.
The **lagoon** is defined as the artificially created water volume between the cube reef and cobble beach.

1.4. Research questions

In this thesis, the responsible mechanisms in the formation of the sand layer will be studied. The mechanisms causing an influx of sediment into the lagoon are needed to understand the morphology around Maasvlakte 2. Furthermore, the future development of the sand layer for the coming years will be discussed. The overarching research question of this thesis is therefore formulated as follows:

Main research question

"Which mechanisms are responsible for the current size of the sand layer at Maasvlakte 2 and how will the sand layer develop in the coming years?"

To be able to answer this research question, the following additional research questions are defined:

Additional questions

1. What are the main mechanisms leading to sediment transport towards the domain between the cube reef and the cobble beach?
2. How large is the respective contribution of the main mechanisms in the formation of the sand layer volume?
3. How will the sand layer develop in the coming (5) years?

1.5. Conceptual model

During previous studies the sand layer is not investigated. We created a conceptual model during several brainstorm sessions to get a better idea of the interest area, as shown in figure 1.9. All potential contributions leading to sediment transport towards the sand layer are indicated. The contributions are separated into hydrodynamic processes (black arrows) and aeolian processes (red arrows). The contribution of each arrow in the formation of the sand layer is studied. In this study we consider the following mechanisms: transport over the cube reef, transport through the cube reef and aeolian transport towards the lagoon. Moreover, we investigate the influence of storm periods and the depth influence at the foreshore in front of the cube reef with respect to the formation of the sand layer.

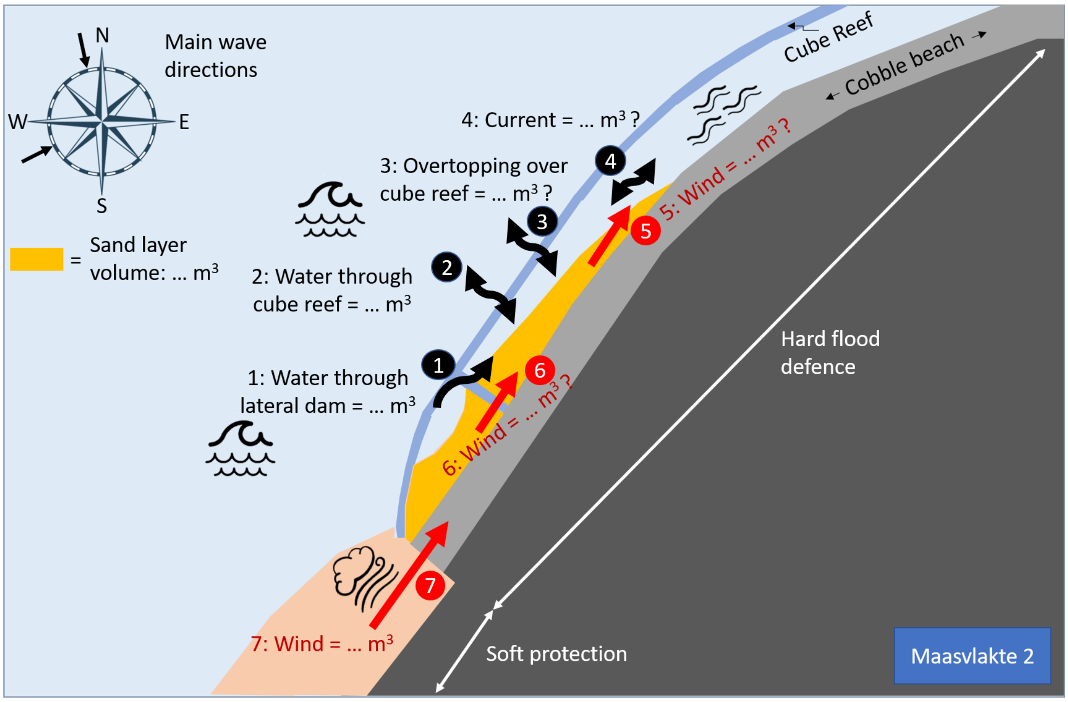

Figure 1.9: Conceptual model for the sand layer area at Maasvlakte 2. The black arrows indicate hydrodynamic transport contributions and the red arrows indicate aeolian transport contributions.

1.6. Research outline

In Chapter 2 the previous studies and model tests by PUMA and Arcadis are briefly explained. Followed by the qualitative observations during seven performed field visits in Chapter 3. Four analyses are performed based on the conceptual model and field observations. First the wave climate is analysed in Chapter 4. Followed by a sediment budget analysis in Chapter 5. In this chapter the satellite images and measurement data from PUMA are analysed. The total sand layer volume is obtained within this chapter. After that, the hydrodynamic and aeolian contributions are separately investigated in Chapters 6 and 7. At the end of Chapters 4, 5, 6 and 7 a short discussion and conclusion of the specific chapter is given. In Chapter 8 a reflection on all obtained results is given, followed by a discussion of the entire system. Finally, the conclusions and recommendations for further research are posed in Chapter 9. The appendices are attached after the bibliography and contain background information plus additional plots and figures.

2
Previous studies

During the design and adaptation period different studies were performed around Maasvlakte 2. This chapter is included in this research to show the prior performed studies by PUMA and Arcadis. It gives an idea of all the prior investigated topics around Maasvlakte 2. PUMA did the design studies and PUMA together with Arcadis performed studies during the adaptation period at the soft protection. Deltares performed model tests during the design studies to test the designed cube reef and cobble beach. The morphological studies by PUMA and Arcadis were only focussed on the soft protection. The sand layer between the cube reef and cobble beach is not investigated during these studies. First the main conclusions from design studies by PUMA are given. Followed by the performed model tests with Deltares. In this section we explain the investigated mechanisms during the model tests. After that we show the main conclusions from the morphological studies by Arcadis. Finally, we give a short summary of all performed studies.

2.1. Studies by PUMA

2.1.1. Design studies

PUMA performed predictions about the available sand at the soft protection and the available cobbles at the hard protection. Erosion of the seabed was expected during the design phase of Maasvlakte 2 (PUMA, 2008b). Due to waves, tides and wind the sand and cobbles will move. At some places more material will be transported than there is supplied in a natural way. This will result in a nourishment (PUMA, 2008c). The safety assessment for the soft protection is based on the fact that there must be a determined volume of sand in the upper part of the profile (between +3m NAP and -5m NAP). See appendix figure B.1 for an overview of a cross-section at the soft protection. Figures of the final design of the hard protection are given in section 1.2. The transition zone between the soft and hard protection was expected to be an erosive part. The area around Maasvlakte 2 is divided and numbered into different sections (see figure 2.1a). In the transition zone some of these cross-sections are not perpendicular on the coast. This part is called "the cone" (see figure 2.1b).

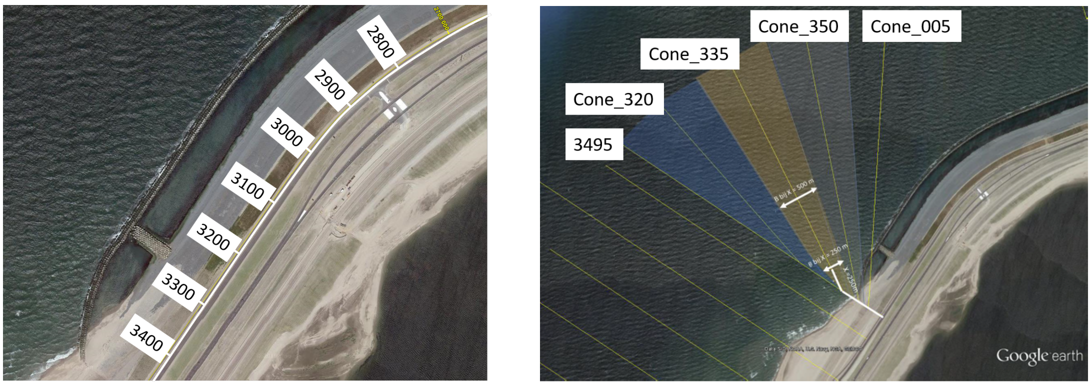

(a) Used KP-numbers for the cross-sections around the sand layer area

(b) This figure indicates the area called 'the cone'

Figure 2.1: Two figures to illustrate the used section numbers around the sand layer

2.1.2. Aeolian transport

During the design phase PUMA performed studies towards the amount of sand transport at Maasvlakte 2. It was expected that the wind would mainly cause for erosion at the dune area. PUMA based their analysis on the little available aeolian transport information along the Dutch coast. With given transport formulas and a year averaged wind climate (obtained from KNMI) the aeolian transport at the soft protection was calculated and expected to be around 75 m^3/m (PUMA, 2008d). Based on experience from other locations along the Dutch coast, PUMA expected that this value will be lower in reality. At other locations along the Dutch coast the sand accumulation in the dunes after a beach nourishment was in the order of 2 - 25 m^3/m. Therefore, the prior mentioned 75 m^3/m was expected to be too high. Vegetation in the dunes and the moisture content after a rainy event will decrease the 75 $m^3/m/year$ (PUMA, 2008d). Finally, PUMA concluded that a sand buffer in the dunes of 50 m^3/m would be sufficient to account for losses by aeolian transport during the first 10 years after construction, which is equal to 5 $m^3/m/year$ (PUMA, 2008d).

During construction of Maasvlakte 2, large sand volumes were found at parking spaces behind the dunes at the soft protection (parking spaces are located at number 1 in figure 2.2). Elevation measurements of 2011 and 2012 were analysed and sand accumulation was found at the dune area. Sand was also visible in the port at number 2 in figure 2.2, these sand volumes were transported from the soft protection. By looking at sections with a similar coast orientation as the sand layer area, an accumulated sand volume was found of 15 $m^3/m/year$ at the sea-side of the dune and at the land-side an average sand volume of 20.6 $m^3/m/year$ was found (PUMA (2012a) and PUMA (2012b)). PUMA placed fences at the sand layer area to prevent that sand would be transported into the cobbles at the hard protection, as shown in figure 2.3.

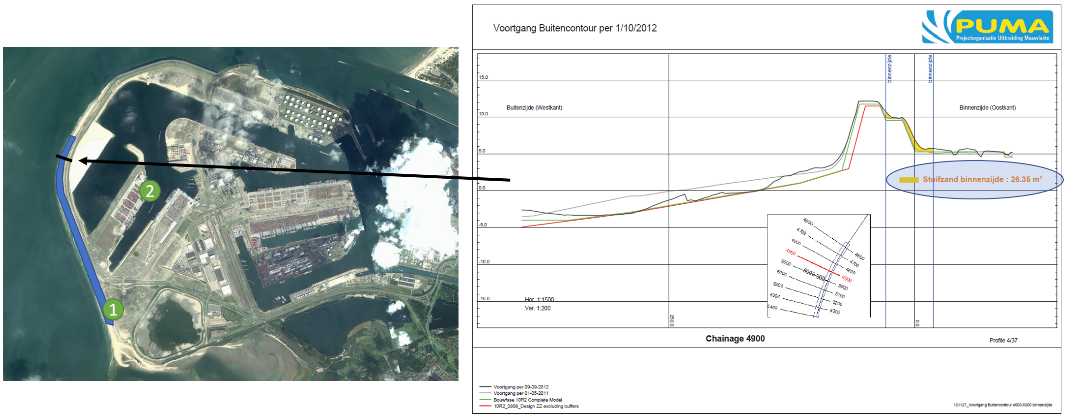

Figure 2.2: Sand volumes found behind the dunes. Elevation measurements are analysed in the blue area of the left figure. Number 1 is indicating the parking spaces and number 2 is the location where large sand volumes were found in the port. For example, the accumulated sand volume in KP4900 at the land side of the dune was 26.35 m^3/m.

Figure 2.3: Small fences are placed to prevent that sand will reach the cobbles at the cobble beach (photo taken on November 20^th, 2018)

As mentioned, it was expected by PUMA that the wind will cause for erosion at the dune area. Based on the large sand volumes at the parking spaces and the performed study afterwards, it is concluded that the assumptions (made during the design phase) were insufficient. Over the past years, research is performed

towards aeolian transport. It is nowadays known that aeolian transport moves sand volumes mainly from the coastline towards the dunes. This was also concluded at the Sand Motor area by Hoonhout (2017). The main sources of aeolian sediment at the Sand Motor mega nourishment were the dry beach area (aeolian zone, 33%) and the intertidal and low-lying supratidal beach areas (mixed zones, 67%). The relative importance of the mixed zones is notable as it is periodically flooded and the majority of the northern mixed zone is oriented unfavorable with respect to the wind (Hoonhout, 2017).
Furthermore, the calculated sand buffer at Maasvlakte 2 by PUMA was too low compared with reality. An average sand volume of 5 $m^3/m/year$ was expected and from measurements an average of around 30-40 $m^3/m/year$ was found in the profile. In sum, the calculated buffer was too low and placed at the wrong location in the profile.

2.2. Model tests during design studies

Different model tests were performed during the design phase. The tests are performed at Deltares in Delft and at HR Wallingford in England. Different variants for the cube reef and cobble beach were made by PUMA and tested at Deltares. The hydraulic conditons were specified by PUMA. The model set-up, measurements, results and observations during the tests of the different variants are described in the report of Hofland and Van Gent (2010). First two series of model tests were performed with two profiles. Those two profiles were also tested on larger scale in the Deltagoot. Combining these two tests the accuracy of the cobble beach could be determined for the smaller scale. Eight variants were tested, which all includes the cube reef and cobble beach. Investigated processes were for example: overtopping, set-up and transmission. According to the observed deviations during construction of the cube reef, the necessary modifications of the design are tested again in the Scheldegoot. The hydraulic stability of the layers in the cube reef and transmission through the cube reef is investigated during the study of Hofland and Van Gent (2011). Moreover, the wave heights behind the cube reef were required for the design of the cobble beach at Maasvlakte 2. Based on model tests at the Scheldegoot (2D) and in the wave basin of HR Wallingford the transmission formula of D'Angremond is calibrated for the cube reef + cobble beach (PUMA, 2009). In 2010 the optimised hard protection is tested in the Deltagoot at Deltares (Van Gent and Van Der Werf, 2010). The cross-shore deformations of the cobble beach and overtopping volumes over the cobble beach are analysed.

In 2007 and 2009 model tests are performed in the Deltagoot of Deltares regarding the transition zone between the soft and hard protection. Different variants are tested for two different cross-sections. The deviations of the cobble beach are analysed. Moreover, tests are performed with sand volumes incorporated in the pores of the cobble beach. At the test of Van Gent and Smith (2007a), the influence of the sand volumes between the pores was minimal on the general profile development of the cobble beach. On the other hand, the influence on the run-up and therefore on the berm development was visible. By a experimental set-up where the toplayer was filled with sand for 50% and the crown was positioned 0,5m higher the overtoppings volumes were three times as high as during the experiment without sand and lower crown ppsition. More about the test set-up and conclusions of all measurements can be found in Van Gent and Smith (2007a) and Van Gent and Smith (2007b). In 2009 additional model tests are performed in the Deltagoot. The main conclusion from the these model tests is that the incorporated sand volumes between the pores increase the erosion resistance of the cobble beach, but overtopping volumes increased as well, more details about the test set-up can be found in (Van Gent and Muttray, 2009) .

2.3. Cobble beach nourishments by PUMA during the adapatation period

The 3.5 km long cobble beach is constructed from 7 million tonnes of quarry stone. Waves will attack the cobble beach and replace the cobbles along the beach. During high water levels the waves will cause for transport of cobbles in cross-shore and longshore direction. The cobbles will move until an equilibrium state is reached. Models are available to predict the so-called S-shape equilibrium profile. In figure 2.4b the cobble movement is visible after a performed suppletion in July 2018.
The cobble beach requires maintenance in the form of regular nourishments of quarry stones. By applying the nourishments, the thickness of the armour layer will be large enough to prevent erosion of the underlying sand layer. See figure 2.4a for an image of the difference between the pre- and post-cobble nourishment in 2018. The applied nourishment volumes turned out to be lower than expected as can be seen in table 2.1. According to Olthoff (2019) the reasons for these lower nourishment volumes were the higher placement of the cube reef, settlement of the subsoil and a different wave climate occurred than during the design phase.

The proposed and executed nourishments in $kton$ are obtained from Olthoff (2019) and PUMA. The executed nourishment volumes in m^3 are obtained by analysing the pre- and post-cobble measurements of 2016 and 2018. According to Olthoff (2019) the porosity of the cobble beach is equal to 0.379.

Date	**Proposed nourishments [kton] (Olthoff, 2019)**	**Executed nourishments [kton] (Olthoff, 2019)**	**Executed nourishments [m3] (obtained from measurements)**
October 2016	34.3	10	5,800
July 2018	37.6	16	10,000

Table 2.1: Predicted and executed nourishment on the cobble beach at Maasvlakte 2

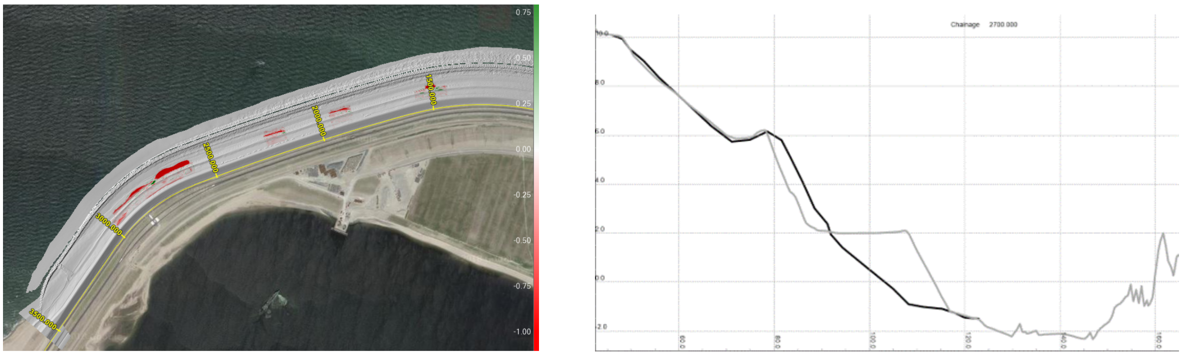

(a) The pre- and post-cobble nourishment in July 2018. The nourishment locations are indicated in red

(b) Deformations of the cobble beach are visible between the post-cobble measurement in July 2018 (grey line) and the GPS-measurement at January 19th, 2019 (black line) for KP2700

Figure 2.4: Performed cobble nourishment in 2018 at Maasvlakte 2

2.4. Morphological studies by Arcadis

Yearly maintenance is necessary to meet the safety requirement for the Maasvlakte. During the adaptation period (2013-2018), the soft protection is monitored extensively. Nourishments were planned to compensate for the occurred erosion. The nourishment lifetime for the soft protection was set to two years, to minimize the effect on the natural equilibrium. Three sand nourishments were planned for the soft protection: 2014, 2016 and 2018. Arcadis was asked to perform four morphological analysis during the adaptation period: Onderwater (2016), Onderwater (2017), Onderwater (2018a) and Onderwater (2018b). These studies were performed to find a practical solution for the occurred erosion in the area, especially at the transition zone.

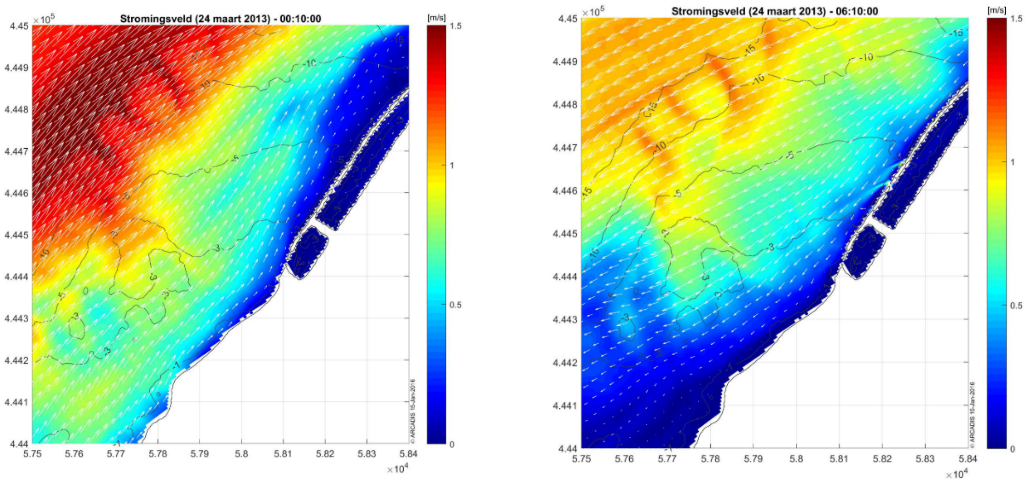

(a) Flood current with measured bathymetry

(b) Ebb currents with measured bathymetry

Figure 2.5: Maximum flood and ebb currents with the measured bathymetry at 24 March, 2013 (Onderwater, 2016)

Onderwater conducted the first morphological study in 2016. The following analysis were carried out: erosion and sedimentation patterns, wave climate observations, different images from Google Earth, analysis of the tidal currents and the combination of waves and tide-induced sediment transports. Delft3D is used to analyse the tidal currents caused by the Nieuwe Waterweg and Haringvliet (Onderwater, 2016). It is observed from figure 2.5 that tide averaged flood-current is visible along the soft protection and an tide averaged ebb-current along the hard protection. At the transition zone a mild, seaward directed, tide averaged current is visible. It is also found by Arcadis and Lako (2019) that the northward directed flood current along the soft protection strengthens the supply of sediment, this sediment settles at the transition zone. The southward directed ebb current along the hard protection is not saturated with sediment and does therefore not cause for any morphological changes. The study by Onderwater (2016) was not focussed on the area within the cube reef. The cube reef is set to impermeable in the models of Onderwater, therefore all velocities are 0 m/s in the lagoon.
During the research of 2016, it was confirmed by Arcadis that the beach area was eroding and the shoreface experiences accretion. Monitoring of the flood defence revealed that, especially near the transition zone more erosion had occurred than initially expected. Furthermore, the nourishment of 2014 was rather ineffective and eroded fast after construction. In Appendix A (figure A.1), the beach nourishment of 2014 is visible. This nourishment of 2014 is not visible anymore in the satellite images in February 2015. This highlighted the importance of the nourishment location. A possible explanation for the erosion could be that the wave climate of the past years is different than the climate of 1979 - 2001 (Onderwater, 2016). Onderwater proposed six solutions to solve the erosion problem. Moreover, the safety assessment was changed by taking into account the 2D effects around the cone and the nourishment locations are redefined.

After monitoring the entire area in April 2017 the assessment requirements were, again, not met. A 2DH process-bases XBeach model was made and the 2D-effects around the hard-soft transition were analysed. The results of this study gave opportunities to adjust the safety assessment.

At the research of Onderwater in 2018 it appeared that the nourishment of 2016 eroded quickly (just like the nourishment in 2014). From the measurements in 2016, after a year of no nourishments, the area seemed to be more stable. Therefore, Onderwater gave the following recommendations: it is recommended not to perform the safety assessment based on layer volumes (required sand volume between +3m NAP and -5m NAP), but on the position of the dune retreat relative to a critical retreat point (similar to the standard safety assessment for uniform coasts from Boers (2012)). Furthermore, it is recommended to interfere less in the system. This can be achieved by nourishing less frequently or avoid nourishments in the active zone (shoreface and foreshore). The solution to avoid nourishments in the active zone is worked out and can be achieved by heightening and widening the dune. The goal of moving the retreat point more seawards is to extend the lifetime of the nourishment and, therefore achieve the requirement of nourishing once every two years. Furthermore, it was observed that if waves are coming from a south-western direction sand is settling in the transition zone. This sand is transported towards the hard protection and settled seawards of the cube reef. Waves coming from a northern direction are able to wash away the accumulated sand.
Comparing the proposed and executed nourishments over all the years, it is visible that the real applied nourishment volume is less than the proposed volume (see Appendix B tables B.1 and B.2). Furthermore, no shoreface nourishments were applied, because this layer constantly had sufficient sediment volume. Instead of shoreface nourishments, more offshore nourishments are placed. The nourishment in December 2018 together with smaller nourishments on the beach should be sufficient to assure the safety for the next two years. See Appendix B for more conclusions from PUMA and Arcadis during the design and adaptation period.

2.5. Summary of all previous studies

Based on all performed studies we concluded that the sand layer is not yet investigated, although the existence of the sand layer is known. Rough predictions are made to account for aeolian transport, but the calculated buffer was too low and placed at the wrong location in the profile. Moreover, all performed morphological studies are about the soft protection and not towards the hard protection. In sum, the problem of a sand layer formation was not foreseen and so far, no attention has been paid to this problem.

3 Field visit observations

The qualitative observations during seven performed field visits are shown in this chapter. Different field visits are performed during this research to obtain information about the processes at Maasvlakte 2. Conditions as aeolian transport, flow velocities in the lagoon and wave heights in the lagoon are observed and analysed. We presented the qualitative observations during the field visits in table 3.1. The observations at the sand layer area are graded as follows: (1) process is not visible, (2) process is clearly visible, (3) extreme manifestaties of the process are visible. In table 3.2 the field conditions during the field visits are shown. The given directions are related to true north (see Appendix B.3 for a wind rose with directions).

Date	Aeolian transport at sand layer	Current within cube reef and cobble beach	Waves within cube reef and cobble beach	Other observations
21 sep	3	3	2	Aeolian transport physically observed Strong northern directed current visible Significant overwash over cube reef
5 nov	1	2	1	No aeolian transport Small southern current (probably tide driven) Very calm conditions at the North Sea
10 nov	2	2	2	Very little aeolian transport Northern directed current visible
20 nov	3	2	2	Aeolian transport physically observed Southern directed current visible
12 dec	1	2	1	No aeolian transport A small current Very calm conditions at the North Sea
08 jan	3	3	2	Aeolian transport physically observed Southern current (large influence of the waves) Cube reef almost under water
11 jan	1	1	1	No aeolian transport Calm conditions and no current

Table 3.1: Qualitative observations during field visits. The observations at the sand layer area are graded as follows: (1) process is not visible, (2) process is clearly visible, (3) extreme manifestaties of the process are visible

Date	Wind velocity [m/s]	Wind direction [degrees]	Wave height [cm]	Wave direction [degrees]	Water level with respect to NAP [cm]
21 sep 2018	13 - 14	270	260	250	≈ +10
5 nov 2018	5	120	40	150	≈ -20
10 nov 2018	8	190	160	210	≈ -60
20 nov 2018	10	90	220	45	≈ +50
12 dec 2018	5	100	70	15	between 0 and -90
08 jan 2019	15-16	315	400	335	≈ +220
11 jan 2019	6.5	320	120	320	≈ -60

Table 3.2: Wind and wave conditions during the performed field visits. Wave conditions are obtained from Europlatform. Water levels and wind conditions are obtained at Hoek van Holland (Rijkswaterstaat, 2018). Directions are related to true north, see appendix figure B.5.

The conditions during the different field visits were sometimes very calm and sometimes extreme. In figure 3.2 the differences during low and high tide and during storm conditions are shown. These pictures are made in northern direction from the lateral dam. The accumulated sand volume between the cube reef and cobble beach is visible in figure 3.2a. We observed sand volumes during the field visits until KP2700, this section is indicated in figure 3.1. During the field visits on September 21th and January 8th rough conditions were present. Especially during January 8th a high water level was combined with high waves and high wind velocities. The large blocks of the cube reef were just visible above the water level (see figure 3.2c). We assumed that during conditions as shown in figures 3.2c and 3.3c, the waves could transport large sand volumes into the lagoon by overtopping. More research is necessary to confirm this assumption. Moreover, we observed that the cube reef is absorbing almost all wave energy. Waves in the lagoon were only visible during the field visits, when wave heights were higher than 120cm outside the cube reef. It is noted that waves were not always observed in the lagoon during wave heights outside the cube reef higher than 120cm. It is difficult to define a general threshold when wave heights are visible in the lagoon. Moreover, wind can create small ripples in the lagoons. From the observations in table 3.1 we observed that aeolian transport is only happening at wind velocities above 8 m/s.

The current velocity in the lagoon was different in size and direction during each field visit. The current direction is changing between being southward or northward directed. During the field visits it could not be confirmed if the observed current is tide, wind or wave driven. It is assumed that the current is tide driven during low wave heights and low wind speeds. This assumption is based on the observation in November 5th, during this day the wind and waves were coming from the south, but the observed current came from the north. This current is probably caused by the tide. On the other hand it is observed that high waves combined with high wind speeds have an influence on the current (September 21th and January 8th). This influence is dependent on the direction of the waves and wind. On September 21th, a strong current was observed with waves and wind from the south-west. During January 8th, the waves and wind were coming from the north-west, but there was no large southern current visible during that day. The waves were approaching the coast with a small angle and most of the water was pushed towards the coastline. Finally, we assumed from the observations that the water level is an important parameter regarding sediment transport towards the lagoon. The water level influences the wave height on the foreshore and in the lagoon, therefore less or more sediment is in suspension.

From all performed field visits the general observations are listed:

- Aeolian transport is physically observed around the sand layer domain when wind speeds are higher than 8 m/s
- The observed current in the lagoon is assumed to be tide driven. High water levels combined with high waves and wind speeds could influence this current direction and velocity.
- The lateral dam is almost fully saturated with sand (see figure 3.3a).
- The cube reef is absorbing the wave energy (see figures 3.3b and 3.3c). Small waves are sometimes able to transmit through the cube reef. This happened during the fieldvisits when wave heights outside cube

reef were higher than 120cm (see figures 3.3e). It was not possible to define a general threshold when wave heights were visible in the lagoon.

- Sand volumes are visible along the cobble beach. This indicates that sand volumes are present between the cobbles until KP2700, see figure 3.1 and 3.3d

Figure 3.1: Sand volumes visible on the cobble beach at November 10^{th}, 2018. The arrows indicate the direction of the taken images.

(a) Image during low tide. Picture is taken in northern direction from the lateral dam.

(b) Image just before high tide. Picture is taken in northern direction from the lateral dam.

(c) Image during storm conditions on January 8^{th}, 2019. The lateral dam is visible at the left side of this picture.

Figure 3.2: Impressions of the sand layer during low and high tide and during storm conditions

(a) Image of the lateral dam, which is full with sand on September 21^{th}, 2018

(b) The cube reef is absorbing the incoming wave-energy on September 21^{th}, 2018

(c) Over-wash over and through the cube reef on September 21^{th}, 2018

(d) Sand volumes visible on the cobble beach on November 5^{th}, 2018. The used GPS-device during the elevation measurements is visible in this figure

(e) Small waves are present in the lagoon on November 10^{th}, 2018. Sand voluems are visible on the cobble beach

(f) The sand layer during low tide on November 10^{th}, 2018 (image taken in northern direction from the lateral dam)

Figure 3.3: Images obtained during the field visits

4

Wave climate analysis

The reason for the existence of the sand layer could be obtained by analysing the occurred wave climate over the last five years. We obtained wave data over the period 01-01-2013 until 12-01-2019 for every 10 minutes from the Europlatform at Rijkswaterstaat and the KNMI (see figure 4.1). The data consists of the following parameters: wave height, wave direction, peak period, wind speed and wind direction. This wave data is used during the analysis of respective mechanisms that contribute to the existence of the sand layer. The wave data is transformed nearshore with the program SWAN.

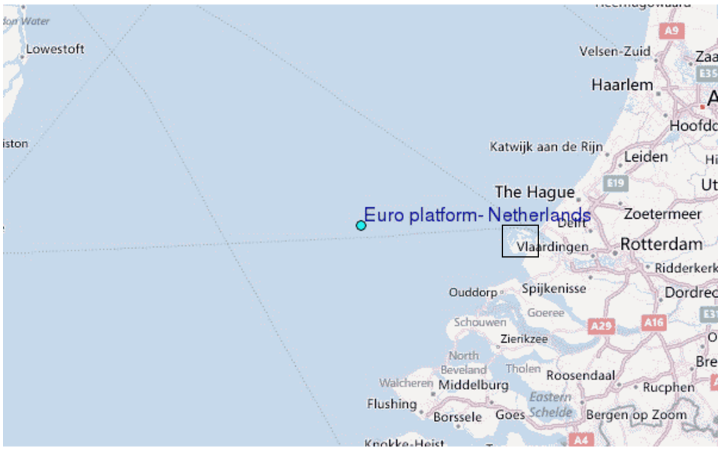

Figure 4.1: Location of the Europlatform offshore, approximately 50 km offshore of Maasvlakte 2

4.1. Year-round wave conditions

The yearly wave conditions are analysed in order to identify differences in the wave climates. In figure 4.2 the wave roses are plotted for each year from 2013 till 2018. In the middle of each figure the percentage of calm conditions is shown (calm conditions corresponds with wave heights under 0.5m). The waves in 2013 were coming from two main directions: south-west and the north. In 2014 and 2015 the waves were mainly coming from the south-west and since 2016 the northern component is getting larger. In 2018 the northern and south-western component are equal in length. In sum, we concluded that the waves were coming from a south western direction in the beginning and that the northern wave direction has increased over the last 5 years. Remarkable is the high percentage of calm conditions in 2017 and 2018.

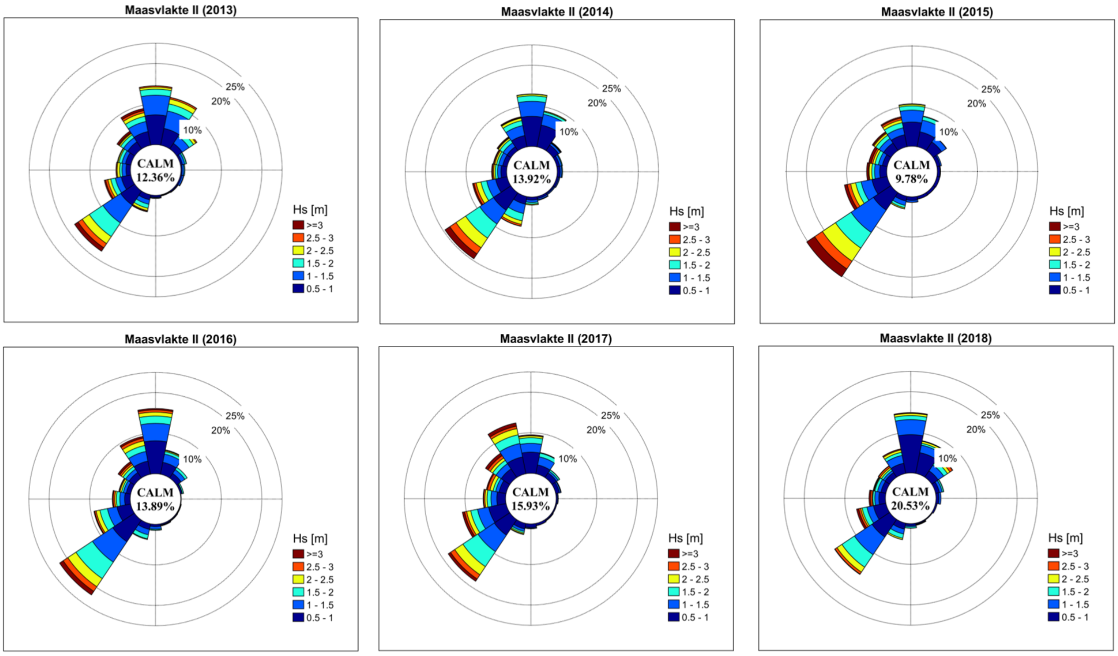

Figure 4.2: Waves roses for the years 2013 - 2018. The colors indicate the wave height and the length of the colorbar represents the percentage of waves from that direction.

4.2. Year-round wave energy fluxes

According to Lako (2019) the wave energy and wave height are defined with a proportion of $E <> {H_s}^{2.5}$. In literature the proportion wave height versus wave energy is also found as: $E <> {H_s}^2$, the exact value for the power is not important during this analysis. In this analysis it is important that the influence of higher wave heights is incorporated in the used relation. With equation 4.1 the magnitude and resulting direction of the wave energy flux can be computed. By looking at the wave energy fluxes the growing northern component is also visible. The resulting wave energy flux is the wave energy obtained from all the individual waves. The incoming waves are separated into bins of 20 degrees between 220 and 40 degrees (see Appendix figure C.1 for the coastal orientation and the wave flux domain). Then equation 4.1 is applied on each individual wave height. The total wave energy flux per bin is obtained by adding up all the individual wave energy values. In table 4.1 the direction and magnitude of the yearly energy fluxes are shown. The increase in waves from a northern direction is visible by comparing the years. The magnitude of 2018 is low compared to other years. The last column of table 4.1 shows that the amount of data points for each year is around the same value. Combined with the high percentage of calm conditions from the wave roses, it is concluded that the wave heights were low in 2018. In figures 4.3a and 4.3b the wave energy fluxes are plotted for the years 2014 and 2017. In 2014 the resulting wave energy flux was 267 degrees and in 2017 it was 287. The contribution of each wave bin is visible in these figures. In appendix figure C.2 the wave fluxes are shown for the years 2013 - 2018.

$$E <> {H_s}^{2.5} \tag{4.1}$$

Year	Resulting direction wave energy flux	Resulting magnitude wave energy flux $[m^{2.5}]$	Data points each year
2013	292	66.561	51.717
2014	267	77.476	52.135
2015	262	108.647	49.588
2016	284	63.444	42.537
2017	287	96.913	51.996
2018	285	44.806	45.780

Table 4.1: Yearly resulting energy fluxes and magnitudes

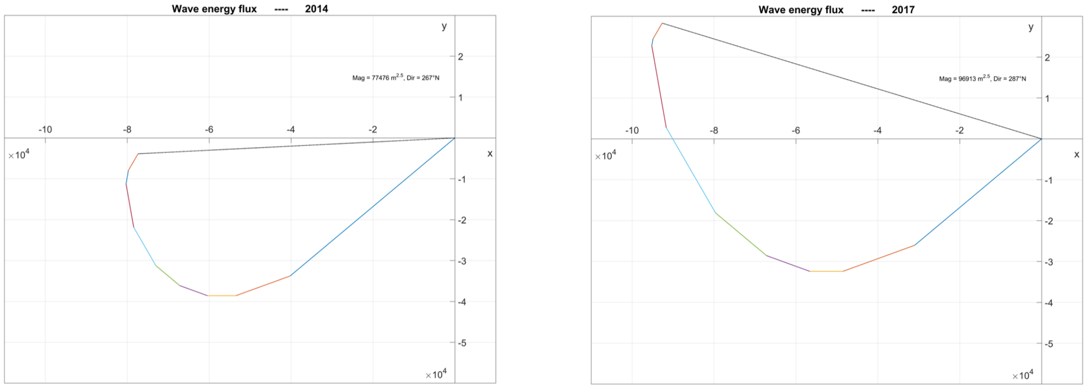

(a) (b)

Figure 4.3: Wave energy fluxes for the years 2014 and 2017

4.3. Winter periods

During the winter periods the waves heights and wind velocities are higher than during the summer period. The higher waves could induce more sediment transport and, therefore it is important to know the conditions during the winter periods. In figure 4.4 the wave roses are shown for the winter periods. The storm season is defined from October 1^{st} until April 15^{th} by Rijkswaterstaat. This storm period is called the winter period in this report. Analysing the winter periods it is observed that the waves were mainly coming from the south west during the winter of 2013-2014 until 2015-2016. A stronger northern component is visible in the winters of 2016-2017 and during the winter of 2017-2018 both directions are equally in size. The same trend is visible by looking at the energy fluxes of the winter periods. The energy fluxes are shown in Appendix figure C.3 and in table 4.2. Remarkable is the lower magnitude of the resulting energy flux during the winter of 2016-2017 compared with the other winter periods, this also visible in the higher calm percentage during 2016-2017 in figure 4.4.

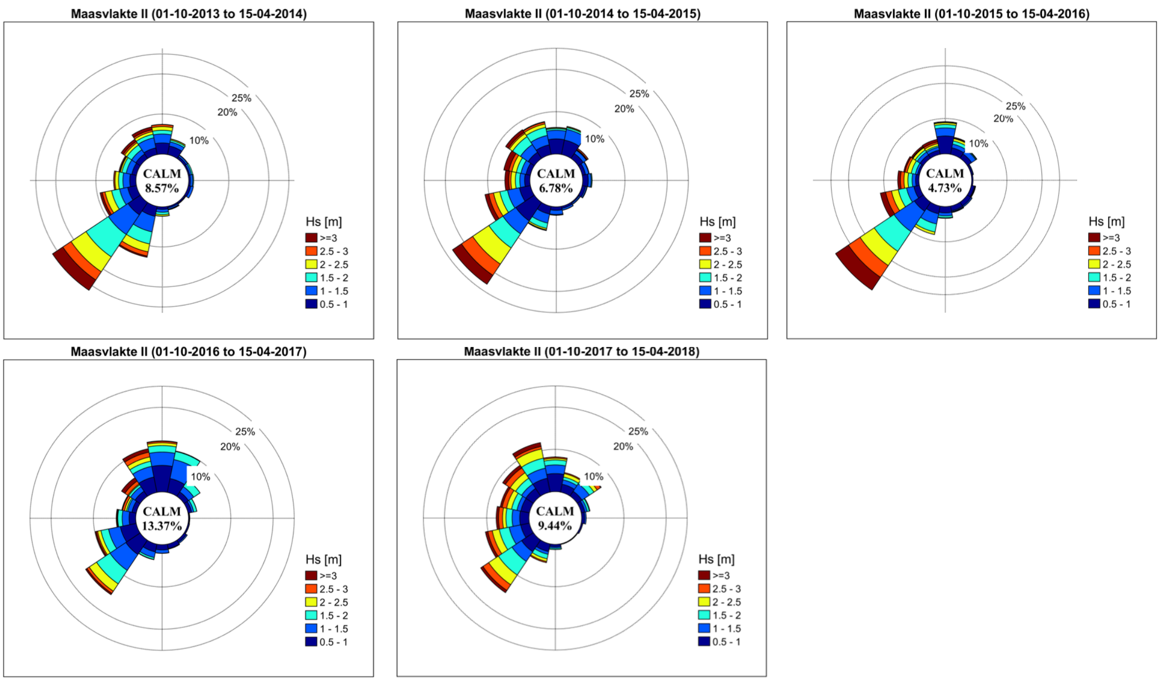

Figure 4.4: Wave roses for the winter periods from 2013 until 2018. The winter is defined from October 1st until April 15th. The colors indicate the wave height and the length of the colorbar represents the percentage of waves from that direction.

Year	Resulting direction wave energy flux	Resulting magnitude wave energy flux [$m^{2.5}$]
2013-2014	261	49.122
2014-2015	262	53.563
2015-2016	255	73.929
2016-2017	303	27.957
2017-2018	288	49.874

Table 4.2: Resulting energy fluxes and magnitudes for the winter periods

4.4. Near-shore wave data

All wave heights from 01-01-2013 until 01-05-2018 are transformed near-shore with the program SWAN, using the bathymetry of 2018. This transformation is performed by a fellow student at Van Oord (Olthoff, 2019). The output points of the transformation are the same output locations which were chosen by Svasek during the design phase of Maasvlakte 2. These 35 transformation points are located from north to south along the toe of the hard protection and a few points are further offshore from the coast. The output data of the SWAN calculation will be used during the hydrodynamic calculations in Chapter 6. In figure 4.5 the wave roses from the Europlatform and a point nearshore are shown. The location of the nearshore wave rose is located 800m offshore (as shown in figure 4.5a). In Appendix figures C.4 and C.5 the near-shore wave roses of this location are shown for the year-round conditions and winter periods. It is observed that almost all waves from the south/south-west are refracted or dissipated by the foreshore (the foreshore is visible in Appendix figure 5.1).

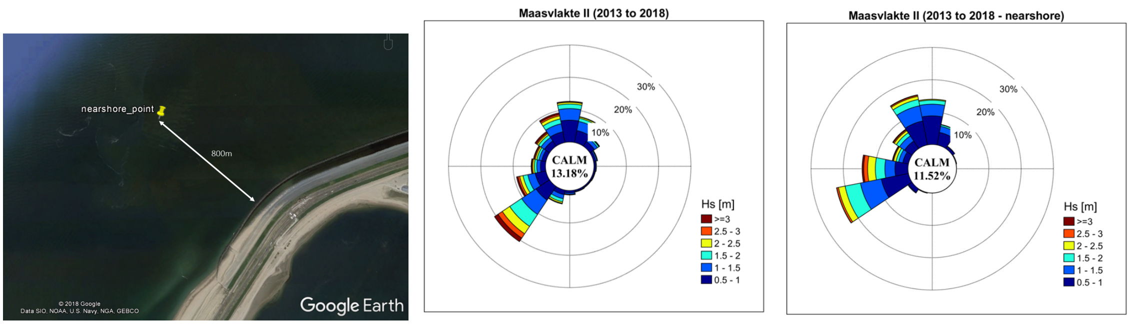

(a) Location of nearshore wave data (b) Wave rose from Europlatform (c) Nearshore wave rose (800m offshore)

Figure 4.5: Waves roses from 2013-2018 obtained from the Europlatform and a point 800m offshore from the sand layer area.

4.5. Conclusions

The waves over the last five years are mainly coming from the southwest and north. Since 2016 the south-western component became less and the northern component became larger. This is observed from both the year-round conditions and winter periods. The energy flux in 2018 is low compared with other years, therefore we concluded that the wave heights were low during 2018. On the other hand the magnitude of the energy flux in 2015 was high compared with other years. Looking at the winter periods it is observed that the waves were mainly coming from the south-west during the winter periods of 2013-2014 until 2015-2016. A stronger northern component is visible in the winters of 2016-2017 and 2017-2018. The magnitude during the winter of 2016-2017 is low compared to other years. The lower wave heights of this winter period are visible by analysing the wave roses. Comparing all wave directions with the coastal orientation (see figure C.1), the nett resulting wave energy flux is still always coming from the left side of the line perpendicular to the coast.

Two main wave directions are visible from the wave roses: waves from the north and the south-west. Between 2014 and 2016 the south-western component was higher than the component from the north. Since 2016 the northern component is growing and the northern component was in 2018 almost equal to the south-western component. Winter periods could induce for more sediment transport towards the lagoon, as wind speeds and wave heights are higher. The exact influence of these winter periods must be investigated.

5
Sediment budget analysis

5.1. Introduction

Within this chapter a data-analysis is performed to analyse the sediment budgets around the sand layer domain. The evolution of the sand layer is investigated over the last five years. PUMA monitored the area around the transition once per year. These measurements are called BIP-measurements and performed to obtain more insight into the processes. Based on these investigations the safety assessment is conducted. By analysing the BIP measurements the sand-volume increase is calculated for each year. Moreover, we analysed satellite images to increase the temporal resolution of the available data. The volumes and satellite images are compared with wave data obtained from Europlatform to identify the influence of storms on the sand layer volume. Finally, elevations of the sand layer area are measured twice during this research to identify differences in pre- and post-storm profiles. The used data sources within this chapter are:

- Bathymetry and coastline measurements by PUMA, called BIP-measurements
- Satellite images during the period 2014-2018 from Satellietbeeld (2018) and Satellietdataportaal (2018)
- Wave, wind and water-level data for the period 2014-2018 from Rijkswaterstaat (2018) and PredictWind (2018)
- Elevation measurements with a GPS-device

5.2. Methodology

5.2.1. Sand volumes

Multiple BIP-measurements are performed by PUMA over the past five years, but not all of them include the sand layer area. The dates of the available BIP-measurement for the sand layer area are: March 2013, April 2014, April 2015, April 2016, April 2017, May 2017 and April 2018. The sand volumes are calculated in reference to the previous year. That means, for example, that the volume calculation of 2015 is the difference between the survey of 2014 and 2015. The volumes are calculated within a predefined polygon (see figure 5.1b). This predefined polygon is drawn based on visual inspection during field visits (shown in Chapter 3) and by analysing the BIP-measurements. Moreover, GPS-measurements are performed. Figure 5.1a shows a measurement with a GPS-device, which includes the sand layer partly. Between 2016 and 2018 the sand layer is measured nine times during low tide. We updated the nearest BIP-measurement with the GPS measurement of the sand layer, therefore more data points are obtained. Still these updated volume calculations are not entirely correct, because only the measured area corresponds exactly with the corresponding measurement. For example the measurement of figure 5.1a is performed in October 26^{th} 2016. The average is taken from the BIP-measurements of April 2016 and April 2017. This average layer is updated with the sand layer measurement of October 26^{th} 2016. Finally, the sand layer volume is calculated with the updated data-file.

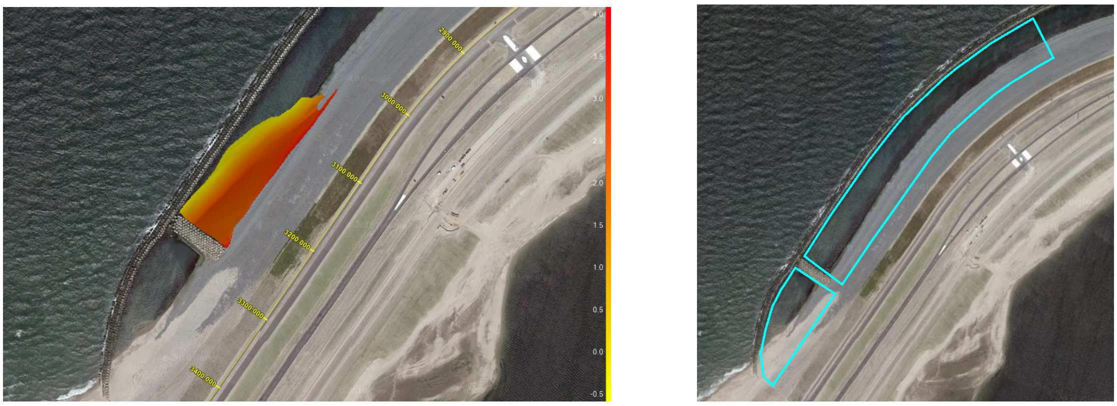

(a) GPS-measurement of a part of the sand layer at 26 October 2016

(b) Used polygons during volume calculations

Figure 5.1: The sand volume outside the cube reef is visible in 2013 and the used polygon during the volume calculation

During construction of Maasvlakte 2, PUMA placed sand volumes between the soft and hard protection to create a gradual transition zone. A sand volume of 7,300 m^3 was placed in the lagoon and also sand was deposited on the foreshore outside the cube reef, as is visible from the elevations in figure 5.2. We took this designed volume into account by calculating the total sand volume in the lagoon. Moreover, PUMA performed nourishments at the soft protection over the last five years. These nourishments could influence the amount of sand transport towards the lagoon, therefore we investigated the influence of these nourishments.

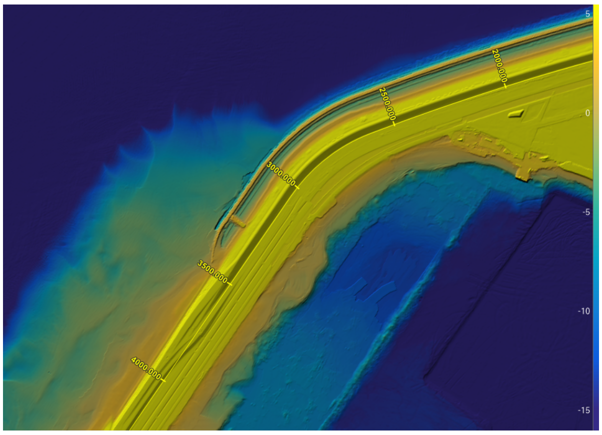

Figure 5.2: The placed sand volume outside the cube reef in 2013. The elevations are shown with the colorbar at the right.

The prior mentioned volume calculation must be corrected for the pore volumes between the cobbles. In figure 5.3 a cross-section is shown along the hard protection (KP3100). In this figure the upward movement of cobbles in the profile is visible between the survey of 2013 and 2014 (red area towards the yellow area). This movement is a natural behaviour of cobbles under wave attack (see section 2.3). The yellow area consists of stones combined with sand in the pores. In the prior mentioned method to calculate the volume increase this area is assumed to be only sand. The volume calculation is therefore an overestimation. To correct for this overestimation, the total volume of the yellow area is calculated and multiplied with the porosity. It is assumed that the pores between the cobbles are for 100% filled with sand. The cobble volume is calculated by applying a cobble porosity of 37.9% (see section 2.3). The calculated cobble volume is subtracted from the total volume. Furthermore, the pores between the cobbles under the sand layer are filled with sand. It is assumed that the pores are filled for 100% where the waves are active and cobbles are moving. The sand particles must move downwards to fill the pores between the cobbles. The only mechanism that can move the sand particles between the cobbles is groundwater, which flows horizontally. Therefore, it is assumed that the pores are filled with sand along the first 0.5m for 70%. The surface area until KP2700 is calculated and multiplied with the porosity and saturation percentage. This volume must be added to the total volume calculation.

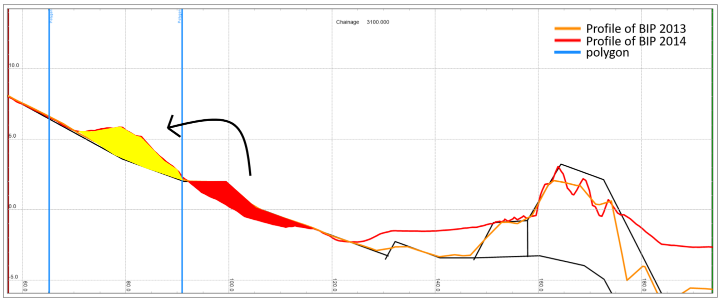

Figure 5.3: The yellow area is the volume of stones that moved upward in the profile (cross-section = KP3100). This volume consist of stones and sand.

5.2.2. Surface areas

Given that only seven BIP-measurements were performed by PUMA, the temporal resolution of the data is increased by analysing 21 satellite images. Satellite images over the period 2013-2018 are available at Satellietbeeld (2018) and Satellietdataportaal (2018) . These images are analysed and shown in Appendix A. With GIS software (i.e. QGIS version 2.18.24) we measured the surface areas of the sand layer. To compare the surface areas with each other, all surface areas must be translated to the same water level of 0m NAP. The exact dates and times of all images are known, therefore water levels at those times are obtained from Rijkswaterstaat (2018). We assumed a constant slope and corrected all surface areas to 0m NAP. Through the fact that we selected the areas by hand, this method could be sensitive for measuring errors. Therefore we compared the obtained surface from the satellite images with calculated surface areas from the BIP-measurements.

5.2.3. Correction factors

By comparing the sand volumes with the surface areas, we made the assumption that the shape of the sand layer is constant over the last five years. Correction factors are defined to investigate this assumption. For all the surface areas between two BIP-measurements the corresponding value on the volume-line is obtained (indicated with V in figure 5.4). We divided these values by the corresponding surface area to obtain a correction factor for the specific period. The correction factor is defined as V/A. The average correction factor between two BIP-measurements is obtained to analyse the evolution of the sand layer. We visualised the described method in figure 5.4.

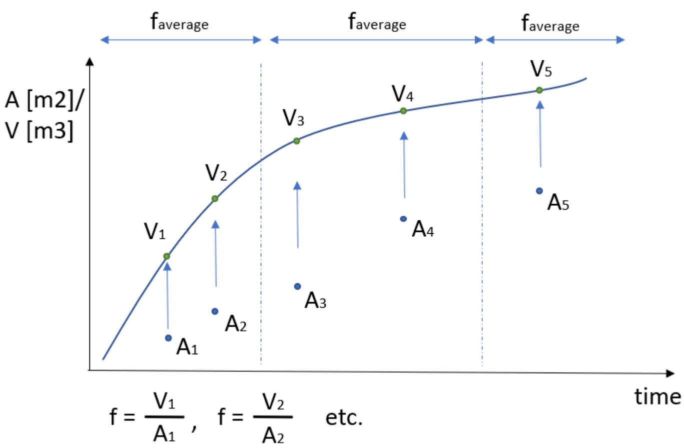

Figure 5.4: The method to calculate the used correction factors

5.2.4. Storm impact

We compared the sand volumes and surface areas with the obtained wave heights from Europlatform. We investigated if a link is visible between the sand layer increase and occurred wave heights. It is known from literature that wave motion reduces the current velocities near the bed, but the near-bed concentrations are strongly increased due to the stirring action of the waves (Van Rijn, 2013). This stirring action could create more sediment transport. The wave heights are higher during storms, therefore the storm influence is investigated. The pre- and post-storm profiles are measured with a GPS-device on November 5^{th}, 2018 and January 10^{th}, 2019. Within this period large wave heights and wind speeds were present. We compared the two measurements with each other to identify differences between the pre- and post-storm profiles. In figure 5.5 the wave rose and wave energy flux are plotted between both measurements. Highest wave heights were coming from the north, as shown in the wave rose. In Chapter 4 the definition energy flux is explained. The measurements are performed with a Trimble GPS-device (accuracy in horizontal and vertical around 10mm).

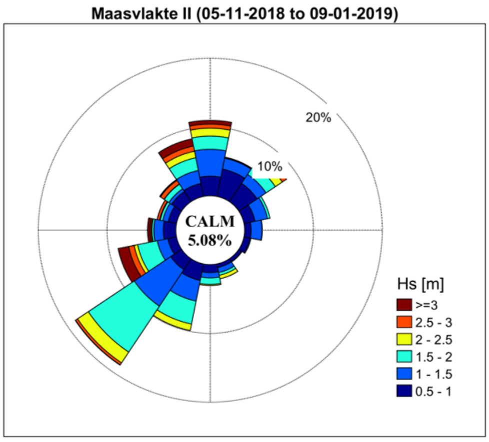

(a) Wave rose for the given period obtained from the Europlatform. The colors indicate the wave height and the length of the colorbar represents the percentage of waves from that direction

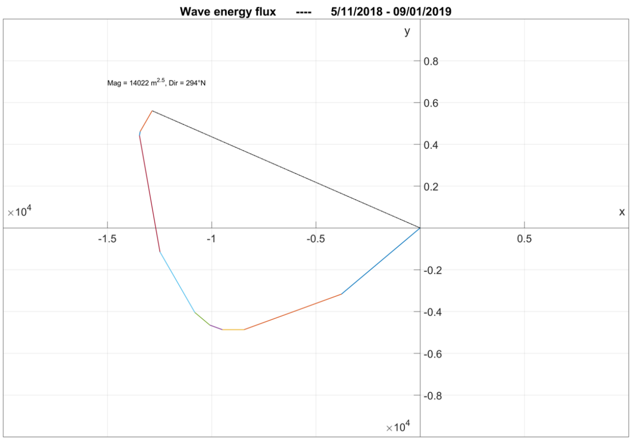

(b) Wave energy flux for the given period

Figure 5.5: The wave rose and energy flux during the period of November 5th (2018) and January 9th (2019)

5.3. Results

5.3.1. Sand volumes versus surface areas

The increase in sand layer volume is visible by analysing the BIP-measurements. In appendix G three cross-sections are shown at the sand layer area. The increase in sand volume from 2013 to 2018 is larger in the southern part than the northern part of the lagoon. From the BIP-measurements the sand layer volume is estimated to have increased with 71,000 m^3. This value is adjusted for the pore volumes by using equation 5.1. The volume of the moved cobbles is substracted and the sand volume in the pores under the sand layer is added to the total volume. In figure 5.6 the surface areas and volumes are plotted. The volume line consist of red and black circles. The black circles are the volumes directly obtained from the BIP-measurements. And the red circles indicate a updated BIP-measurement with a GPS-measurement of the sand layer. A change in the volume increase is visible at the beginning of 2017. Looking at the surface areas it seems that around the winter period the surface areas are increasing for the years 2015 and 2016. For the years 2017 and 2018 this winter increase is less visible. The winter periods are highlighted in red in figure 5.6. Looking at the near-shore waves heights higher than 2.5m in the lower graph, we observed that high waves are present during the winter periods. This could indicate that waves are important by analysing the sand layer increase. Looking at the nourishment dates in figure 5.6 it is visible that the volume line is increasing after a nourishment. No decrease of volume is visible after a nourishment.

$$\begin{aligned} \text{Correct for moving cobbles} &: 9,100m^3 \times 0.379 = 5,700m^3 \\ \text{Correct for sand within cobbles under sand layer} &: 66,000m^2 \times 0.5m \times 0.379 \times 0.7 = 8,750m^3 \end{aligned} \tag{5.1}$$

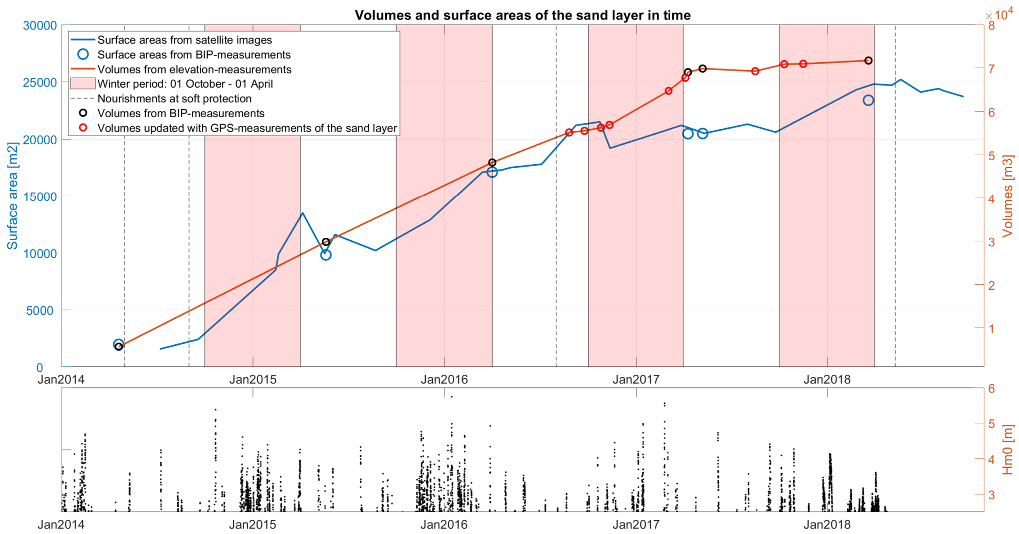

Figure 5.6: The top graph shows the sand volumes versus surface areas and in the lower graph near-shore wave heights higher than 2.5m are plotted. The following lines and symbols are plotted in the top graph: the sand layer volumes from the BIP-measurements with the red line (fitted through the black and red circles, whereby the red circles indicate a updated volume with GPS-data), the surface areas from the BIP-measurements with the blue circles, the surface areas from the satellite images with the blue line, the nourishments at the soft protection with the black stripes and the winter periods are highlighted in red.

In figure 5.7b the volumes and surface areas are plotted with the corrected surface areas from the satellite images. The volumes are obtained from only the BIP-measurements. The correction factors are calculated for each satellite image between two BIP-measurements. The four averaged correction factors are plotted in figure 5.7a. It is visible that the value for the first period is higher compared with the other three factors.

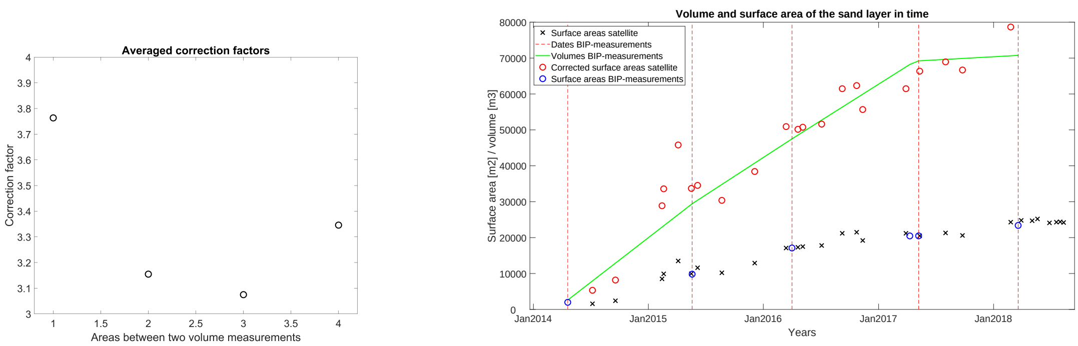

(a) Average correction factors between two BIP-measurements

(b) The volume versus the surface areas of the sand layer with the corrected values in red. The volumes are obtained from only the BIP-measurements.

Figure 5.7: The correction factors (left) and the profiles of 3 BIP-measurements (right)

5.3.2. Storm impact

In figure 5.8b the erosion and accretion areas are shown by subtracting the two elevation measurements at November 5th (2018) and January 10th (2019). For the sand layer domain between KP3250 and KP2950 the volume decrease is 1,500 m^3 over two months (see figure 5.8a). We observed from figure 5.8a that sand volumes accreted higher in the profile and lower in the profile mainly erosion has occured. During field visits it is observed that the area within the white square is dominated by moving sand volumes and the the area within the yellow square is dominated by moving cobbles. The cross-sections at the black lines of figure 5.8b are plotted in Appendix D.1 for a more detailed view of the elevation differences.

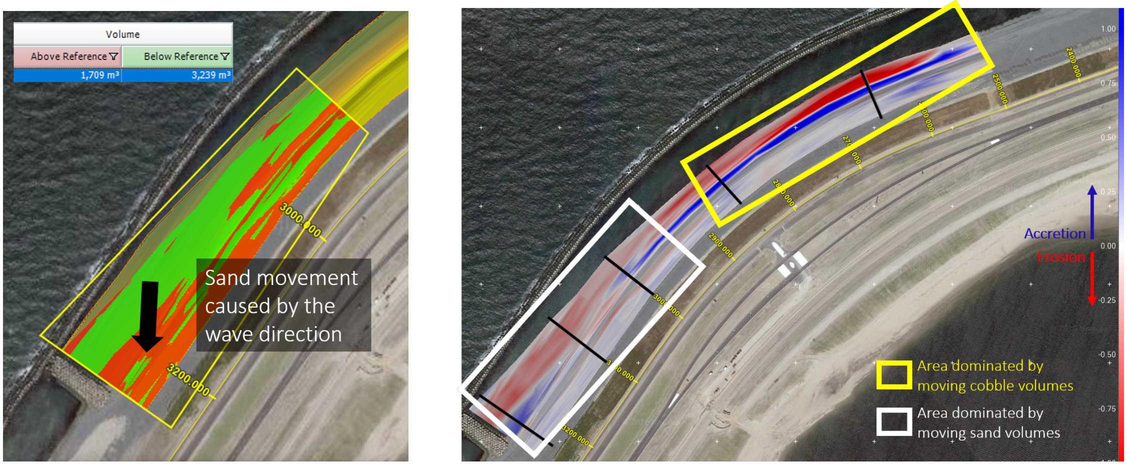

(a) Erosion (green) and accretion (red) for the sand layer area

(b) The erosion areas (red) and accretion areas (blue) at the sand layer domain. The cross-sections of the black lines are shown in Appendix D

Figure 5.8: The areas with erosion and accretion during the period: 5 November 2018 until 10 January 2019.

5.4. Discussion

From the analysis in this chapter the sand layer increase is visible over the last five years. This increase in volume is visible by looking at the cross-sections in Appendix G. In figure 5.6 the sand volumes and surface areas are plotted in time. The observed change in volume increase around January 2017 in figure 5.6 is difficult to explain. From the wave analysis in Chapter 4 it was observed that the waves over the last five years were mainly coming from the south-west and the north. Since 2016 the northern component is increasing in size and the south-western component is decreasing. Looking at the winter periods it is observed that the waves were mainly coming from the south-west during the winter periods of 2013-2014 until 2015-2016. A stronger northern component is visible in the winters of 2016-2017 and 2017-2018. From figure 5.6 it can also be observed that the wave heights were lower during the winter of 2016-2017 and 2017-2018 (this is also visible from the lower energy fluxes in table 4.2). But looking at the coastal orientation, the nett resulting wave energy fluxes are still always coming from the left side of the line perpendicular to the coast. This is the case during each year over the last five years (as mentioned in the conclusions of Chapter 4).

Additionally, from figure 5.6 it can be observed that the surface areas from the satellite images follow the surface areas from the BIP-measurements good. Furthermore, the surface areas are following the trend of the volume-line until the end of 2016. From that moment it seems that the ratio between the sand volume and profile changes. The surface area values are further away from the volume-line than before the end of 2016. We assume that the cross-profile changed around 2017. Looking at the cross-section of KP3075 in figure 5.9, it is visible that the surface area (looking from above) is slightly increasing from 2016 to 2017, but not as much as the relative volume increase. In 2018 the surface area becomes bigger again and the volume is just slightly increasing (looking at the profile of 2017 versus 2018).

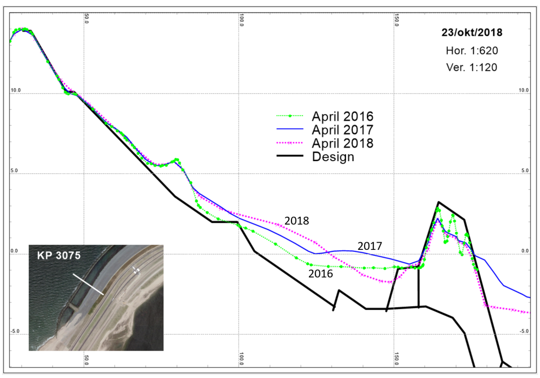

Figure 5.9: Three profiles from the BIP-measurement in 2016, 2017 and 2018

Looking at the calculated correction factors, the value for the first area is higher compared with the other three factors. This is probably through the fact that the system is dynamic during the first period after construction. The assumption of a constant shape of the sand layer may be not valid for this first part. The correction factors for the other three periods are around the same value. An explanation could be that the sand layer is growing more stable after the first period. The last value is a little higher than the middle two factors. This could be through the fact that the volume and surface area line are further away than in the middle part in figure 5.6. Another explanation for the higher correction factor could be the nourishment strategy of PUMA. PUMA monitored and intervened during the adaptation period at the soft protection. In the satellite image of 2014 a large nourishment is visible at the transition zone (see appendix figure A.1). This nourishment influences the sand transport in this area. Moreover, PUMA artificially removed a sand volume in August 2015 of around 10.000/20.000 m^3 from the lagoon. They thought to solve the sedimentation problem in the lagoon by removing a sand volume, but this sand volume was back within a few months. From the satellite image in Appendix figure A.3 the removed sand volume is visible.

From the two elevation measurements at November 5th (2018) and January 10th (2019) we observed that sand volumes are pushed higher in the profile around KP3250 (close to the lateral dam). The northern waves transported the sand volumes higher in the profile in southern direction. But the sand was not able to pass the lateral dam, therefore the sand has accumulated higher in the profile against the lateral dam. More northwards, around KP3100, erosion of the sand layer is visible. And northwards of KP2950 the upward movement is caused by moving cobbles. The areas of sand and cobble movements are indicated in figure 5.8b. From Appendix figures D.4 and D.5 the stone movement is visible by comparing the black and blue lines. Looking at the wave rose it is visible that the higher wave heights came from the north and south-west (350 and 260 degrees). Looking at the wave energy flux the resulting wave direction was 294 degrees. The higher wave heights have a large contributions to the resulting energy flux. As said the sand layer encountered a nett erosion during the mentioned period. This is probably caused by the higher waves from the north.

Moreover, the boundary until which sand was visible in the lagoon is analysed using the BIP-measurements of 2013 and 2018. In the field observations of Chapter 3 we observed sand volumes until KP2700 (as shown in figure 3.1). In figure 5.10 we present two cross-sections for the BIP-measurements of 2013 and 2018. Looking at the two cross-sections, a smooth (grey) line is visible lower in the profile at KP2850, which is probably sand (around x = 140). And at section KP2650 (which is a little more northwards) a bumpy (grey) line is visible lower in the profile, which are probably cobbles. We indicated the mentioned areas with a blue circle in figure 5.10.

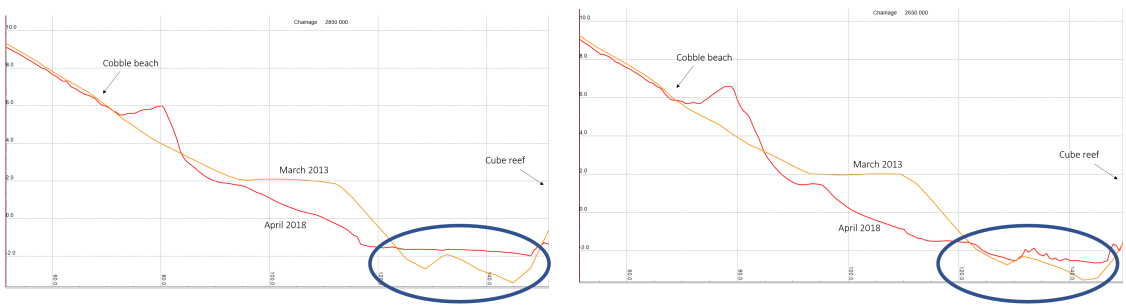

(a) Cross-section at KP2850

(b) Cross-section at KP2650

Figure 5.10: Two cross-sections obtained from the elevation measurement at April 5th, 2018

5.5. Conclusions

From this chapter we observed that the sand layer volume has increased over the last five years. From the BIP-measurements the total sand volume in April 2018 is estimated to be 71,000 m^3. This volume is much more than the predicted value of 20,000 m^3 from PUMA. An increased data resolution is obtained by calculating the surface areas from satellite images. From the satellite images it appears that the sand volume increased mainly during the winters of 2015 and 2016. From the volumes and surface areas it follows that the sand volume has not increased that much during the winters of 2017 and 2018. There is a change in volume increase around January 2017, which is difficult to explain. The direction and size of the waves could be the reason for this change. From the wave analysis in Chapter 4 it was observed that more waves were coming from the north over the past 2 years. The northern and south-western wave component were almost equal in size during the winter of 2017-2018. It could be that the impact of both waves directions was equal and that the sand layer is therefore stable during this winter period. Moreover, the winters of 2016-2017 and 2017-2018 had a higher calm percentage than the years before. Overall, we concluded that the size and direction of the waves have an influence on the size of the sand layer.

From the BIP-measurements the total sand layer volume is estimated to have increased with 71,000 m^3 until April 2018. From the satellite images it appears that the sand volume increased mainly during the winters of 2015 and 2016. From the volumes and surface areas it follows that the sand volume has not increased that much during the winters of 2017 and 2018. The wave height and direction may be the reason for this change. We concluded that the wave height and direction are important by analysing the sand layer volume. Especially during the winter periods, when wave heights are highest, the sand layer volume is changing.

6
Hydrodynamic transport

6.1. Introduction

In this chapter, we investigate the role of hydrodynamic transport in the formation of the sand layer. Hydrodynamic transport is divided into two mechanisms: overtopping over the cube reef and transport caused by the tide (see arrows 2 and 3 in figure 1.9). Both mechanisms transport water volumes into the lagoon, which contain sand particles that could settle in the lagoon. Wave data and flow velocities are required to calculate the sediment concentration profile as a function of depth. This sediment concentration is required to calculate the sand transport of both mechanisms. We performed measurements at Maasvlakte 2 to obtain the flow velocities in the lagoon and wave data is obtained from Europlatform and a nearshore location. Finally, the transported sand volumes by overtopping and the tide are calculated.

6.2. Methodology

6.2.1. Flow velocity measurements

We performed flow velocity measurements on December 12th 2018 in the lagoon. During other field visits at the lagoon we observed a current in northern or southern direction, as shown in Chapter 3. The measurements could help to clarify the processes behind this observed current. Moreover, the current velocity is needed as input parameter in order to calculate the sediment concentration as a function of depth. Measurements are performed with a Valeport106 current meter and GPS-drifters. A Valeport106 (figure 6.1a) can measure the flow velocities at different depths, by submerging and then manually adjusting the depth of the device. The GPS-drifters (figure 6.1b) are floating devices with a GT31-GPS on top, which log their location and velocity each second. As a result, using the drifters it is possible to obtain flow velocities and directions in the top part of the water column.

(a) Valeport106 current meter obtained from Van Oord

(b) Used GPS drifters from the TU Delft. A GT31 GPS is located on top of the floating construction.

(c) Impression of the performed flow velocity measurements. Wetsuits and boat were arranged to ensure the safety

Figure 6.1: Measurement devices during performed flow velocities measurements at Maasvlakte 2

The measurements are performed at different locations along the sand layer domain (between KP2000 and KP3000). The conditions on December 12^{th} were calm, as evidenced by wind and wave parameters in table 6.1. An important note is that the tide direction was changing during the measurements. In Appendix E.1 a detailed explanation of the tide direction is given. Furthermore, we placed oranges in the lagoon during two other field visits (around KP2850 on the 10^{th} and 20^{th} of November 2018). Flow velocities are obtained by measuring their travel time and distance. While this is a rougher method than using the GPS drifters, it may still give a useful indication of the flow velocity in the top part of the water column.

Date	Wind velocity [m/s]	Wind direction [°]	Wave height [cm]	Wave direction [°]	Water level with respect to NAP [cm]
10 nov 2018	8	190	160	210	≈ -60
20 nov 2018	10	90	220	45	≈ +50
12 dec 2018	5	100	70	15	between 0 and -90

Table 6.1: Wind and wave conditions during the measurements. Wave conditions are obtained from the Europlatform. Water levels and wind conditions are obtained at Hoek van Holland (Rijkswaterstaat, 2018). Directions are related to true North, see Appendix figure B.5.

6.2.2. Sediment concentration as a function of depth

We estimate the sediment concentration as a function of depth in order to obtain a better prediction of the volume of sand transported into the lagoon. The two main modes of sand transport in the water column are bed-load transport and suspended load transport. Bed-load transport is caused by particles that are in close contact with the bed. These particles are dominated by flow-induced drag and gravitational forces. On the other hand, suspended load transport is the irregular motion of particles through the water column, as a result of turbulence-induced drag forces on the particles (Van Rijn, 2013). Since the particles that could be transported into the lagoon are suspended in the water column, suspended load transport is used to calculate the sediment transport arising from tide and overtopping. As expected, observations show that the suspended sediment concentrations decrease with increasing height above the bed (Van Rijn, 2013). According to Van Rijn (2013), the rate of decrease depends on the ratio of the fall velocity and the bed shear velocity (w_s/u^*).

The reference concentration (C_a) is located close to the bed and necessary to obtain the sediment concentration profile, as shown in figure 6.2. The reference concentration is based on the critical shear stress from Shields and the effective bed-shear stress caused by the current and waves (Van Rijn, 1984). The reference concentration is calculated with equation 6.1.

$$\text{Reference concentration:} \qquad c_a = 0.015 \times \rho_s \times \frac{d_{50}}{a} \times \frac{T^{1.5}}{D_*^{\,0.3}} \qquad [kg/m^3] \tag{6.1}$$

d_{50} = particle size $\quad a$ = reference level

T = Dimensionless bed-shear parameter $\quad D_*$ = Dimensionless particle diameter

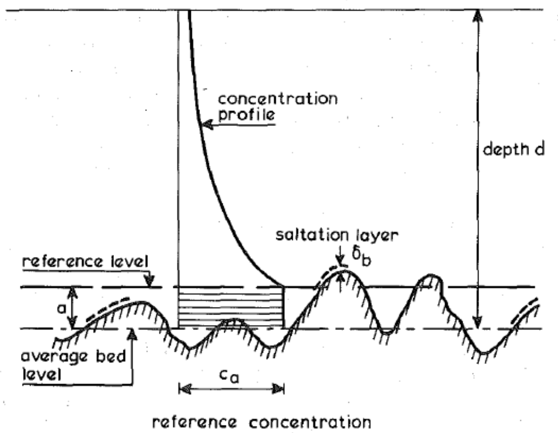

Figure 6.2: Definition sketch to indicate the reference concentration = C_a (Van Rijn, 1984)

The wave height, wave period, water level, water depth, and flow velocity are required inputs for the reference concentration. For the flow velocity we will use the values we have measured, while the wave height, wave period and water level are obtained hourly from Rijkswaterstaat (2018). The concentration profile can be expressed by the Rouse profile, see equation 6.2 (Deltares, 2014). All necessary equations to obtain the reference concentration profile are shown in Appendix E.2.

$$\text{Rouse profile:} \qquad \frac{c(z)}{c_a} = \left(\frac{z}{h-z} \times \frac{h-z_a}{z_a}\right)^{w_s/\kappa u^*} \qquad [-] \tag{6.2}$$

h = water depth $\quad z_a$ = reference level $\quad u^*$ = bed-shear velocity

z = height above the bed $\quad w_s$ = particle fall velocity $\quad \kappa$ = Von Karmann coefficient (= 0.41)

6.2.3. Overtopping volumes

High water levels together with high waves can lead to water transport over the cube reef, and since this water contains suspended sediment, this may contribute to sand transport into the lagoon. We have observed overtopping during field visits with high water levels and high waves, as shown in figure 6.3 for two separate occasions.

We will now estimate the volume of sand transported into the lagoon through overtopping. For simplicity, we assume that the sediment suspended in the overtopped water volume remains in the lagoon. This assumption may be justified by considering that conditions outside the cube reef are rough compared to the mild conditions in the lagoon. Due to reduced turbulence, the sediment now has a chance to settle in the lagoon. Water without sediment then returns through the cube reef, given that the lagoon is closed at the northern and southern end and that the water level in the lagoon cannot increase indefinitely. Water (containing little sediment) thus flows in the offshore direction through the cube reef, while overtopping volumes (containing sediment) are transported into the lagoon. Hence, the following steps are performed to obtain the transported sand volume through overtopping in cubic meters:

1. Calculate the overtopping volume/hour for the nine output locations, see figure 6.4

2. Calculate the reference concentration and define the Rouse profile for each time step (see section 6.2.2)

3. Calculate total transported sand volume for the defined output locations $[m^3/m/5years]$

4. Apply the porosity and alongshore distance to obtain the total sand volume $[m^3/5years]$

(a) Overtopping observed during a field visit at September 21, 2018

(b) Overtopping observed during a field visit at January 8, 2019

Figure 6.3: Overtopping volumes over cube reef were visible during the performed field visits

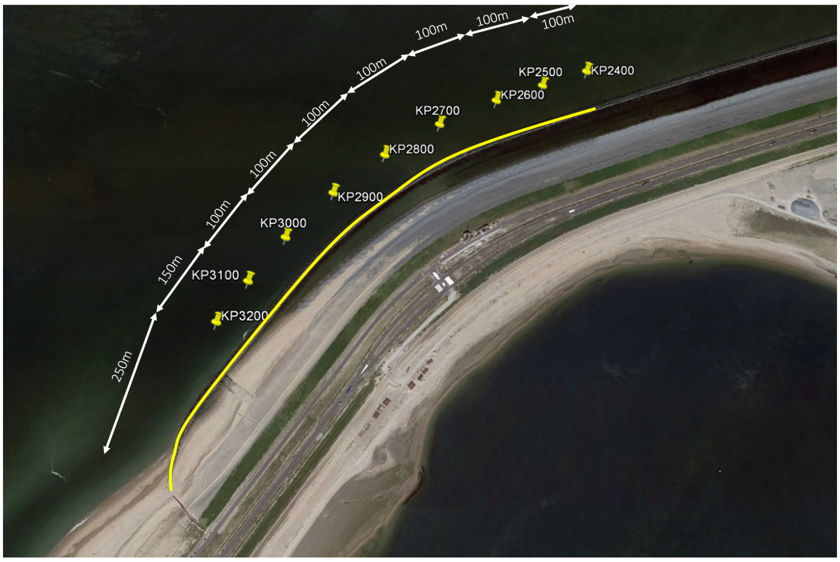

Figure 6.4: The nine locations at which the overtoppings volumes are obtained (yellow pins). The yellow line indicates the alongshore length over which the overtoppings volumes are calculated

The overtopping equation from Van Der Meer et al. (2014) is used to calculate the amount of overtopping over the cube reef (equation 6.3). This formula is based on the formulas treated in the EurOtop (Pullen et al., 2007). For structures with a slope, overtopping at low and zero freeboard conditions have often been overlooked in physical model studies, but they represent important situations, e.g., in analysis of performance of partially constructed breakwaters and of low-freeboard, lower-cost defences (Van Der Meer et al., 2014). It was clear that familiar, exponential-type formulas work poorly in these regions. Analysis has therefore been performed to bring together the conventional exponential formulas with the few reliable datasets including very low and zero freeboard (Van Der Meer et al., 2014). For the data points at zero freeboard, the equations would significantly overpredict the amount of overtopping. Figure 6.5 shows the old and new formula based on available data. For the cube reef at Maasvlakte 2 the relation R_c/H_{m0} will be close to 0. Therefore, the new proposed equation 6.3 from Van Der Meer et al. (2014) is used to calculate the amount of overtoppping.

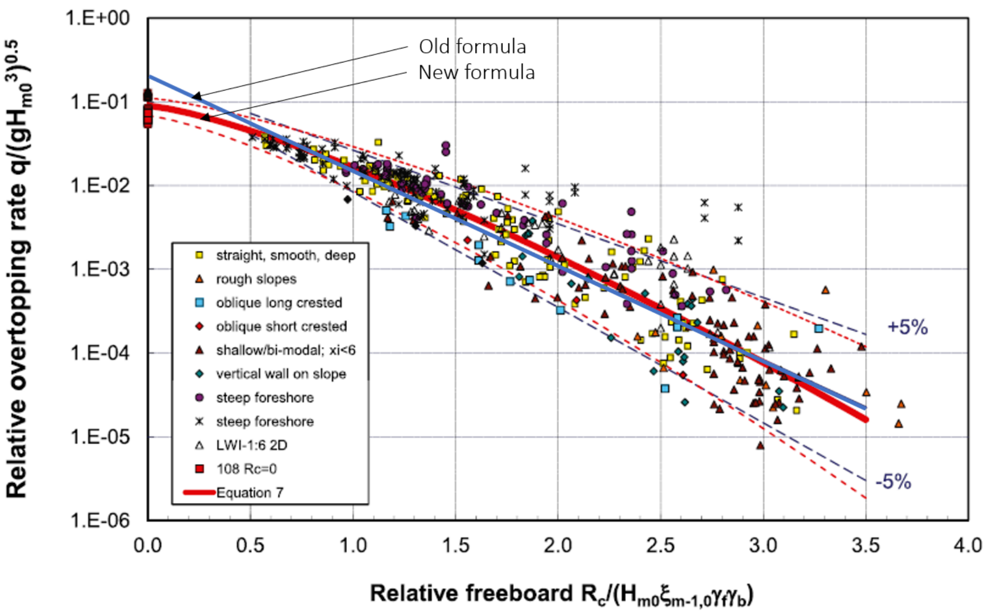

Figure 6.5: Old en new formula to calculate the amound of overtopping. Obtained from the Eurotop (Pullen et al., 2007) and Van Der Meer et al. (2014)

The wave height, wave direction, and amount of freeboard are the input parameters for equation 6.3. Hourly wave data is obtained at the toe of the cube reef for the period 01-01-2013 until 01-05-2018, this period is referred to as 5 years during this thesis (see section 4.4 for the near-shore wave heights). The different locations at the toe of the cube reef are indicated with the yellow pins in figure 6.4. The free-board (R_c) is defined as the difference between the water level and the height of the cube reef. If $R_c < 0$, the free-board is set to 0 in equation 6.3. A negative free-board happens when the waterlevel combined with wave height is higher than the cube reef height. The height of the cube reef is an important parameter in the overtopping equation. Analysing the BIP-measurements, we observed that the average height of the highest tips of the blocks from the cube reef varies over the years 2013-2018 between 2.0m and 2.5m along the sand layer domain (with respect to still water level). The overtopping volumes are therefore calculated for a height of 2.0m, 2.25m, and 2.5m. Furthermore, the roughness parameter γ_f and wave angle parameter γ_β are required in equation 6.3. γ_f is calibrated for concrete armour units in non-breaking conditions using the CLASH database. For the cube reef a 2-layer slope of cubes is used (γ_f = 0.47 according to the EurOtop (Van der Meer et al., 2018)). γ_β is implemented to include the effect of oblique waves (equation 6.4), which we adjust according to the coast orientation for each position. The angle of wave attack is defined as the angle between the wave crest and the structure. As expected, wave crests parallel to the cube reef, where the direction of propagation is thus perpendicular to the coast, give the highest overtopping discharges. We apply equation 6.3 at nine locations along the sand layer domain: KP2400 through KP3200 (see figure 6.4).

$$\text{Overtoppings formula:} \quad \frac{q_h}{\sqrt{g \times H_{m0}^3}} = 0.09 \times exp(-(1.5 \times \frac{R_c}{H_{m0} \times \gamma_f \times \gamma_\beta})^{1.3}) \quad [m^3/m/sec]$$

$$q_h = \text{overtoppings volume} \qquad \text{Hm0} = \text{wave height} \qquad R_c = \text{free-board}$$

$$y_f = \text{Roughness paramater} \qquad y_\beta = \text{Wave angle parameter} \tag{6.3}$$

$$\text{Wave angle parameter:} \quad \gamma_\beta = 1 - 0.0063 \times |\beta| \qquad \text{for } 0^\circ \le \beta \le 80^\circ \qquad [-]$$

$$\beta = \text{the angle between the wave crest and the structure}$$

$$\text{for } \beta > 80^\circ \text{ the result } \beta = 80^\circ \text{ can be applied} \tag{6.4}$$

The sediment concentration as a function of depth is dependent on the water depth and wave conditions, whereby the water depth of the foreshore is varying over the last five years (as shown in table 6.2). The depth at each output location is obtained from the annual BIP-measurements by PUMA. The water depth is linearly interpolated between those depth measurements.

	KP3200	KP3100	KP3000	KP2900	KP2800	KP2700	KP2600	KP2500	KP2400
March 2013	3.5	5.4	5.5	7.1	9.5	10	10.7	11.5	11
April 2014	2	2.5	4.1	6.4	8.8	10	10.7	11.5	11
April 2015	2	2.4	3.1	3.7	6	9	10	10,8	11
April 2016	2	2.2	4.1	4.5	4.2	7.5	9.5	10	10.5
May 2017	1.8	2,2	3.2	4.5	4.7	7.2	9	9.8	10.5
April 2018	2.3	3.1	4	4.7	4.7	6.3	8.5	9	10

Table 6.2: Varying depths (in meters) at the toe of the cube reef per section over the past five years. The depth are obtained from the performed BIP-measurements by PUMA. These water dephts are with respect to still water level. In Appendix figures E.14 and **??** the water depths are shown around the sand layer domain.

The Rouse profile (explained in section 6.2.2) is hourly defined for the used output points. As mentioned in section 6.2.2, the suspended sediment concentrations decrease with increasing height above the bed. In figure 6.6a we define the height "Δ" in order to estimate the sediment concentration in the water volume transported through overtopping. The height "Δ" is defined at the wave trough. The area under the Rouse profile between Δ and the water level is calculated and divided by the vertical height. Thereby the weighed average is obtained over the mentioned area. We assumed that this area of water will flow over the cube reef by overtopping. Given this method, a higher wave height will result in a higher sediment concentration. At each time step the sediment concentration is determined and multiplied by the water volume. All calculated sand volumes are summed up, which gives a total sand volume per meter at each output location. To obtain the total sand volume in $m^3/5years$, the alongshore length is defined for each location and a porosity of 0.4 is applied (the alongshore lengths are shown in table 6.3 and figure 6.4). No wave data is available for the sections south from the lateral dam, therefore the obtained volume/meter at KP3200 is multiplied with 250m to include the southern part.

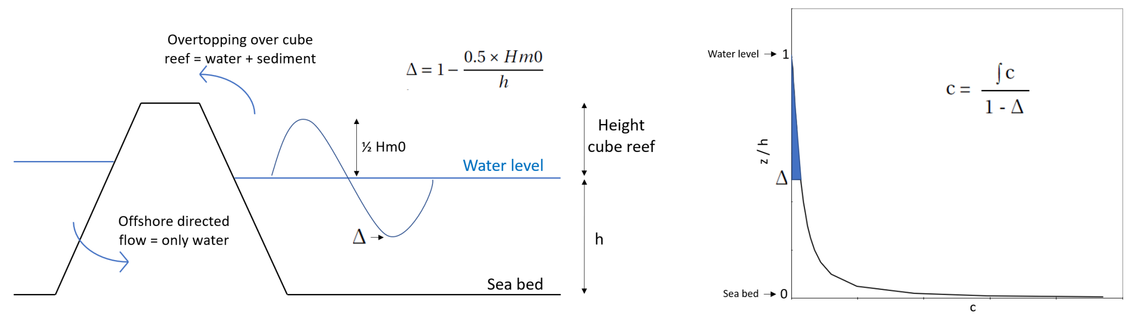

(a) Figure to illustrate the depth Δ in the water column

(b) Method to calculate the used sediment concentration

Figure 6.6: Method to define the used sediment concentration for each time step

KP number	3200	3100	3000	2900	2800	2700	2600	2500	2400
Applied alongshore length [m]	250	150	100	100	100	100	100	100	100

Table 6.3: The applied alongshore lengths per section

6.2.4. Tide induced transport

In this section the sand volume transported by the tide is estimated. In figure 6.7 a large section of the hard protection of Maasvlakte 2 is shown. The volume of sand transported through the tide is dependent on two parameters: the flow opening and the lagoon area filled by the tide. A smaller flow opening will cause for higher velocities at the opening, which results in more sediment transport. Moreover, a larger area that is filled by the tide in the lagoon will also cause for higher velocities at the opening. The flow opening and a possible area are illustrated in figure 6.7.

A gradient in flow velocities could indicate a difference in discharge between two points (for example the two white crosses in figure 6.7). We assumed that this difference in discharge is transported through the dam between those two points. It could be investigated if a difference in discharge is present at the lagoon by analysing the performed flow velocity measurements of section 6.2.1. The width of the flow opening could be obtained by analysing the flow velocity measurements. The filled area in the lagoon by the tide is difficult to define. Therefore, two different areas are defined and the transport by the tide is calculated for those areas, as shown in figure 6.7.

We calculate the difference in maximum- and minimum water level and multiply this by the lagoon area. This water volume enters the lagoon twice per day. Given this approach, we estimate the total water volume that flows in the lagoon over the past 5 years. This water volume is multiplied by the sediment concentration to obtain the total volume of sand transported by the tide. The sediment concentration is calculated by using the Rouse profile, which is explained in section 6.2.2. The water depth, wave height, wave period, and flow velocity are required to calculate the sediment concentration as a function of depth. Average conditions are chosen for these hydrodynamic parameters to calculate sediment concentration. The whole method to obtain the sediment concentration in the water is shown in section 6.2.2.

Figure 6.7: Method to calculate the transport caused by the tide

6.2.5. Uncertainty overtopping calculation vs variability nature

We assume that the tide transport is a order of magnitude lower than overtopping over the cube reef, therefore the uncertainty of the overtopping calculation is estimated to obtain a better feeling for the maxima and minima of the used equations. A benchmark for the maximum uncertainty for an analysis to be useful is the sensitivity of the results to natural variations. The uncertainty of the overtopping calculation is therefore compared with the nature variability.

The method to calculate the amount of overtopping consists of two parts. The first part is the amount of overtopping over the cube reef, which is obtained from Van Der Meer et al. (2014). And the second part is about the sediment concentration in the water, which is obtained from Van Rijn (1984). For both methods we created the cumulative distributions. In figure 6.5 all performed overtopping experiments from literature are shown together with equation 6.3 and the 5% bandwidths. According to Van Der Meer et al. (2014) the uncertainty of equation 6.3 is given by $\sigma(0.09) = 0.013$ and $\sigma(1.5) = 0.15$. Given those values the cumulative distribution is obtained. The second part of the overtopping calculation the sediment concentration in the water volume. According to Van Rijn (1984) the total sediment load cannot be predicted with an inaccuracy less than a factor 2 because the accuracy of the main controlling parameters is too low, while also the total load data used for calibration and verification show deviations up to a factor 2. The equation has been determined by fitting of measured and computed concentration profiles for a range of flow conditions. This means that the calculated sediment concentrations during this research can be two times higher or lower in reality. Therefore, we assume that the 2.3 percentile is 0.5 × the sediment concentration and the 97.7 percentile is 2 × the sediment concentration. The other percentiles are linearly interpolated.

To obtain insight in the sensitivity of the results for natural variations, first the standard deviation, mean value and percentiles of all monthly water levels between 2013-2018 are compared with the water levels between 1990-2019. Since these values were similar, the dataset of 2013-2018 is used to calculate variability of nature. The variability of nature is calculated according to the following steps:

1. Selecting all hourly water levels per month. Doing this, the variation in storm seasons can be included in the analysis. That gives, for example, 5 months of water levels for the month January from the dataset 2013-2018
2. All high waters are selected in order to estimate the variability of the water levels. Normally there are two high waters per day
3. Obtain percentiles from the high water cumulative distributions per month
4. Obtain monthly variations by subtracting the mean from the chosen percentiles, which gives the water level variability per month
5. Apply the monthly variations on all water levels of the used data set

It is important to note that the uncertainty of the overtopping calculations is on the conservative side. We assumed that both used equations are independent, which is not the case in reality. Moreover, the calculated nature variability is an underestimation, because in reality a change in water level will also change, for example, the wave height. This is not considered during this analysis. But, comparing the theoretical formulas with the variability of nature may still give a useful indication of the reliability of the used equations.

6.3. Results

6.3.1. Flow velocity and sediment concentration in lagoon

We performed measurements with the Valeport device at 10 different locations along the coastline in the lagoon. Three during the first measurement and seven during the second measurement. In figure 6.8 all velocities and directions of both measurements are plotted. In Appendix figures E.3 until E.13 all locations and results are shown separately at each location. During the first measurements the flow velocities are higher in the top part of the water column. This is probably caused by the wind velocities, which were in the same direction as the tide direction. During the second measurement the tide direction was opposite from the wind direction. Therefore, the wind induced velocity profile is not visible. The average measured velocity with the Valeport device is in the range of 0.10-0.20 m/s. The prior mentioned change in tidal direction from section 6.2.1 is visible by looking at the measured directions of the Valeport device (see figures 6.8b and 6.8d).

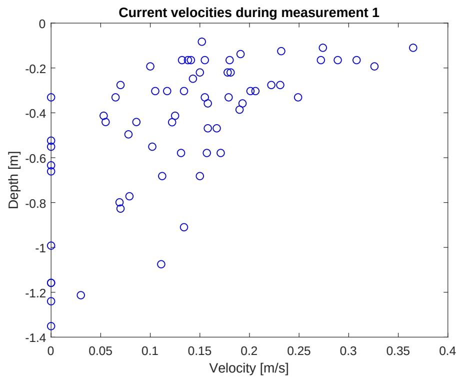

(a) All current velocities during measurement 1

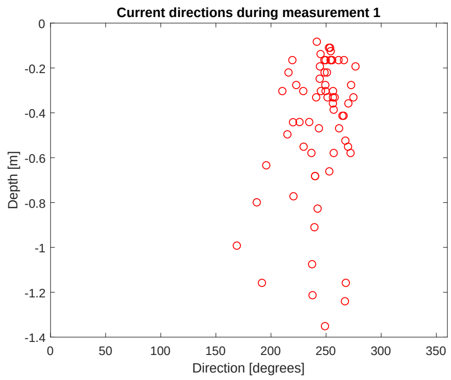

(b) All current directions during measurement 1 (south-western direction)

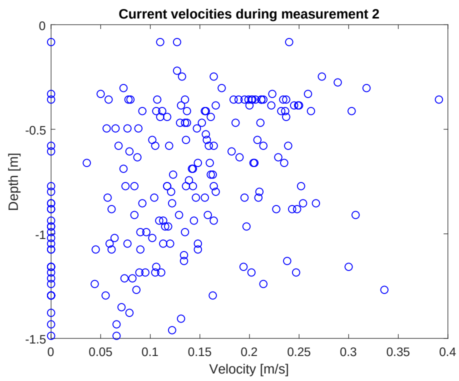

(c) All current velocities during measurement 2

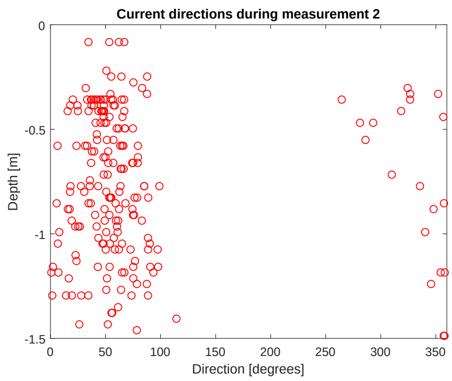

(d) All current directions during measurement 2 (north-eastern direction)

Figure 6.8: All current velocities and directions from the Valeport measurements

In figure 6.9 the results of three different GPS-drifters are plotted. It is visible that all drifters were flowing in western direction (which was the same as the wind direction). Moreover, the velocities during the first measurement are higher than during the second measurement. The average velocity obtained from the GPS-drifters is in the range of 0.5 - 0.6 m/s. These velocities are higher than the velocities measured with the Valeport device. In table 6.4 the average velocities of each measurement are shown. The velocities from the measurements with the oranges are also shown in this table. It is visible that the velocities from the oranges and the Valeport are around the same value.

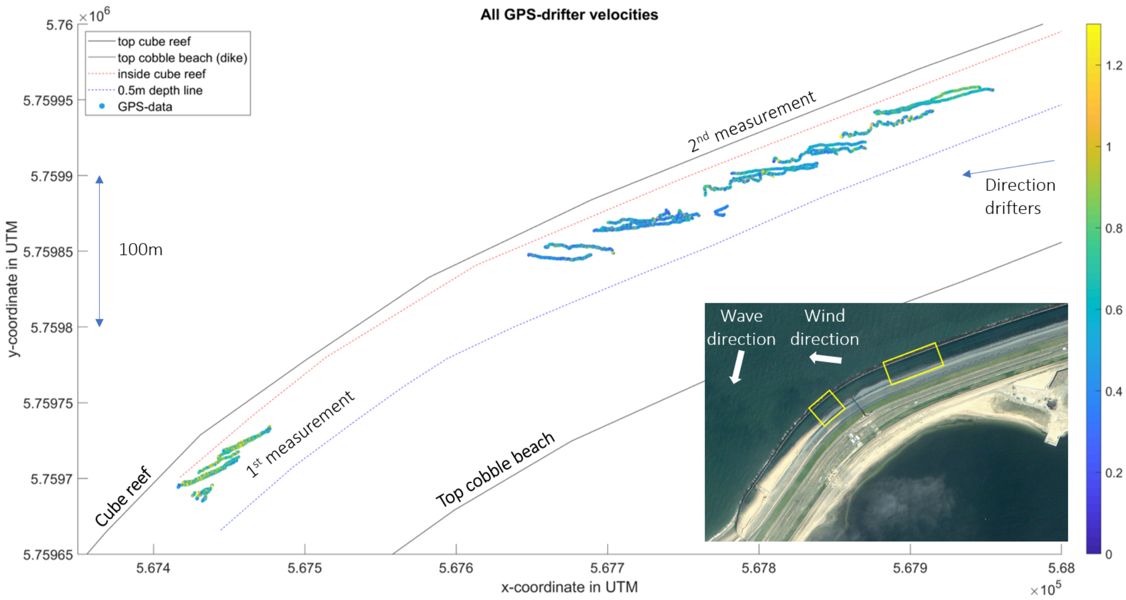

Figure 6.9: Result of the GPS measurements at 12 December, 2018. The colorbar indicates the velocities of the GPS drifters in m/s

	Measured flow velocity [m/s]
Orange measurement (10nov 2018)	0.23 - 0.25
Orange measurement (20nov 2018)	0.15 - 0.18
Valeport 106 current meter (12dec 2018)	0.10 - 0.20
GPS-drifters (12dec 2018)	0.50 - 0.60

Table 6.4: Current velocities for different performed measurements

The flow velocity we have measured is used to define the sediment concentrations as a function of depth. Given that the wave conditions and water depths are different in time, the sediment concentration is also changing in time. In figure 6.10 the Rouse profile is drawn for two different wave conditions. According to Van Rijn et al. (1993) a larger wave height leads to larger sediment concentrations and to a more uniform concentration profile. These larger concentrations are visible in figure 6.10. Given this figure it is also observed that the highest concentrations are at the bed and the suspended sediment concentrations decrease with increasing height above the bed.

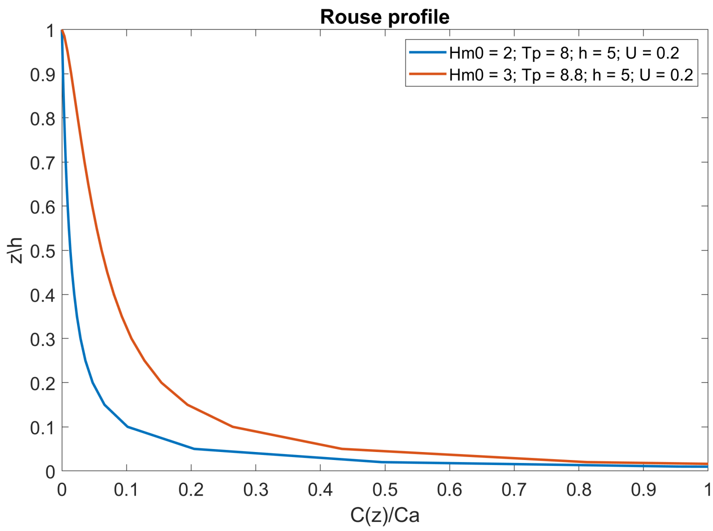

Figure 6.10: Rouse profile for two different conditions

6.3.2. Overtopping volumes

In table 6.5 the sand volumes per meter are shown for the nine output locations (as shown in figure 6.4). It can be seen that the transported sand volumes into the lagoon at KP2400 are lower than at KP3200. Furthermore, a jump in transport volume is visible between KP2600 and KP2700. With the porosity and alongshore length the total volume of sand transported by overtopping is 9,500 - 25,000 m^3 over the last 5 years. This range is dependent on the height of the cube reef.

KP number	**Sand volume** $[m^3/m]$ **(cube reef = 2m)**	**Sand volume** $[m^3/m]$ **(cube reef = 2.25m)**	**Sand volume** $[m^3/m]$ **(cube reef = 2.5m)**
2400	4.1	2.9	2.3
2500	4.3	3.3	2.4
2600	5.1	3.8	2.8
2700	11.2	8.5	6.4
2800	25.6	18.3	12.8
2900	18.4	12.2	8.0
3000	13.9	8.3	4.9
3100	18.4	9.7	5.0
3200	12.7	5.8	2.6

Table 6.5: Sand volumes for KP2400 until KP3200 caused by overtopping given in m^3/m.

In Appendix Table E.1 the transported sand volumes for an equal water depth at all sections are presented. Given that the wave heights are higher at KP2400 (compared with KP3200), the transported sand volumes are also higher at KP2400. In reality the water depth is deeper at KP2400, therefore less sediment is located in the top part of the water column. We present Table E.1 to highlight the influence of the water depth and wave height on the transported sand volumes.

6.3.3. Tide induced transport

We observed no difference in discharge by analysing the flow velocity measurements of section 6.2.1. There is a small difference in flow velocity between the two locations, but no clear differences to obtain a discharge distinction. Given that result, we assumed that the flow opening is the straight part as indicated in figure 6.11. The transport is calculated for two different lagoon areas, which are indicated in figure 6.11.

The total volume of water transported by the tide is calculated through the water level difference multiplied by the lagoon area. The average difference between low and high water is 1.8m. The total transported water volumes for the two lagoon areas are 2.63e08 m^3 and 5.26e08 m^3. We assumed average hydrodynamic conditions to calculate the sediment concentration: wave height = 2m, wave period = 8sec and a water depth of 4.5m. The volume of sand transported by the tide is shown in equation 6.5 for the two lagoon areas, using a porosity of 0.4.

$$
\begin{aligned}
&\text{Total sand volume transported by the tide into lagoon} = \\
&\frac{2,63e08 \times 0,000010}{0.6} = 4.380 m^3 \text{sand} \\
&\frac{5,26e08 \times 0,000010}{0.6} = 8.760 m^3 \text{sand}
\end{aligned}
\tag{6.5}
$$

Figure 6.11: Transport caused by the tide

6.3.4. Uncertainty overtopping calculation vs variability nature

The results from sections 6.3.2 and 6.3.3 verifies the assumption that the sand transport by overtopping is larger than the transport by the tide. In this section we present the results from the uncertainty calculation of overtopping versus the variability of nature. During this analysis the height of the cube reef is set between 2m and 2.25m. We assume that this range is more realistic than the prior used range of 2m and 2.5m. This assumption is more discussed in section 6.4.2. In figures 6.12 and 6.13 the cumulative distributions are plotted for both cube reef heights. The uncertainty distributions of overtopping and sediment concentration are plotted against the variability of water levels. As shown in these figures, the distributions of overtopping and sediment concentration are close to each other. Moreover, the results show that the variability of water levels is around the same order of magnitude as the uncertainty of the overtopping and sediment concentration calculation. This analysis is performed to determine if improvement is needed in the used methods during this research. If the nature variability is an order larger than the uncertainty of the performed calculation, the method is accurate enough to trust the outcome. But as shown, both uncertainties are in the same order of magnitude, therefore we conclude that improvement is possible in the accuracy of the performed methods during this research.

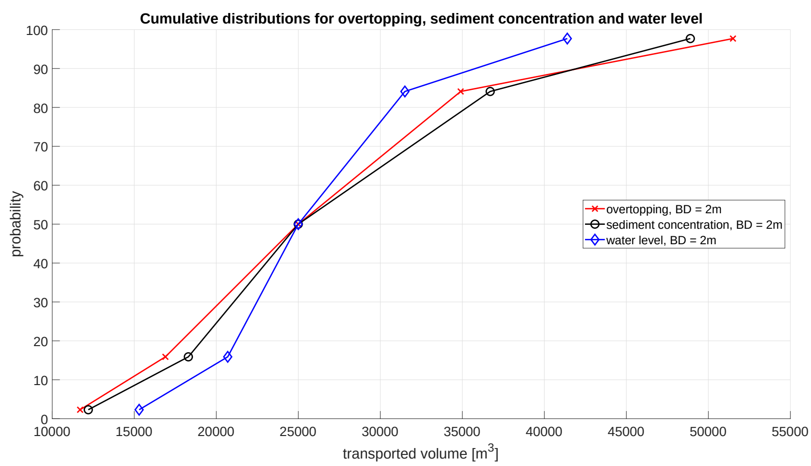

Figure 6.12: Cumulative distributions for a cube reef height of 2m

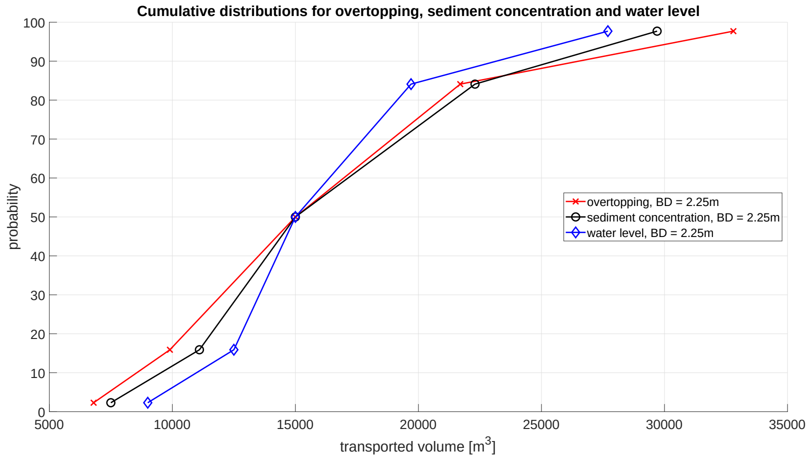

Figure 6.13: Cumulative distributions for a cube reef height of 2.25m

6.4. Discussion

6.4.1. Flow velocity in lagoon

From table 6.4 it is observed that there are differences in flow velocties between the performed measurements. The results of the orange measurement and the valeport measurement are close to each other. The differences between the two individual orange measurements are due to the different wave and wind directions. During the measurements it is observed that the wind had a large influence on the movement of the GPS-drifters. This is also visible from the results, because the drifters are flowing in western direction, which is the same as the wind direction during the measurement. One of the drifters was located lower in the water (see the lower drifter in figure E.2a). The observed velocity of this lower located drifter was lower, because this drifter is less influenced by the wind. Another result are the higher velocities during the first measurement compared with the second measurement. As mentioned in section 6.2.1, the tide direction was different at both GPS measurements. During the first measurement the tide direction was equal to the wind direction. And during the second measurement the tide was changing against the wind direction. The drifters during the second measurement were still flowing with the wind direction. Another reason for the higher velocities during the first measurement is the lower water depth at the location of the first measurement. Wind velocities have more influence where the water depth is lower. According to the reports of Arcadis in section 2.4, the tidal velocities close to the cube reef are always lower than 0.5 m/s. Based on this and on the observations it can be concluded that the velocities of the drifters are too high, because they are wind driven.
The average measured velocity with the Valeport device is in the range of 0.10-0.20 m/s. During the first measurement the water level was lower, therefore the depths measured with the Valeport were lower (see Appendix figure E.1). Furthermore, during the first measurements a wind induced profile is observed. This can be explained through the fact that the wind velocities and tide directions are in the same direction. Another reason for the wind induced profile is that wind velocities have more influence where the water depths are lower. The wind induced profile is not visible during the second measurement, because the wind and tide directions are against each other and the water depths are larger. Based on the change in direction of the Valeport device, it is concluded that the measured velocities are caused by the tide.

The current velocity in the lagoon can be influenced by the wind and wave conditions. When the waves heights and wind velocities are low, the tide induced current direction was visible during the field visits. For example at November 5, the wind and waves were coming from the south, but the observed current came from the north. The same process was measured with the Valeport device. Combining the observations of the field visits from Chapter 3 with the measurement results it is concluded that the observed current in the lagoon is tide driven.

The current velocity is used as input to obtain the sediment concentration over depth. The conditions during the measurements were calm and therefore the influence of high wind speeds or high waves on the current velocity was not investigated. According to Van Rijn (1991) a strong current velocity increases the concentrations in the water column. And a weak current superimposed on the waves hardly affects the concentration profile. The influence of the current direction on the concentration profile is relatively small (Van Rijn, 1991). During the calculations (to obtain the transported sand volume into the lagoon) a measured velocity of 0.2 m/s is used. Velocities between the 0.1 and 0.4 m/s are obtained during the measurements. Calculate the transported sand volumes into the lagoon with velocities of 0.1 and 0.4 m/s gave total transported sand volumes that were +/- 2% higher or lower compared with a velocity of 0.2 m/s, which is negligible. According to the model simulations of Arcadis in section 2.4, the tide velocities will not be higher than 0.5 m/s. It is not known if the flow velocities will be higher than 0.5 m/s during conditions with high waves and high wind speeds. The influence of the flow velocity is therefore not further investigated.

6.4.2. Overtopping

Using hourly wave data in the overtopping calculations results that the sediment concentrations are an average over time. In reality waves create turbulence in the water column and through this turbulence a sand volume rises from the bottom into the water column. After some time the sediment swirls downwards again. As a result of the used average wave height, a large time dependence is included in the calculations. More research towards this turbulence caused by the waves could give a more precise sediment concentration. No better formulas or methods were found in literature to estimate the sediment concentration over depth during this research.

The cube reef height has an influence on the transported volumes by overtopping. A lower height will result in more water transport over the cube reef. The height of the cube reef is determined from the BIP-measurements. The height of the cube reef is not a constant value over the alongshore length. The chosen range of 2-2.5m is obtained by looking at the BIP-measurements. Furthermore, holes are present between the cubes due to the placement structure of the cubes. This results in height fluctuations along the sand layer domain (as shown in figure 6.14), which makes the definition of height of this structure unclear. The chosen range in height resulted in a transported sand volume between 9,500 - 25,000 $m3$. Looking at, for example, figure 6.14 it is concluded that the highest value of 2.5m is too high and not realistic. An average value of 2.25m will be conservative, through the fact that holes are present between the cubes. In figure 6.3a it is visible that water is transported through these holes into the lagoon. Probably the most realistic height will be a weighted average between the 2m and 2.25m. Therefore the transported sand volume by overtopping will be between 15,000 and 25,000 m^3, this range is without the performed uncertainty analysis.

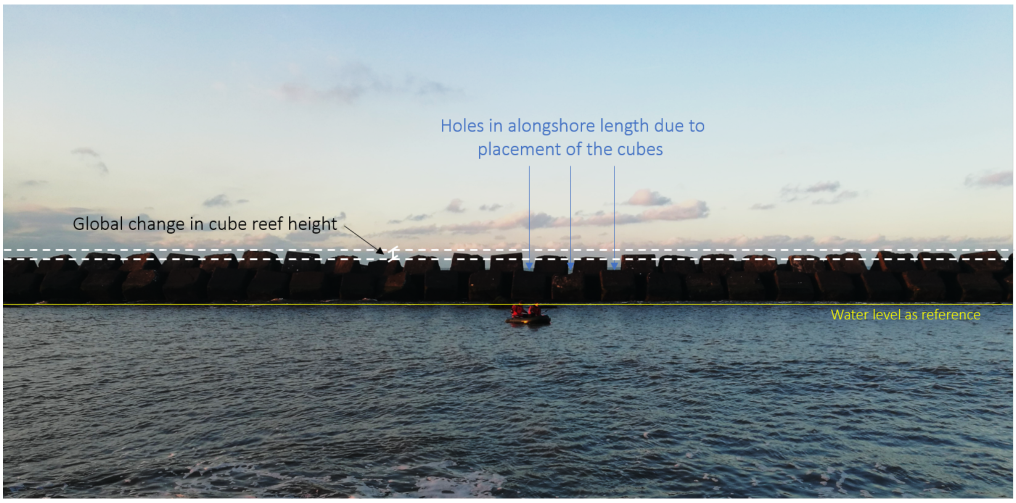

Figure 6.14: Difference in height of the cube reef and holes between the cubes due to the placement structure of the cubes .

The overtoppings volumes are calculated for the sections between KP2400 and KP3200. These sections are visible in figure 6.4. Analysing table 6.5 it is visible that there is a jump in transported volumes between KP2600 and KP2700. The transported volumes at KP2400 until KP2600 are lower than at the other sections. This is due to the larger water depths at those sections. Lower sediment concentrations are present in the higher part of the water column. Sand volumes were visible between the cobbles until KP2700 during performed field visits, see figure 3.1. The same boundary can be seen from these overtopping volumes. The influence of the water depth is shown by increasing the water depth with 1.5m at KP2400. This gives a transported sand volume that is twice as small.

Furthermore, the waves used in this calculation are transformed nearshore by SWAN. During this calculation the bathymetry of 2018 is used (as mentioned in Chapter 4). From table 6.2 it is visible that the water depth is decreasing from 2013 towards 2018. The waves at the output locations during the years before 2018 could be higher, through the fact that the water depth is higher. A higher wave height will result in more overtopping. The real influence of different wave heights is not investigated, because the waves are only transformed nearshore for the bathymetry of 2018.

Moreover, it happens that the water level combined with the wave height is higher than the height of the cube reef. As mentioned in section 6.2.3, a negative free-board is not possible in equation 6.3. If Rc < 0, the free-board is set to 0, which gives less transport into the lagoon than is happening in reality. It happens rarely that the water level + wave height are higher than the cube reef, but if it happens, large volumes of water (with sediment) will flow into the lagoon. Moreover, it must me mentioned that the cube reef is different than the type of structure where the formula is intended for. This causes for (potentially large) uncertainties.

The uncertainty of the overtopping calculation is investigated in section 6.3.4. Moreover, the results show that the variability of the water levels is around the same order of magnitude as the uncertainty of the overtopping and sediment concentration calculation. According to Gallach-Sánchez et al. (2018), the overtoppping equation of Van Der Meer et al. (2014) have a good accuracy for mild slopes and steep slopes. But for very small and zero relative crest freeboards (0 < Rc/Hm0 < 0.11) there is a consistent under-prediction across all the slope ranges by the equation of Van Der Meer et al. (2014). Based on these two conclusions of Gallach-Sánchez et al. (2018) we assume that the overtopping volumes are higher than the calculated values in this research. Looking at the results in sand transport over the cube reef by overtopping, the uncertainty of the overtopping equation is estimated between 7,500 and 50,000 m^3.

6.4.3. Tide induced transport

The size of the filled area by the tide through the flow opening is unknown. Therefore, two areas are chosen and the sediment transport is calculated for those to areas. This resulted in a sand volume of 4,300 and 8,700 m^3. Even with the largest area the transported sand volume by the tide is small compared with the total sand layer volume of 71,000 m^3. Based on this relatively simple calculation it is concluded that the sand transport by the tide will not be an important process that is responsible for the total sand layer volume.

Furthermore, it is not taken into account that sediment is able to settle in the cube reef, when water is flowing towards the lagoon during the flood current. And it is not taken into account that water volumes (which could include sand volumes) are flowing in offshore direction during the ebb phase. This could transport sand volumes out of the lagoon. Both processes reduces the transported sand volume caused by the tide.

6.5. Conclusions

In this chapter the respective contribution of hydrodynamic transport is investigated compared with the total sand volume of 71,000 m^3. The hydrodyanmic transport is divided into two mechanisms: overtopping over the cube reef and the transport caused by the tide. The sediment concentration over depth is calculated and multiplied with the transported water volume to estimate the transported sand volume of each process. Measurements are performed to obtain the flow velocities in the lagoon. The flow velocity is necessary as input parameter to calculate the sediment concentration in the water. It is observed during the measurements that the current velocity in the lagoon is tide driven and in the range of 0.10-0.20 m/s. The exact influence of the wind and waves depends on the direction of the wind and waves. It is not known if the current velocity increases during high waves and high wind speeds.

The total sand volume transported into the lagoon by overtopping is between 9,500 and 25,000 m^3 over the last 5 years. The transport caused by the tide is estimated to be between 4,300 and 8,700 m^3. Even the maximum transported sand volume by the tide is just 12% of the total sand layer volume. Therefore, the tide will not be the most important mechanism that is responsible for the sand layer volume.
As mentioned in the discussion, the height of the cube reef is an important parameter in the overtopping calculations. The transported volume range depends on the height of the cube reef. Probably the most realistic

height will be a weighted average between the 2m and 2.25. Therefore, the sand volume caused by overtopping is estimated to be between 15,000 and 25,000 m^3. This is equal to 21 - 35% of the total sand layer volume. Moreover, the uncertainty analysis shows that the variability of the water levels is around the same order of magnitude as the uncertainty of the overtopping and sediment concentration calculation. The uncertainty of the overtopping equation is estimated between 7,500 and 50,000 m^3, which is around a factor 2 compared with the mean values.

From the hydrodynamic analysis in this chapter, it can be concluded that the sand layer volume will increase infinitely if no counter measures are taken. The exact increase in sand layer volume will depend on the foreshore evolution. This conclusion is based on the fact that water volumes including sediment are transported into the lagoon and only water volumes are transported out of the lagoon (mentioned in section 6.2.3). Furthermore, it is concluded that only small sediment volumes could be transported out of the lagoon by the tide. This is not investigated into detail, but the influence of the tide is small compared with the total sand layer volume.

> Overtopping is responsible for a sand transport towards the lagoon between 21 - 35% of the total sand layer volume. Transport caused by the tide is estimated to be maximal 12%. Therefore overtopping is an important mechanism that is responsible for the total sand layer volume. Moreover, we concluded that the sand layer volume will increase infinitely if no counter measures are taken. The exact increase in sand layer volume will depend on the foreshore evolution.

7
Aeolian transport

7.1. Introduction

In this chapter, we investigate the role of aeolian transport in the formation of the sand layer (aeolian transport is indicated with arrow 6 in figure 1.9). Aeolian processes occur wherever there is a supply of granular material and atmospheric winds of sufficient strength: in deserts, on beaches, and in other sparsely vegetated areas, such as dry lake beds (Kok et al., 2012). The sand particles can occur in different modes, as shown in figure 7.1a. The type of transport mode depends mainly on the particle size and wind speed. The D_{50} at the Maasvlakte is 330 μm (Onderwater, 2018b). Sand transport was physically observed during field visits until around 1m height, therefore saltation will be the main transport mode at the sand layer domain. At Maasvlakte 2 the sand is transported by the wind from the soft protection towards the sand layer domain. In figure 7.1b the aeolian transport is visible at the cobble beach. Waves cannot bring sand to these (high) locations in the profile, therefore it must be delivered by the wind. In this chapter the aeolian transport capacities are calculated with the Bagnold formula (Bagnold, 1937). This formula is compared with measurement data around Maasvlakte 2.

The prediction of PUMA for the aeolian sand losses at the soft protection was 5 $m^3/m/year$ for the first 10 years after construction (as shown in section 2.1). As mentioned in section 2.1, this value of 5 $m^3/m/year$ is not found in reality during construction of Maasvlakte 2. It is concluded that the predicted aeolian transport by PUMA was too low and the sand buffer was located at the wrong location in the profile.

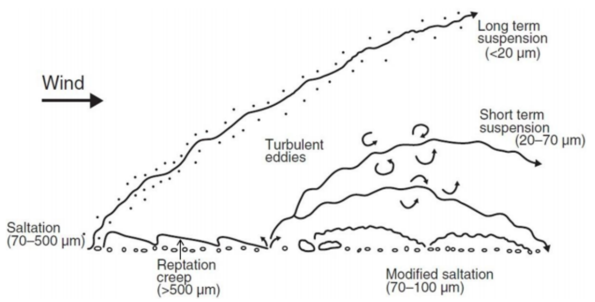

(a) Different modes of aeolian transport (Kok et al., 2012)

(b) The effect of aeolian transport is visible higher in the profile

Figure 7.1: The different aeolian transport modes (left) and the aeolian transport is visible in the profile (right)

7.2. Methodology

Three methods are applied to estimate the aeolian transport at Maasvlakte 2. In the first method the Bagnold formula is applied. With this formula the aeolian transport capacity is calculated. From experience it is observed that the calculated transport capacity from the Bagnold formula is never reached along the Dutch coast, because the supply of sediment is not large enough. To account for this overestimation, the Bagnold formula is compared with the two other methods. One of these methods is based on the dune volume increase over the past 5 years. From research it is observed that aeolian transport is moving sand volumes from the water line towards the dunes. The dune volume increase is acquired from the performed BIP-measurements by PUMA. The third method is based on field experiments, in which sand volumes have been captured in bins at Maasvlakte 2. Comparing methods 2 and 3 with the Bagnold formula of method 1 gives an estimation of the aeolian transport around Maasvlakte 2.

7.2.1. Bagnold formula

The Bagnold formula (Bagnold, 1937) is used to determine the transport capacity of aeolian transport. Equation 7.1 shows the Bagnold formula, all parameters are explained in Appendix F. In this version of the Bagnold formula the effects of sand moisture are not included. The influence of the wind velocity is implemented with a power 3 in equation 7.1. That means that if the wind is twice as strong, the transport capacity will increase with a power 3. The outcome of this formula can therefore be seen as a theoretical upper limit. Hoonhout (2017) compared four equilibrium sediment transport formulations at the Sand Motor area in the Netherlands. The Bagnold formula overestimated the measured aeolian transport rates less compared with the alternative formulations (Bagnold overestimated with a factor 3-4). Therefore, the Bagnold formula is used in this research.

$$\text{Bagnold formula:} \qquad q_a = C \times \frac{\rho_{air}}{g} \times \sqrt{\frac{d}{D}} \times (u_* - u_{*th})^3 \qquad [kg/m/s] \tag{7.1}$$

Hourly wind directions and velocities over the period 01-01-2013 until 01-05-2018 are obtained from Rijkswaterstaat (2018). The representative wind directions are specified using the coast orientation. The coast orientation is defined as 207 degrees (related to true North). All wind directions coming from a direction between 207 and 297 are taken into account (as shown in figure 7.2b). The outcome of the Bagnold formula is in the unit of $kg/m/s$. A domain is defined to acquire sand volumes in m^3. In figure 7.2a the sand layer domain is indicated and four possible aeolian transport directions are given. As said, for aeolian sediment transport you need a supply of granular material combined with atmospheric winds of sufficient strength. Both requirements are only available at arrow 1. Therefore, all other arrows are neglected and only the alongshore wind components in north-eastern direction are used. The outcome of equation 7.1 is divided into alongshore and cross-shore components, as shown with f_θ in equation F.3. This factor is included to account for respectively the onshore and alongshore wind directions only. Moreover, the outcome of the Bagnold formula is multiplied with the length perpendicular to the coastline = Δ_y in figure 7.2b. This length is the distance over which the sand volumes enter the domain between the cobble beach and cube reef. This distance is changing over the year, therefore satellite images are used to estimate this distance (see appendix A for the satellite images). A minimum and maximum distance is yearly determined and the relative percentage of occurrence per year is estimated. Finally, the outcome from the Bagnold formula is translated from kg to m^3 by using the density of sand and a porosity of 0,4 (shown in equation F.3).

$$Q = \frac{q_a \times \Delta_y \times \Delta_t}{\rho_s \times (1-p)} \times f_\theta \qquad [m^3] \tag{7.2}$$

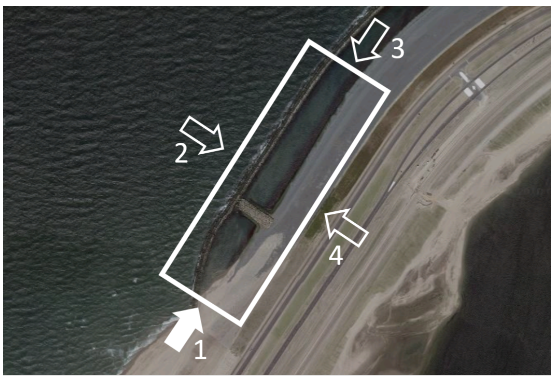

(a) Four directions of available (aeolian driven) sand transport into the specified domain

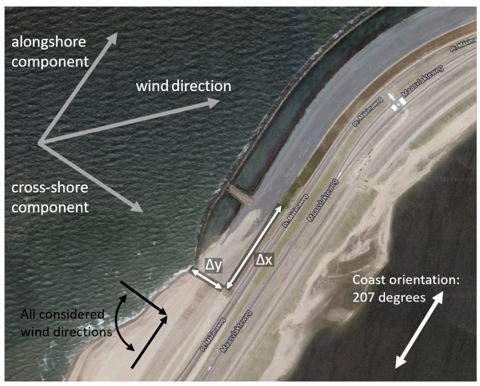

(b) Divide the main component in an alongshore and cross-shore component

Figure 7.2: Definitions to apply the Bagnold formula

7.2.2. Dune volume increase

From the performed BIP-measurements by PUMA the dune volume increase have been calculated between 2013 and 2018. The dune area is defined from +2m NAP and higher in the profile. At +2m NAP fences were placed by PUMA at the sand layer area to capture the transported sand by the wind, therefore this height is chosen to define the dune area. In figure 2.3 the placed fences are visible. Polygons are drawn around the defined dune area and the dune volume increase is calculated within these polygons. The calculated dune volume increase can be compared with the outcome of the Bagnold formula (equation 7.1). The wind speeds are used in the Bagnold formula and then the outcome is translated to the cross-shore component of the wind direction (with factor f_θ in equation F.3). In figure 7.3 all considered wind directions are shown. The dune increase is calculated for three different alongshore lengths. In figure 7.3 the polygon is drawn for an alongshore length of 600m. Polygons are also made for lengths of 200m and 400m.

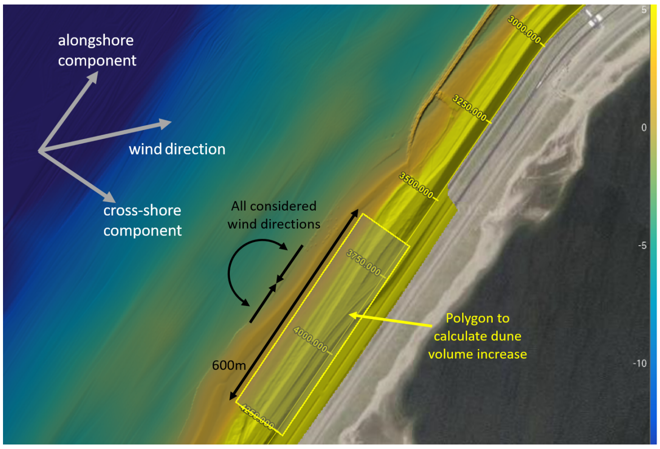

Figure 7.3: The specified polygon to calculate the dune volume increase. The elevations are shown with the colorbar on the right.

7.2.3. Measurements at Maasvlakte 2

During five different field measurements the aeolian transport is estimated. Sand volumes are captured by placing bins in the wind direction and measuring the difference in weight between start and end time of the experiment. The captured sand volume is translated into the unit $grams/meter/hour$. In figure 7.4 an image of the located bin at the start (left) and end (right) of a measurement is shown. These figures are from the measurement done on November 20^{th}, 2018. Through the fact that the center of gravity at aeolian transport is close to the ground, we assumed that almost all sand particles are captured by the bins. The wind velocities during the field visits were in the range of 5-10 m/s. According to Van Rijn (2018) the critical wind velocity for dry, loose sand particles with a particle size of 330 μm is 7 m/s. Which means that aeolian sediment transport theoretically happens at wind velocities above 7 m/s.

(a) The bins at the start of the measurement

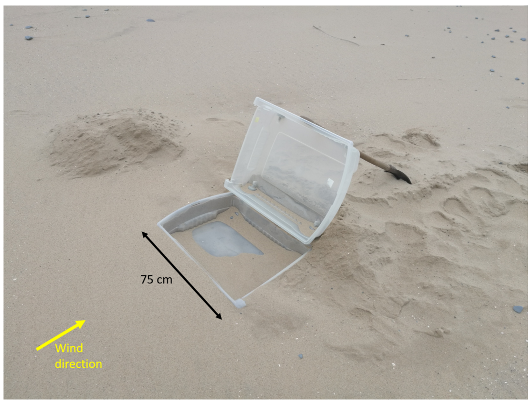

(b) The bins at the end of the measurement. The width of the bin is 75 cm.

Figure 7.4: Aeolian transport capacity measurement with the located bins at November 20, 2018

7.3. Results

7.3.1. Bagnold formula

In figure 7.5 the transported sand volumes by aeolian transport towards the sand layer domain are plotted. The aeolian transport is between 37,000 and 52,000 m^3 sand over the period 01-01-2013 until 01-05-2018. Both the maximum and minimum values are theoretical upper limits. The range in sediment transport depends on the maximum and minimum cross-shore distance based on the yearly satellite images. An average aeolian transport of 45,000 m^3 is obtained by defining two cross-shore lengths per year multiplied by the percentage of occurrence per year. The blue dots in figure 7.5 show the hourly transported volumes. It is visible from the cumulative plots that the aeolian transport increases the most during the winter periods.

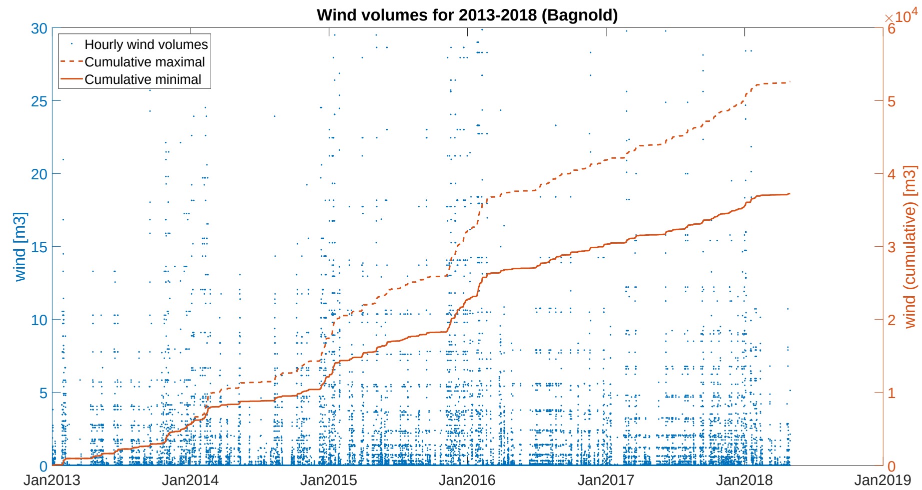

Figure 7.5: The sand volumes transported by the wind (using Bagnold formula). The blue dots are all volumes per hour. The red lines are the cumulative values of the lower and upper limit.

7.3.2. Bagnold formula vs measurement data

In table 7.1 the increase in dune volume is shown for the five different alongshore lengths from 2013 to 2018. In the second column the transported sand volumes are given by using the cross-shore component of the Bagnold formula. In the most right column the volume calculated with the Bagnold formula is divided by the measured dune volume increase, which is named 'factor' in table 7.1. In general the measurements differ a factor 3,1 with the results of the Bagnold formula. In figure 7.6 the Bagnold formula is plotted against the dune volume increase in time. The overestimation of the Bagnold formula is visible in this figure. The Aeolian transport is plotted for two different alongshore lengths (300m and 500m). Until around January 2015 the trend of all lines is similar. From January 2015 until 2018 the Bagnold formula is overestimating lines from the dune increase. From 2017 to 2018 the dune volume did not increase. The dune volume shows a decrease in 2018 for length 1 of the dune volume calculation. The reason for this decrease is unclear.

	Increase in dune volume $[m^3]$	**Bagnold formula (cross-shore component)** $[m^3]$	**Factor** $[-]$
200m	26,500	84,500	3.18
300m	47,560	129,197	2.73
400m	52,300	169,000	3.23
500m	68,019	211,995	3.12
600m	81,500	254,000	3.12

Table 7.1: The calculated dune volume increase and the transported sand volumes with the Bagnold formula over the past 5 years (2013-2018). In the last column the volume calculated with the Bagnold formula is divided by the measured dune volume increase

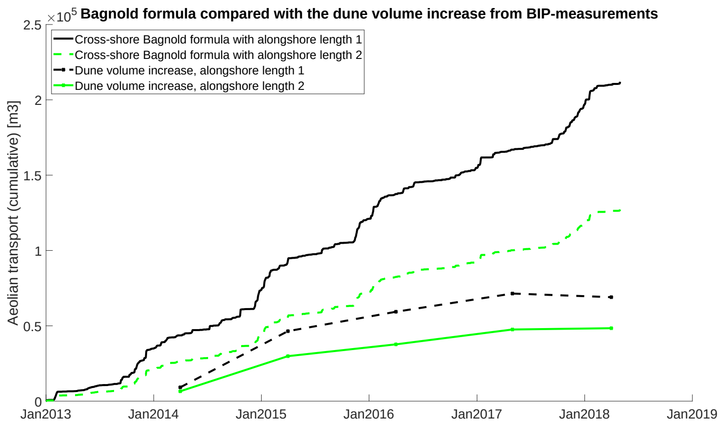

Figure 7.6: The Bagnold formula compared with the dune volume increase from the BIP-measurements.

Moreover, as mentioned in section 7.2.3, field measurements are performed during this research at the sand layer area. Sand volumes are captured in square bins during five different field visits. In table 7.2 the conditions and observations are shown during the field visits. The critical wind velocity of 7 m/s (Van Rijn, 2018) for sediment transport by the wind is visible from the field visits. The captured sand volumes by the bins are shown in the most right column of table 7.2. During three field visits no sand volumes were captured in the bins, because the wind velocities were too low.

Date	**Wind direction [degrees]**	**Wind velocity [m/s]**	**Observations**	**Measured Aeolian transport [g/m/h]**
21 sep 2018	270	13 - 14	Aeolian transport physically observed	-
5 nov 2018	120	5	No aeolian transport	0
10 nov 2018	190	8	Very little aeolian transport	1330
20 nov 2018	90	10	Aeolian transport physically observed	8637
12 dec 2018	100	5	No aeolian transport	0
08 jan 2019	315	15-16	Aeolian transport physically observed	-
11 jan 2019	320	6.5	No aeolian transport	0

Table 7.2: Wind conditions and observations during the performed field visits. Wind speeds are obtained from a location 3km offshore (Rijkswaterstaat, 2018). Also the capured sand volumes are shown in the last column. No measurement is indicated with the symbol:"-"

In figure 7.7 the results of the field measurements are plotted against the Bagnold formula. We observed that the transport volumes from Bagnold are higher than the measured volumes during the field visits. The difference between the Bagnold formula and the performed measurement is on average a factor 7.

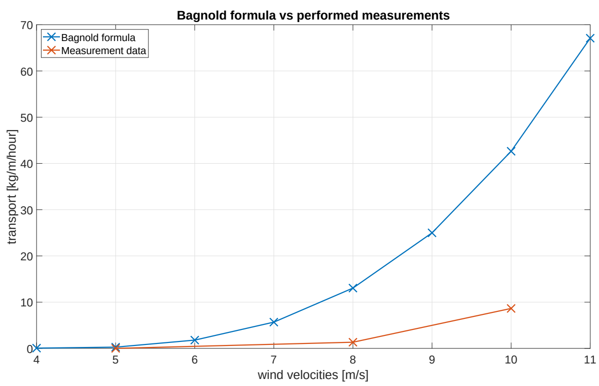

Figure 7.7: The Bagnold formula for different wind velocities compared with the measurements

7.4. Discussion

Three analysis are performed to estimate the aeolian transport towards the sand layer domain. All methods result in a transport volume by the wind. From experience it is observed that the calculated transport capacity from the Bagnold formula is never reached along the Dutch coast, because the supply of sediment is not large enough. Therefore, the transport capacity of Bagnold is compared with real transported volumes at Maasvlakte 2. Through the fact that the Bagnold formula is the upper limit, the estimated aeolian transport must always be lower than this value.

Comparing the increase in dune volume from the BIP-measurements with the cross-shore component of the Bagnold formula, an average overestimation factor of 3.1 was found. Comparing the performed field-measurements with the Bagnold formula an average factor of 7 was found. Applying these factors on the aeolian transport found with the Bagnold formula, gives the following ranges for aeolian sediment transport at Maasvlakte 2:
- apply factor 3: 12,300 - 17,300 $m^3/5years$
- apply factor 7: 5,300 - 7,400 $m^3/5years$

Whereby the increase in dune volume is based on a time series (just as the Bagnold formula) and the field experiments are performed within a time-frame of maximum 2 hours. Moreover, an overestimation factor of 3 to 4 was found for the Bagnold formula at the Sand Motor in the research of Hoonhout (2017). Therefore it is concluded that method based on dune volume increase is more accurate than the field experiments.

Furthermore, PUMA performed an analysis in 2012 by comparing elevation measurements of 2011 and 2012, as shown in the reports of PUMA (2012a) and PUMA (2012b). From this analysis a dune volume increase of 30-40 $m^3/m/year$ was acquired (as shown in section 2.1). The analysis by PUMA is done on data over 1 year during construction and the analysed sections are located more southwards than the analysis of this chapter (the coast orientation is different for the sections more southwards). The dune volume increase in this research was around 25 $m^3/m/year$, which is the same order of magnitude as found in the research by PUMA in 2012. The reason for the higher values in 2012 is probably the different coast orientation of the analysed sections (those sections have a coast orientation which is more perpendicular to the wind direction).

7.5. Conclusion

In this chapter the role of aeolian transport in the formation of the sand layer is investigated. Three analysis are performed to estimate the aeolian transport. The Bagnold formula is applied and compared with measurement data. Measurement data is used to calculate the dune volume increase and field measurements are performed to calculate the transport capacity of aeolian transport. PUMA made a prediction for a sand buffer to account for aeolian transport at Maasvlakte 2 (PUMA, 2008d). During construction it was already concluded by PUMA that the predicted buffer was too low and it was placed at the wrong location in the profile. Therefore it is not possible to compare the prediction by PUMA with the real aeolian transport.

From experience we observed that the calculated transport capacity by the Bagnold formula is never reached along the Dutch coast. Therefore, the outcome of the Bagnold formula is taken as upper limit: the estimated aeolian transport must always be lower than this value. The aeolian transport calculated with the Bagnold formula is between 37,000 and 52,000 m^3, with an average value of 45,000 m^3. Based on literature and the performed analyses in this chapter, we assumed that the Bagnold formula overestimates with a factor 3. Therefore, the aeolian transport is estimated between 12,300 - 17,300 $m^3/5years$ sand. This is equal to 17-24% of the total sand layer volume.

The analyses performed in this chapter are based on measurement data. In other studies an equal factor of overestimation was found by Hoonhout (2017), thereby we assumed that the found aeolian transport volumes in this research are accurate. We concluded that the aeolian transport will not be twice as large in reality.

> Aeolian transport is estimated to be responsible for a sand transport towards the lagoon of 17-24% of the total sand layer volume. The performed analysis is based on real data and the result is therefore assumed to be accurate. Aeolian transport is not considered as the largest transport mechanism, but aeolian transport can not be neglected by looking the total sand layer volume

8
Discussion

The objective of this thesis is to determine the morphological mechanisms in, and their respective contributions to, the formation of the sand layer. In this chapter we present the obtained results of the previous chapters. We started with a conceptual model in Chapter 1. Subsequently, we performed three volume investigations based on this conceptual model: a sediment budget analysis (Chapter 5), a hydrodynamic analysis (Chapter 6), and an aeolian analysis (Chapter 7). At the end of these chapters an individual section with a discussion is included. These discussions were on the assumptions, simplifications and choices made to calculate the respective transportation contribution. The discussion in this chapter will be more on the interpretation of the entire system. This helps to put the investigated results into perspective and strengthens the conclusions. We first give an overview of the conceptual model with the final transportation values, followed by the influence of storm periods on the sand layer volume. Then we present the qualitative insights from satellite images and finally the future development of the sand layer is discussed.

Overview of transport contributions

The sediment budgets of the sand layer area are analysed in Chapter 5, this analysis is based on available elevation measurements and satellite images. We found that the total sand layer volume was 71,000 m^3 in April 2018. In Chapter 1 all possible transport mechanisms are shown in the conceptual model. The results of each investigated mechanism is shortly given in this section.

Hydrodynamic transport, investigated in Chapter 6, is divided into two mechanisms: overtopping over the cube reef and transport by the tide. The volume of water transported over the cube reef is calculated and multiplied by the sediment concentration in the water to investigate the role of overtopping in the formation of the sand layer. As a result, the calculation shows a transported sand volume between 15,000 and 25,000 $m^3/5years$ due to overtopping. This is equal to 21-35% of the total sand layer volume. This range is dependent on the height of the cube reef. It is ambiguous how to define the height of the cube reef through the alongshore height fluctuations and the available gaps between the cubes. Moreover, the structure is different than what the formula is intended for, which also give uncertainties in the calculation. These uncertainties are not included in this given range. Furthermore, the transported sand volume due to tidal currents is obtained by multiplying the transported water volume from low to high tide with the sediment concentration in the water. This results in a sand transportation between 4,300 and 8,700m^3 over 5 years, equal to a maximum of 12% of the total sand layer volume. The exact lagoon area filled by the tidal current is unknown. Therefore two areas are chosen, which results in the given range for transport by the tide.
Finally, the transported sand volume through aeolian transport is investigated in Chapter 7 using Bagnold's formula. We compared the outcome of this formula to measurements and ultimately estimate aeolian transport to be between 12,300 and 17,300 $m^3/5years$, equal to 17-24% of the total sand layer volume. The range in aeolian transport is dependent on the width perpendicular to the coast. Sand volumes are transported in the lagoon by the wind through this width (= Δ_y in figure 7.2b). This width changes over the year, wherefore a range is applied during the calculation.

In table 8.1 we present the transport range from each mechamism and the parameter that influence the specific transport range. The last column of table 8.1 shows the calculation accuracy of each investigated mechanism. Uncertainties are present within the different analyses, but the total sand layer volume of 71,000 m^3 is assumed to be accurate. Based on the results from all analyses, overtopping appears to be responsible for most transport into the lagoon. Our estimates indicate a total maximum sand layer volume of 25,000 + 8,700

+ 17,300 = 51,000 m^3. That leaves 20,000 m^3 of sand unaccounted for in our estimated 71,000 m^3 volume of sand in the lagoon.

Mechanism	**Range in transported volume**	**Parameter that causes the transport range**	**Accuracy of performed calculation**
Overtopping	15,000 - 25,000 m^3	Ambiguous how to define the cube reef height	Large uncertainty, which is shown in Chapter 6
Aeolian transport	12,300 - 17,300 m^3	Width perpendicular to coastline changes over the year	Accurate, because it is compared with real measurement data and with literature
Tidal current	4,300 - 8,700 m^3	Size of filled lagoon area by the tidal current is unknown	Uncertain, but already a factor 2 is implemented in the analysis and even the maximum value is still small compared with the total sand layer volume

Table 8.1: The transport ranges from the performed analyses in this research

As mentioned in Chapter 7, the calculated volume by aeolian transport is compared with real measurement data and in literature the same transportation values were found. It is therefore assumed that this value for aeolian transport is accurate and will not be twice as large in reality. Aeolian transport is unlikely to be responsible for the missing volume. Moreover, within the calculation of the transportation volume due to tidal currents the filled area is already multiplied with a factor 2. Even with the largest area the transported volume by the tide is small compared with the total sand layer volume of 71,000 m^3. We conclude that transport by the tide is not responsible for the missing volume. Furthermore, the maximum calculated transport by overtopping is 25,000 m^3. We showed in Chapter 6 that the uncertainty of this calculation depends on the overtopping formula and the sediment concentration formula. The uncertainty of the calculation is estimated between 12,000 - 50,000 m^3, as shown in figure 6.12. Therefore, we conclude that only the uncertainty in the overtopping calculation can explain the missing volume of 20,000 m^3. Overtopping is set to 45,000 m^3 in figure 8.1, whereby the sum of all transport mechanisms correspond with the total volume of 71,000 m^3. In figure 8.1 all final transport values are shown for each mechanism. In this research the measurement uncertainties are not considered. The measurement uncertainties are order of magnitudes lower than the uncertainties of the performed analyses.

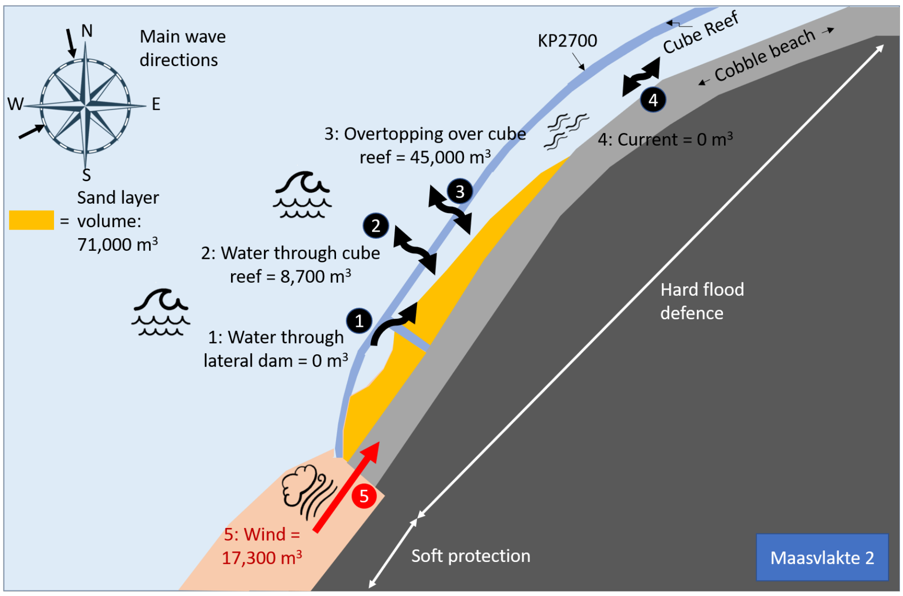

Figure 8.1: Created conceptual model, whereby black arrows indicate a hydrodynamicmechanism and red arrows an aeolian mechanism.

Arrows 2, 3 and 5 of figure 8.1 are already explained in this section. Arrow 1 is set to zero, because we assume that hydrodynamic sand transport through the lateral dam did not contribute to the formation of the sand volume in the lagoon. This assumption is based on observations during field visits and the designed placement structure of the cubes in the lateral dam.
Moreover, we observed sand volumes at the cobble beach reaching KP2700 during the field visits, but from the hydrodynamic analysis we observed that sand volumes are brought into the lagoon by overtopping also further northwards of KP2700 (KP2700 is indicated in figure 8.1). Based on this, we conclude that the current velocity is able to transport the incoming sand volumes in the lagoon. The sediment has a chance to settle in the lagoon due to the mild conditions. Due to these mild conditions we assume that the current velocity can only transport little sand volumes for short distances. Therefore, arrow 4 is also set to 0 m^3.

Influence storm periods

The results of the sediment budget analysis in Chapter 5 show that the sand layer volume is increasing during winter periods. This result can be justified by considering that wind speeds and wave heights are highest during winter periods. Prior in this chapter we concluded that overtopping and aeolian transport were the most dominant transportation mechanisms. It is interesting to look at the conditions that cause for sand transportation to the lagoon. In figure 8.2 the fraction of overtopping volumes are cumulatively plotted for each section combined with the cumulative normalised aeolian transported volumes. A vertical line is included at y = 0.1. With this line it is visible that, for example, 12.5% of all aeolian conditions are responsible for 90% of the total aeolian transport. The horizontal axis corresponds with the fraction of time and the vertical axis with the fraction of total transported volume. Note the start value of the x-axis.

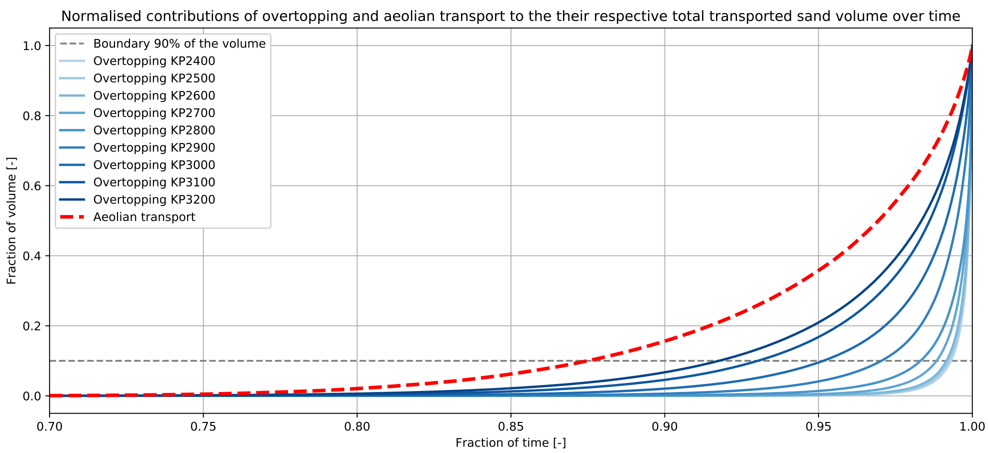

Figure 8.2: Normalised contributions of overtopping and aeolian transport to the their respective total transported volume over the past 5 years. Note the start value of the x-axis.

We observed that 90% of the total transported volume of each respective line is caused by less than 15% of all occurred conditions over the past 5 years. For overtopping it is even less, for example the total transported volume for KP2400 is caused by less than 5% of all occurred conditions. Looking at the overtopping volumes per section, it is clear that KP2400 is the steepest and KP3200 the least steep. Which means that the total volume of overtopping at KP2400 is dominated by less events. Analysing the characteristics of the conditions that are responsible for this sand transport we observed that only conditions with high water levels and high wave heights are able to transport sand volumes in the lagoon, which are the extreme events. The responsible conditions are different for KP2400 compared with KP3200. This is probably due to the fact that the water depth is lower at KP3200, therefore the waves break earlier than at KP2400. Moreover, we conclude from figure 8.2 that the total volume of aeolian transport is driven by more events than the overtopping volumes. Aeolian transport is therefore less dependent on extreme events than overtopping.
As shown in figure 8.3, we found a correlation between the wave height and wind speed. Most of the times high wave heights happen at the same time as high wind speeds. Moreover, high wind speeds can create a set-up of the water level at sea, which could induce for more overtopping over the cube reef. As expected, high

wind speeds are also responsible for more aeolian transport. The observed increase of the sand layer volume during wind periods is justified with the demonstrated correlation combined with the observed dependency on extreme events.

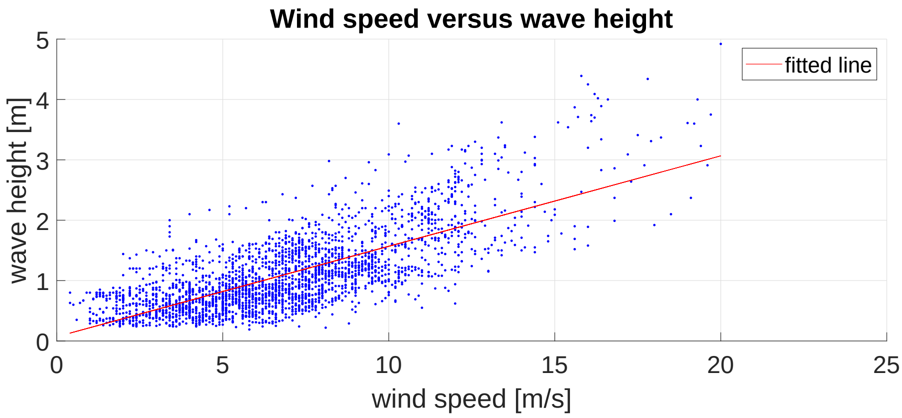

Figure 8.3: Correlation between wind speed and wave height. Wave heights are from Europlatform and wind speeds at Hoek van Holland. Both obtained from Rijkswaterstaat (2018)

In Chapter 4 we found that the wave component from the north-west increased from 2013 to 2018. The south-western and north western component were almost equal in size during 2018. This is not necessarily a trend for years ahead, but it did influence the approach angle of the waves over the last 5 years. More waves from the north-west lead to a more perpendicular wave approach on the cube reef, resulting in more wave overtopping. This change in wave direction is observed in the wave data of Europlatform and from the nearshore data, as shown in Chapter 4. The change in wave direction is therefore not caused by the growing foreshore in front of the cube reef. On the other hand, this foreshore is breaking the waves coming from the south-west. As shown in the bar-plots of Appendix figures E.16 and E.17 we observed that the overtopping volumes of KP2400 are mainly caused by higher waves from the north-west. And that overtopping volumes of KP3200 are mainly caused by lower waves from a western direction. Which could be explained by the fact that the water depth is deeper at KP2400, therefore less wave breaking is present. But through the deeper water depth, more wave turbulence is necessary to stir the sediment up in the water column. The combination of water depth and sediment supply is important for the hydrodynamic transport capacity.

Qualitative insights from satellite images

Hydrodynamic and aeolian transport are the important transport mechanisms in the formation of the sand layer. Aeolian transport is coming from the south-west and hydrodynamic transport happens through or over the cube reef. Looking at the satellite images in Appendix A the growing sand layer is visible over time. The importance of aeolian and hydrodynamic transport is discussed based on these satellite images. Several images indicate that the sand layer is created by aeolian transport and other images indicate the importance of hydrodynamic transport.

From the satellite images it can be observed that the sand layer is growing from south to north, which is the same direction as aeolian transport. Especially the sharp edge of the sand layer in February 2015 seems to highlight the importance of aeolian transport, as shown in figure 8.4a. Hydrodynamic transport is not able to create a sharp pattern as is shown in this satellite image. It can indicate that aeolian transport is responsible for a uniform migration of the sand layer in northern direction. On the other hand, in May 2015 it is visible that water is present south of the lateral dam. And aeolian transport is not able to move sand in a northern direction through this water volume over the lateral dam. It is not known if this water volume in May 2015 is just a small layer of water, which will be gone if the tide drops a bit. Probably if aeolian transport will continue, it is just a matter of time until this southern part is totally filled up with sediment. Moreover, the sand color in for example March 2017 is very bright and sand volumes are visible on the cobble beach, as shown in figure 8.4b. This indicates both the presence of aeolian transport, but on the other hand the layer thickness of these visible sand volumes is unknown. It could only be a few centimetres, which does not justify the importance of aeolian transport.

(a) Observed sharp edge of the sand layer shape

(b) Shape of the sand layer at March 2017

Figure 8.4: Satellite images of 2015/02/18 (left) and 2017/03/28 (right)

The satellite image of March 2017 shows a pattern of the sand layer indicating the importance of hydrodynamic transport in the formation of the sand layer. The alongshore sand volume attached to the cube reef indicates transport through the cube reef. But if sand is transported through the cube reef, one would expect to see sand volumes at more locations in the lagoon. This can be justified by considering that the current is able to transport the incoming sand volumes in the longshore direction. From the hydrodynamic analysis in Chapter 6 we observed that sand volumes are transported into the lagoon until around KP2400. Moreover, the water depths increase in northern direction towards water depths of 11m at KP2400. The required wave turbulence at the sea-bottom to induce sediment transport is decreasing for larger water depths.
PUMA artificially removed a sand volume from the lagoon in August 2015. They thought to solve the sedimentation problem in the lagoon by removing the sand, but this sand volume was back within a few months. This indicates the presence of marine processes. The removed sand volume is visible by comparing the satellite images of May 2015, August 2015 and March 2016 in Appendix A.
Different theories in the formation of the sand layer are possible based on the satellite images. Both aeolian and hydrodynamic transport is visible. As mentioned in the beginning of this chapter, we concluded that aeolian transport cannot be responsible for the entire sand layer volume. Even the maximum value of the calculated aeolian transport is not equal to the entire sand layer volume. This is also not the case for hydrodynamic transport, but the inaccuracy of this calculation shows the variability of the used formulas.

Future development of sand layer

As mentioned in Chapter 6 the sand layer volume will increase indefinitely (until the lagoon is filled) if no counter measures are taken. The responsible processes for sediment transport to the lagoon will not change in the nearby future. Aeolian transport will always happen if there is a supply of granular material and atmospheric winds of sufficient strength. The source for aeolian and hydrodynamic transport is the, southern located, soft protection. Since nourishments are necessary to secure the safety of the soft protection, the supply of sediment will remain.
In chapter 6 we made the assumption that conditions outside the cube reef are rough compared to the mild conditions in the lagoon. And due to the reduced turbulence inside, the sediment now has a chance to settle in the lagoon. Water without sediment then returns through the cube reef, given the fact that the lagoon is closed at the northern and southern end and that the water level in the lagoon cannot increase indefinitely. Water (containing little sediment) thus flows in the offshore direction through the cube reef, while overtopping volumes (containing sediment) are transported into the lagoon. This assumption justifies the consideration that the sand layer will increase indefinitely until the lagoon is filled, as sediment is flowing in more than flowing out. The amount of overtopping is dependent on the depth of the foreshore. From the analysis in Chapter 6 we observed that the overtopping volumes reduce in northward direction from KP2800. This is due to the fact that the water depths are deeper and the created wave turbulence is not enough to move the sediment from the bottom to the top of the water column. It is not known if the foreshore is able to extend in northern direction by internal longshore transport. As mentioned, during overtopping there is probably no outflux of sediment, but the tide transport, which is likely responsible for a lower order of magnitude, could create an outflux of sediment. The outflux is not investigated during this research.

In Chapter 5 we analysed the sediment budgets in the lagoon. The formation of the sand layer volume is plotted in figure 5.6. From this figure we observed a volume change around the beginning of 2017. The sand

layer volume did not increase much in 2017 and 2018. We assume that this change in volume increase is due to a difference in wave height and direction. As shown in the wave analysis of Chapter 4, the calm percentages of 2017 and 2018 were higher than the years before 2017. Especially the calm percentage of 2018 was higher than the years before, moreover the resulting wave energy flux was low in 2018. In figure 8.5 we present the normalised overtopping volumes over the last 5 years at four sections. The increase during winter periods for KP3200 is highlighted with the black arrows. A larger increase is visible for 2015 and 2016, than for 2017 and 2018. Moreover, as shown in Chapter 7 (figure 7.5), the volume of sand transported by wind was also lower for the years 2017 and 2018. The change in sand layer volume increase in 2018 may be justified by the lower wave energy flux and lower wind speeds in 2018.
Furthermore, the growing foreshore has an influence on the amount of overtopping. A lower water depth require less turbulence to stir the sediment up in the water column. On the other hand, a lower water depth result in more wave breaking and therefore less turbulence and less overtopping. As already mentioned, it is unknown if the foreshore is able to grow in northern direction. Currently, the water depth northwards from KP2700 is too deep to stir the sediment up in the water column. Probably a large part of the longshore transport, coming from the soft protection, flows into the deeper water depths around the foreshore. It will take time before the water depths in the northern sections are low enough to create large sand transport by overtopping. As mentioned, the sand layer volume will increase indefinitely until the lagoon is filled, it will depend on the foreshore evolution until which section the lagoon is filled by overtopping.

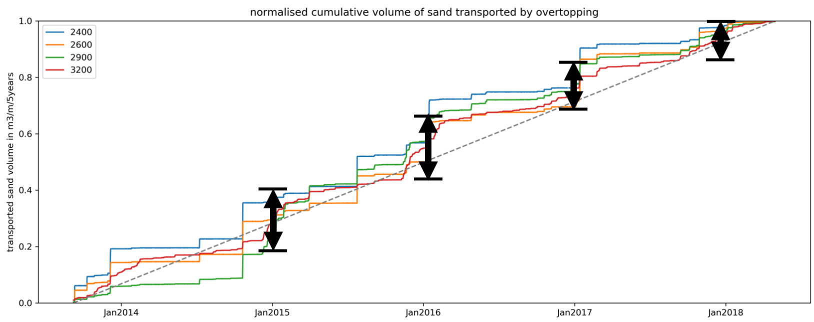

Figure 8.5: Normalised overtopping volumes of KP2400, KP2600, KP2900 and KP3200. The arrows indicate the winter increase of KP3200.

Mitigating measures

As mentioned in the introduction (Chapter 1), The sand volumes between the cobbles could increase the amount of run-up on the cobble beach, which could induce for more overtopping. It is difficult to clean the sand volumes from the pores between the cobbles. The sand volumes in the lagoon will be transported in northern direction by water or wind if no counter measures are taken. That means that a larger area of the cobble beach will be saturated with sand. Moreover, it is not known what the effect of accumulated sand will be for the functionality of the cube reef. It is unknown if the safety requirement of Maasvlakte 2 still holds for this increased run-up. Currently, the cube reef is absorbing almost all wave energy. When the cube reef is totally saturated with sand, the wave could roll over the cube reef and is able to reach the cobble beach with more wave energy. On the other hand, the foreshore combined with the sand layer will cause for wave dissipation. The sand layer will act as a extended foreshore, which will dissipate more wave energy. It must be investigated what a storm will do on an increased foreshore. PUMA has to convince Rijkswaterstaat that the sand volumes will not influence the safety standards of Maasvlakte 2.

Regardless of the fact that research is necessary towards the amount of dissipation of the sand layer, it is probably better to prevent that the sand is transported in northern direction along the cobble beach. Because this northern directed sand transport will cause for more saturated pore volumes at the cobble beach. There are different options to prevent sand from moving in northern direction. One option is to remove the entire sand layer volume, but it is not proven that this sand is negative for the safety standards of Maasvlakte 2. Another option is to keep the sand in its current position and to maintain it by placing, for example, vegetation on the sand layer. Building with nature has become a hot topic in hydraulic engineering over the last years. The real added value of vegetation at Maasvlakte 2 must be investigated, as it could be a solution. Vegetation can keep the sediment at its location, dissipating the wave energy.

9 Conclusions and recommendations

9.1. Conclusions

The objective of this research is to determine the morphological mechanisms and respective contributions in sediment transport into the domain between the cube reef and cobble beach. This research is performed by creating a conceptual model with all processes that could contribute to the formation of the sand layer. These processes were then studied by means of a literature study, wave climate analysis, sediment budget analysis and a separate hydrodynamic and aeolian analysis combined with field experiments. This research has provided more insight in the mechanisms responsible for the sand layer formation. This has resulted in a better understanding of coastal transition areas. The conceptual model with al final transport values is shown and explained in Chapter 8 (figure 8.1). This chapter presents the conclusions of this study by answering the research questions posed in Chapter 1.

Research questions

In this section the research questions are handled. First the additional question and finally the main research question is answered.

> **1. What are the main mechanisms leading to sediment transport towards the domain between the cube reef and the cobble beach?**

The investigated mechanisms are aeolian and hydrodynamic transport. Hydrodynamic transport is divided into overtopping over the cube reef and transport by the tide. Both mechanisms transport water from the foreshore towards the lagoon. The main mechanisms that contribute to the formation of the sand layer volume are overtopping over the cube reef and aeolian transport, whereby overtopping over the cube reef is the largest mechanism. Sediment is moved by aeolian transport from the soft protection in northern direction. Moreover, it is found that the sand layer formation is dependent on extreme events and that the sand layer is mainly increasing during the winter periods. During winter periods the wave heights and wind speeds are higher than in other seasons. The responsible events that transport sand volumes into the lagoon by overtopping are events with high water levels and high wave heights. Moreover, we showed that high wind speeds and high wave heights are correlated. The observed increase during the winter periods is justified with the demonstrated correlation between wind speed and wave height combined with the fact that the sand layer formation is dependent on extreme events.

> **2. How large is the respective contribution of the main mechanisms in the formation of the sand layer volume?**

The total sand layer volume is estimated to be 71,000 m^3. The respective calculated contributions of each mechanism are listed from largest to smallest:
- Transport by overtopping: 25,000 m^3
- Aeolian transport: 17,300 m^3
- Transport by the tide: 8,700 m^3

Based on these values, overtopping and aeolian transport are assumed to be the main responsible mechanisms responsible for the sand layer volume, whereby overtopping over the cube reef is the largest mechanism. Our estimates indicate a total maximum sand layer volume of 25,000 + 8,700 + 17,300 = 51,000 m^3. That leaves 20,000 m^3 of sand unaccounted for in our estimated 71,000 m^3 volume of sand in the lagoon. The accuracy of each calculation is analysed in order to clarify the missing volume compared with the total sand layer volume. The calculated aeolian transport is compared with real measurement data and in literature the same transport values were found. It is therefore assumed that the found value for aeolian transport is accurate. Moreover, within the calculation of the transportation volume due to tidal currents the filled area is already multiplied with a factor 2. Even with the largest area the transported volume by the tide is small compared with the total sand layer volume of 71,000 m^3. Finally, the uncertainty of the overtopping calculation is estimated between 12,000 - 50,000 m^3. Therefore, we conclude that only the uncertainty in the overtopping calculation can explain the missing volume of 20,000 m^3.

3. How will the sand layer develop in the coming (5) years?

As mentioned, the total sand layer volume is estimated to be 71,000 m^3. High wind speeds and high waves will cause for sand transport towards the lagoon. Therefore, we concluded that the sand layer will increase indefinitely, until the lagoon is completely filled. Depending on the foreshore migration in the northern direction, the sand layer will also increase in northern direction. Currently, the water depth northwards of KP2700 is too deep to stir the sediment up in the water column and transport sand in the lagoon. If these water depths will decrease, the waves could transport sand volumes in the lagoon.

After the maintenance period in 2023, the responsibility for the maintenance of Maasvlakte 2 goes to Rijkswaterstaat. PUMA has to convince Rijkswaterstaat that the sand volume will not influence the safety standards of the flood defence of Maasvlakte 2. The sand volumes between the cobbles could increase the amount of run-up on the cobble beach, which could induce for more overtopping. On the other hand could the sand volume dissipate the incoming wave energy and decrease the run-up on the cobble beach. There are many discussions about whether the formation of the sand layer volume is an advantage or disadvantage. It is unknown if the safety requirement of Maasvlakte 2 still holds with the sand volume in the lagoon. More research should show if saturation of the pores at the cobble beach influences the safety standards, and based on this investigation the sand layer volume will be removed or not. If the sand layer volume will not be removed, the future development depends partially on the wind and wave climate and partially on the foreshore evolution.

Finally, the main research question is answered:

Which mechanisms are responsible for the current size of the sand layer and how will the sand layer develop in the coming years?

The main responsible mechanisms for the sand layer volume are thought to be overtopping and aeolian transport. Based on the results of this research, many conclusions can be drawn in a qualitative way, but quantitatively the calculated numbers do not entirely match the total sand layer volume. The difference with the estimated total sand layer volume likely lies in the overtopping calculation, or in other words: the missing volume compared with the total sand layer volume can be found in the uncertainty of the used equations during the overtopping calculation. We concluded that the sand layer will increase indefinitely, until the lagoon is completely filled. The source for aeolian and hydrodynamic transport is the, southern located, soft protection. Since nourishments are necessary to secure the safety of the soft protection, the supply of sediment will remain. And high wind speeds and high waves from the north-west will cause for sand transport towards the lagoon. There are many discussions about whether the formation of the sand layer volume is an advantage or disadvantage. The future development of the sand layer depends on the safety standard, which will be discussed during the contractual negotiations between PUMA and Rijkswaterstaat.

9.2. Recommendations

The recommendations are divided in two different categories, namely the recommendations regarding the application of this research and the recommendations for further research are proposed.

Application

This research improved the system understanding at the transition zone at the protection of Maasvlakte 2. The improved system understanding showed which processes are responsible in the formation of the sand layer. Moreover, the future development of the sand layer volume is discussed. This research opens the possibility for modelling the area into more detail. The approach of this research was to define the main mechanisms and to estimate the contributions of the different transportation mechanisms. More in depth calculations could be an improvement to this research. We concluded in this research that the sand layer volume will probably increase indefinitely until the lagoon is entirely filled with sand. But the future development of the sand layer will probably depend on the contractual negotiations between PUMA and Rijkswaterstaat.

A large sand volume could dissipate much of the incoming wave energy. However, the sand volumes in the pores between the cobbles will cause for more run-up on the cobble beach. It is not sure what the effect of wave dissipation is compared with the increased run-up. It will take time before a real dune is present in the lagoon that can withstand storms. But it is suggested to conduct more research into the wave dissipation by the sand volume. Why should we remove the sand volume if the safety requirement could still hold with the sand volume in the lagoon? It would be a shame if we unnecessarily remove the sand volume in the lagoon. Maybe vegetation can keep the sediment at its location and vegetation will dissipate even more wave energy.

Research recommendations

Within this research certain assumptions are made and the following suggestions are proposed in order to improve the model uncertainty of this research project. The research recommendations are divided into recommendations for data collection and recommendations for model improvement.

Further research: data collection

- We performed flow velocity measurements in the lagoon during this research. More measurements would strengthen the obtained flow velocities. Especially during storm/heavier weather conditions it is unknown what the flow velocities are. During this research it was not possible to perform measurements during heavy conditions. At mild conditions we assume that the tide velocity is the main driving mechanism behind the flow velocity in the lagoon. The effect of waves and wind on the flow velocity during storm conditions must be investigated. Moreover, aeolian transport measurements are performed within this research by placing bins at the sand layer. There are more measurement techniques available to obtain the aeolian transport capacity. Measurement devices as a laser-scanner, leatherman sand trap, saltiphone or wengler fork laser could give more insight in the aeolian transport at the lagoon.

- During this research the BIP-measurements by PUMA were used to calculate the volume increase over the past 5 years. Yearly BIP-measurements are only performed by PUMA in April or May. It would be useful to have also field data in between, for example around November. Within this research an increased data resolution is obtained by calculating the surface areas from satellite images. But it would be better to have more BIP-measurements in order to say something about the shape development of the sand layer.

Further research: model improvement

- During this research we translated the waves from Europlatform for the years 2013-2018 nearshore using the bathymetry of 2018. The alongshore sand transport in northern direction extended the foreshore in front of the cube reef. Therefore, the bathymetry in, for example, 2014 was different than in 2018. The water depth was deeper for several sections in 2014, therefore higher waves are present in front of the cube reef, which are responsible for more overtopping. The real effect of a different bathymetry must be investigated.

- To decrease the uncertainty of the overtopping calculation, the large inaccuracy of the sediment concentration in the water column by Van Rijn (1984) must be investigated. The total sediment load cannot be predicted with an inaccuracy less than a factor 2 because the accuracy of the main controlling parameters is too low, while also the total load data used for calibration and verification show deviations up to a factor 2. Physical modelling or field investigations are necessary to reduce the uncertainty of the overtopping calculation.

- Within this research only the uncertainty of the overtopping calculation is investigated. The uncertainty of the transport by the tide and aeolian transport could also be analysed. This would complete the uncertainty analysis and thereby a better explanation could be given for the 20,000 m^3 of sand unaccounted for in our estimated 71,000 m^3 volume of sand in the lagoon.

- We assumed during this research that there is probably no outflux of sediment during overtopping. The outflux of all mechanisms is not investigated during this research. More investigation into the outflux can add value to this research.

- The transport by the tide is estimated as the volume of water between low and high tide multiplied by the sediment concentration in the water. More research towards the propagation of a water volume through the cube reef is necessary. The knowledge about the sediment movement through the cube reef is limited.
- The used overtopping equation has his limits by applying it on a structure like the cube reef. There is no literature about the overtopping rates over a structure like the cube reef. Large holes are present between the cubes, therefore the overtopping volumes are probably larger in reality than the outcome of the formula. These holes are not taken into account by defining the amount of free-board. The amount of free-board is defined as the difference between the highest point of the cube reef and the water level.
- Based on the results of this research, many conclusions can be drawn in a qualitative way, but quantitatively the calculated numbers do not entirely match the total sand layer volume. Investigation towards the transition zone with more detailed models like Delft3D or XBeach could give more information about the foreshore development in northern direction. Before these models can be applied, it must be investigated how the cube reef can be incorporated in these models. The cube reef makes it hard to model the transition zone.

Bibliography

Aeroview b.v. Luchtfotografie. URL `http://www.aeroview.nl/`.

R.A. Bagnold. The transport of sand by wind. *Geographical journal*, 1937.

M. Boers. Technisch rapport duinwaterkeringen en hybride keringen. Technical report, Deltares, 2012.

J. Bosboom and Marcel J.F. Stive. *Coastal Dynamics I, Lecture notes CIE4305*. Delft Academic Press, 2015.

Deltares. Delft3D FLOW User Manual. Technical report, Deltares, 2014.

D. Gallach-Sánchez, P. Troch, and A. Kortenhaus. A Critical Analysis and Validation of the Accuracy of Wave Overtopping Prediction Formulae for OWECs. *Energies*, pages 1–20, 2018. doi: 10.3390/en11010133.

Havenbedrijf Rotterdam NV. 'stenig duin met blokkendam', 2010. URL `https://www.maasvlakte2.com/uploads/factsheet_harde_zeewering.pdf`.

Havenbedrijf Rotterdam NV. Maasvlakte 2, 2013a. URL `https://www.portofrotterdam.com/en/news-and-press-releases/maasvlakte-2`.

Havenbedrijf Rotterdam NV. Maasvlakte 2, van plan tot uitvoering, 2013b. URL `https://www.maasvlakte2.com/nl/index/show/id/109/aanleg`.

Havenbedrijf Rotterdam NV. Maasvlakte 2: five years of operation, 2018. URL `https://www.portofrotterdam.com/en/news-and-press-releases/maasvlakte-2-five-years-of-operation`.

B. Hofland and M. Van Gent. Maasvlakte 2 Harde Zeewering, Stenig Duin + Blokkendam: Meetrapport van aanvullend 2D schaalmodelonderzoek Scheldegoot - Proevenseries 1 t/m 10. Technical Report no. 1001806-016, Deltares, 2010.

B. Hofland and M. Van Gent. Maasvlakte 2 Harde Zeewering, Stenig Duin + Blokkendam: Meetrapport van aanvullend 2D schaalmodelonderzoek Scheldegoot - Proevenseries 11 t/m 21. Technical Report no. 1001804-019, Deltares, 2011.

B. Hoonhout. *Aeolian Sediment Availability and Transport - Proefschrift*. 2017. ISBN 978-94-6332-152-5.

J.F. Kok, E.J.R. Parteli, T.I. Michaels, and D. Bou Karam. The physics of wind-blown sand and dust. *Reports on Progress in Physics*, 75(10):1–119, 2012. ISSN 00344885. doi: 106901.

A. Lako. Morphodynamic behaviour of coastal hard-soft transitions. Master's thesis, Delft University of Technology, 2019.

G.J.A Loman. " Maasvlakte 2 " project : the winning DCM bid with an EMSAGG focus on the innovative cobble sea defense. Technical report, EMSAGG Conference, Rome, Italy, 2009.

T. Olthoff. Longshore transport of coarse-grained material. Master's thesis, Delft University of Technology, 2019.

M. Onderwater. Optimalisatie van beheer en onderhoud rondom noordelijke beeindiging van zachte zeewering van Maasvlakte 2. Technical report, Arcadis, 2016.

M. Onderwater. Maasvlakte 2, noordelijk deel van ZZ en Conus - Uitwerking werkelijke standzekerheid t.b.v. aanpassing keuringsmethodiek. Technical report, Arcadis, 2017.

M. Onderwater. Memo - Effect van meer zand in het duin bij Kp3.495 op de Standzekerheid en onderhoudsfrequentie. Technical report, Arcadis, 2018a.

M. Onderwater. Maasvlakte 2, noordelijk deel van ZZ en Conus - Uitwerking werkelijke standzekerheid t.b.v. aanpassing keuringsmethodiek. Technical report, Arcadis, 2018b.

PredictWind. Ocean Racing & Americas Cup proven, highest resolution wind & marine forecasts on the web., 2018. URL https://forecast.predictwind.com.

T. Pullen, N.W.H. Allsop, T. Bruce, A Kortenhaus, H. Schüttrumpf, and J.W. Van der Meer. EurOtop: Manual on wave overtopping of sea defences and related structures. page 185, 2007. ISSN 01613782. URL www.overtopping-manual.com.

PUMA. Buitencontour: Beheer- & Instandhoudingplan (BIP) van Instelperiode van zandige Buitencontour. Technical Report no. puma-p-mo-onb05, Projectorganisatie Uitbreiding Maasvlakte, Rotterdam, 2008a.

PUMA. Maasvlakte 2: Prognose van grootschalige ontgronding van voorland. Technical Report no. puma-p-po-onb01, Projectorganisatie Uitbreiding Maasvlakte, Rotterdam, 2008b.

PUMA. Zachte Zeewering: Prognose van onderhoudsuppletie. Technical Report no. puma-p-mo-onb07, Projectorganisatie Uitbreiding Maasvlakte, Rotterdam, 2008c.

PUMA. Zachte Zeewering: Beperking van hinder stuifzand. Technical Report no. puma-p-mo-onb08, Projectorganisatie Uitbreiding Maasvlakte, Rotterdam, 2008d.

PUMA. Harde Zeewering: Calibratie van golftransmissieformule voor variant SD+B. Technical Report no. puma-p-jwm-mo06, Projectorganisatie Uitbreiding Maasvlakte, Rotterdam, 2009.

PUMA. Voortgang binnencontour per 1/10/2012. Technical report, Projectorganisatie Uitbreiding Maasvlakte, Rotterdam, 2012a.

PUMA. Voortgang buitencontour per 1/10/2012. Technical report, Projectorganisatie Uitbreiding Maasvlakte, Rotterdam, 2012b.

PUMA. Samenvatting keuringen en ervaringen Instelperiode: Volume morfologische schillen. Technical Report no. puma-bc-tvij-mi904, Projectorganisatie Uitbreiding Maasvlakte, Rotterdam, 2018.

Rijkswaterstaat. Open data rijkswaterstaat, 2018. URL https://www.rijkswaterstaat.nl/zakelijk/open-data.

Satellietbeeld. Satellite images for the netherlands, 2018. URL http://satellietbeeld.nl/.

Netherlands Space Office Satellietdataportaal. Satellite images for the netherlands, 2018. URL https://satellietdataportaal.nl/.

J. Ter Brugge. 'maasvlakte 2: polderen in de zee', 2006. URL https://www.historici.nl/maasvlakte-ii-polderen-in-de-zee/.

J. Van Der Meer, M. Asce, and T. Bruce. New Physical Insights and Design Formulas on Wave Overtopping at Sloping and Vertical Structures. *Journal of Waterway, Port, Coastal, and Ocean Engineering*, pages 1–18, 2014. doi: 10.1061/(ASCE)WW.1943-5460.0000221.

J.W. Van der Meer, N.W.H. Allsop, T. Bruce, J. De Rouck, A Kortenhaus, T. Pullen, H. Schüttrumpf, P. Troch, and B. Zanuttigh. EurOtop: Manual on wave overtopping of sea defences and related structures. page 304, 2018. URL www.overtopping-manual.com.

M. Van Gent and M. Muttray. Maasvlakte 2: Zachte Zeewering, Sectie Noordelijke Beëindiging: Meetrapport van aanvullend 2D schaalmodelonderzoek, Proevenseries 7 t/m 12. Technical report, Delft Hydraulics, 2009.

M.R.A Van Gent and G.M. Smith. Maasvlakte 2: Zachte Zeewering, sectie Noordelijke Beëindiging: Meetrapport van 2D schaalmodelonderzoek, Doorsnedes 1 en 2, Proevenseries 1 t/m 6. Technical report, Delft Hydraulics, 2007a.

M.R.A Van Gent and G.M. Smith. Appendix bij rapport over Maasvlakte 2: Zachte Zeewering, sectie Noordelijke Beëindiging: Meetrapport van 2D schaalmodelonderzoek, Doorsnedes 1 en 2, Proevenseries 1 t/m 6. Technical report, Delft Hydraulics, 2007b.

M.R.A. Van Gent and I.M. Van Der Werf. Maasvlakte 2: Harde Zeewering, Stenig Duin + Blokkendam: Meetrapport van aanvullend 2D schaalmodelonderzoek Deltagoot, Proevenseries 13 t/m 15. Technical report, Deltares, 2010.

Van Oord. Contractor puma completes first part of maasvlakte 2, 2013. URL `https://www.vanoord.com/news/2013-contractor-puma-completes-first-part-maasvlakte-2`.

L.C. Van Rijn. Sediment transport, Part II: Suspended load transport. *Journal of Hydraulic Engineering ASCE*, pages 1–29, 1984. ISSN 0733-9429/84/0011-1613/01.00.

L.C. Van Rijn. Sediment transport in combined currents and waves. *Euromech 262 - Sand transport in Rivers, Estuaries and the Sea*, 1991.

L.C. Van Rijn. Simple general formulae for sand transport in rivers, estuaries and coastal waters, 2013. URL `www.leovanrijn-sediment.com`.

L.C. Van Rijn. Aeolian transport over a flat sediment surface, 2018. URL `www.leovanrijn-sediment.com`.

L.C. Van Rijn, M.W.C. Nieuwjaar, T. Van Der Kaay, E. Nap, and A. Van Kampen. Transport of fine sands by currents and waves. *Journal of Waterway, Port, Coastal, and Ocean Engineering*, 1993. ISSN 0733-950X/93/0002-0123.

L.C. van Rijn, J.A. Roelvink, and W. ter Horst. Approximation formulae for sand transport by currents and waves and implementation in delft-mor. Technical report, Delft Hydraulics, 2001.

L.C. Van Rijn, D.J.R. Walstra, and M. Van Ormondt. Description of transpor2004 and implementation in delft3d-online. Technical report, Delft Hydraulics, 2004.

P. Zaalberg. The relation between cobble revetments, sand and overtopping. Master's thesis, Delft University of Technology, 2019.

A
Satellite images Maasvlakte 2

All images are obtained from Satellietdataportaal (2018) and Satellietbeeld (2018).

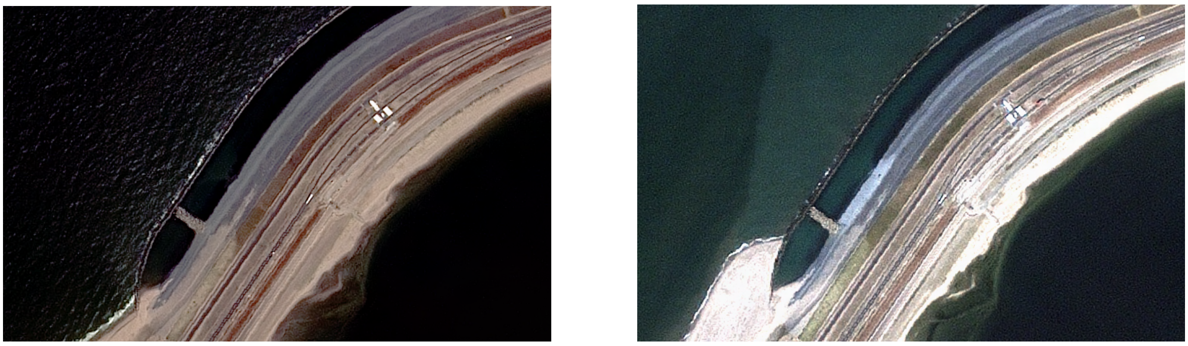

Figure A.1: Satellite image of 2014/07/07 (left) and 2014/09/18 (right). In the right picture the beach nourishment is visible

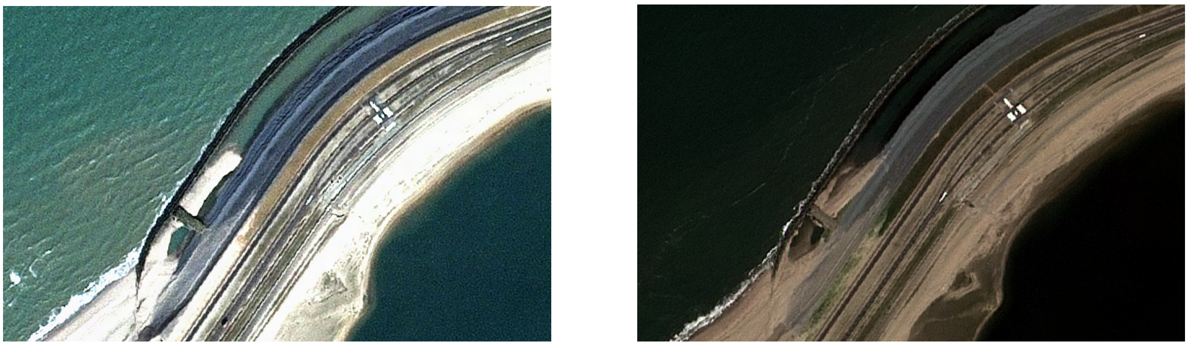

Figure A.2: Satellite image of 2015/02/18 (left) and 2015/05/17 (right)

Figure A.3: Satellite image of 2015/08/22 (left) and 2016/03/13 (right). In the left figure, the artificially removed sand volume is visible

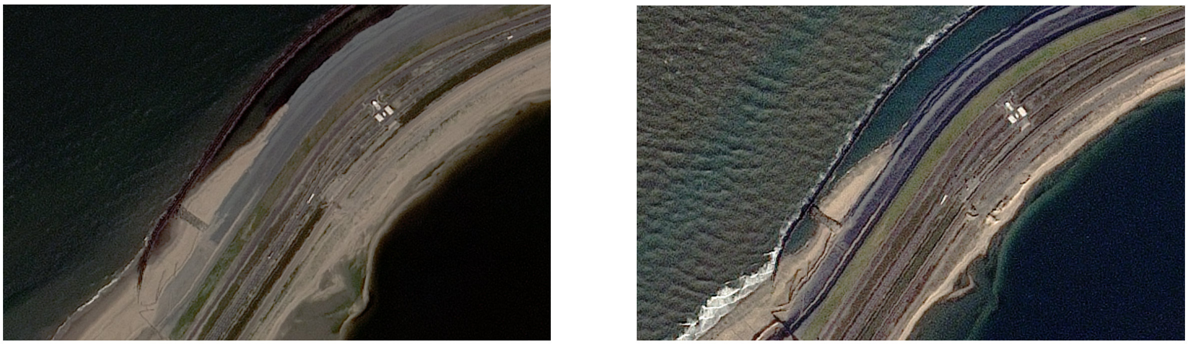

Figure A.4: Satellite image of 2016/07/04 (left) and 2016/11/11 (right)

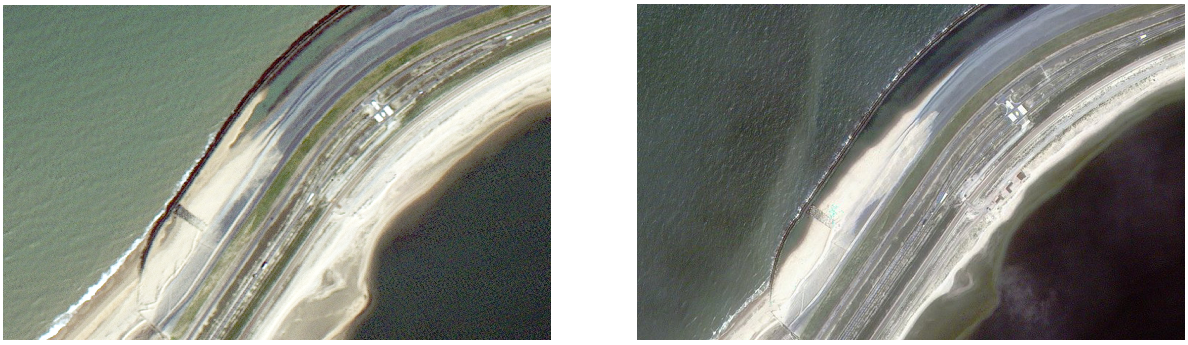

Figure A.5: Satellite image of 2017/03/28 (left) and 2017/08/01 (right)

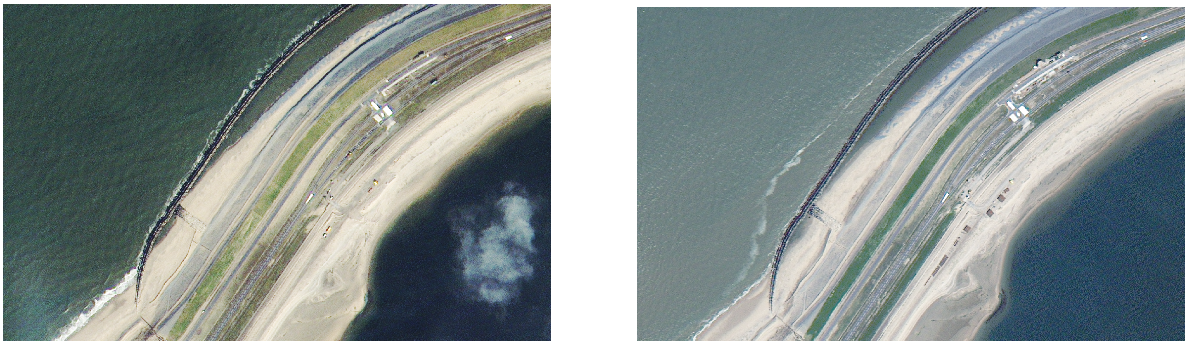

Figure A.6: Satellite image of 2018/03/29 (left) and 2018/05/03 (right)

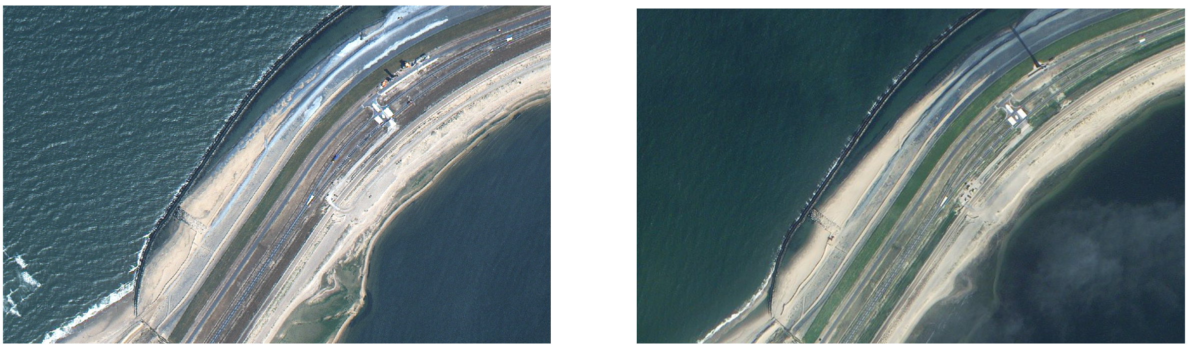

Figure A.7: Satellite image of 2018/06/27 (left) and 2018/09/17 (right)

B

Recent research Maasvlakte 2

During the design and adaptation period different studies were performed around Maasvlakte 2. PUMA did the design studies and PUMA + Arcadis performed studies during the adaptation period at the soft protection. During these analysis the profiles of the soft protection are categorized into four morphological zones (see figure B.1):

- Dune (= Duinreep) : profile above NAP+3m
- Beach (= Strandoever) : profile between NAP+3m en NAP-4m
- Shoreface (= Vooroever) : profile between NAP-4m en NAP-8m
- Offshore (= Kustfundament): profile between NAP-8m en NAP-20m, this section is again divided into a shallow and deep part

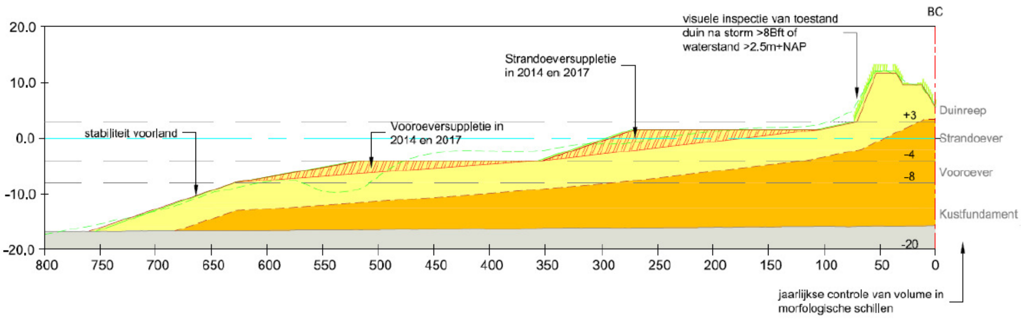

Figure B.1: The different morphological zones in the profile

During the design period the main (hydraulic) causes for sediment losses for the soft protection are investigated by PUMA and stated as follows (PUMA, 2008c):

- cross-shore transport caused by incoming waves
  - (wave induced) cross-shore transport can re-profile the profile. A storm can cause for large changes.
- large-scale erosion at the toe of the constructed profile
  - this erosion is caused by the contraction of the tides (mainly the northern directed flood-current).
- different cross-shore transport as a result of toe-erosion
  - if the shoreface is deeper, higher waves can reach the beach. And through the fact that bottom slopes become steeper, the seaward-directed cross-shore transport is increasing. Which result in erosion.
- longshore transport caused by oblique incoming waves, combined with tide- and wind-driven currents
  - to indicate sediment losses, the spatial gradients are important. These gradients can appear as a result of different hydraulic conditions (waves and tides), coastal orientation and differences in sediment supply. For example, the soft protection ends quite abruptly at the transition zone. Waves from a northern direction cause for a southern directed current and, therefore transport. But at the hard flood defence is no sand available, therefore the transport capacity starts at zero in the transition zone. This abrupt ending of the hard flood defence influences the sediment capacities.

B.1. Adaptation Period - studies performed by Arcadis

Arcadis performed four investigations towards the sand transport at the soft protection: Onderwater (2016), Onderwater (2017), Onderwater (2018a) and Onderwater (2018b). The main conclusions of these studies are given in this section. The morphological studies were performed with the main objective to find a practical solutions for the excessive erosion in the area, and to reformulate the method for assessing the safety of the system, such that the requirements, set by the Port of Rotterdam, can be met after the adaptation period.

Study of Onderwater (2016):
During this first study of Arcadis, it appeared that several transects did not have enough spares to be able to withstand the expected erosion for the coming year. During the adaptation it was observed that the nourishment strategy was not working as expected. Therefore, Arcadis was asked to conduct a first, morphological study. The main conclusions from this study were:
1. A rotation of the coastline was visible: the northernmost 300m coastline of the soft flood defence was rotated with an angle to the original orientation.
2. A characteristic cross-shore profile was visible, with a sand bar and a trough.
3. Natural dynamics: at the transition zone, large gradients in sediment transport are present.
4. The beach nourishments in 2014 on the cone turned out to be rather effective and eroded quite fast. The shoreface volume appeared to be rather stable and even bigger than the required volume.

Arcadis observed the profile changes of different measurements. It appears that in the upper part of the cross-section the differences between the measurements were unstructured. And in the lower part of the profile the changes are more gentle and in the direction of the dominant tide. Therefore it was concluded that the sediment transport higher in the profile (above NAP-8m) is dominated by the waves and lower in the profile by tides. It is also concluded that the tide-dominated transport is not influenced by the waves and the other way around. These conclusions are confirmed by the results of a created Delft3D model.
With the Delft3D model the currents are modelled caused by the tides from the Nieuwe Waterweg and Haringvliet. From these results a large flood-current is visible along the soft protection and a large ebb-current along the hard protection. At the transition zone a mild, seeward directed, current is visible. See figures B.2, B.3 and B.4. The complexity of the transition zone creates dynamic processes. Large sediment gradients are present in this area.

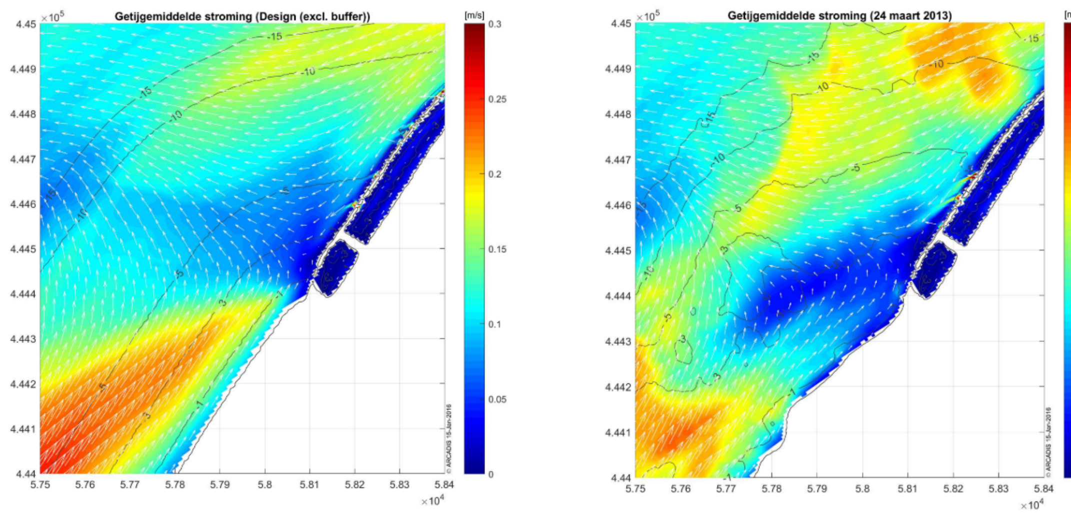

(a) Tide averaged current with design bathymetry

(b) Tide averaged current with the measured bathymetry

Figure B.2: Tide averaged current with the design and the measured bathymetry at 24 March, 2013

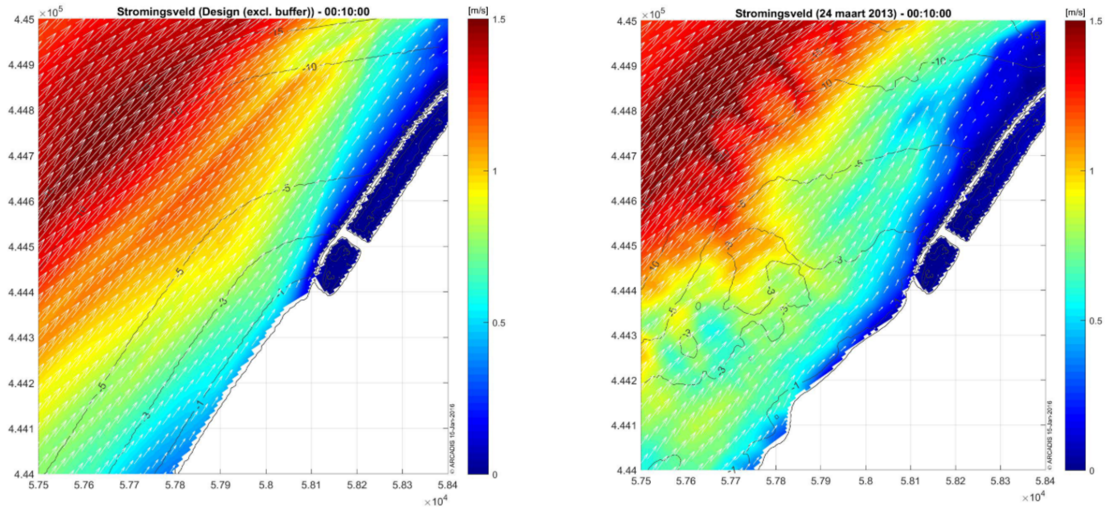

(a) Flood current with design bathymetry

(b) Flood currents with the measured bathymetry

Figure B.3: Flood current with the design and the measured bathymetry at 24 March, 2013. Showing maximum flood velocities

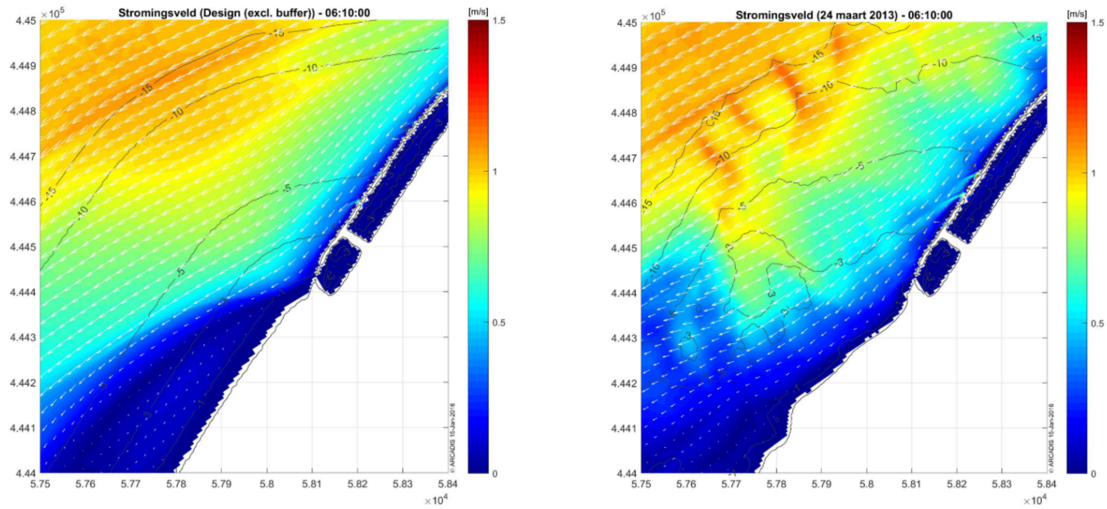

(a) Ebb current with design bathymetry

(b) Ebb current with the measured bathymetry

Figure B.4: Ebb current with the design and the measured bathymetry at 24 March, 2013. Showing maximum ebb velocities

Study of Onderwater (2017):

XBeach is used to better understand the 2D-effects around the Maasvlakte. During this study the assessment method was investigated. An advantage of this model is that physical processes can be investigated better. A disadvantage is that the safety assessment is more complex. The XBeach results are not used to perform the safety assessment. The bar-trough was again visible (was also visible in the study of 2016). The beach erosion higher in the profile and sedimentation lower in the beach profile was shown. Another obtained result was that the relatively larger shoreface volume, causes for more wave damping, which resulted in a decrease of dune retreat of about 7 to 8 meters.

Study of Onderwater (2018a) and Onderwater (2018b):

The most important conclusion from this report was that it appears from the 2017 measurements that the nourishment of 2016 eroded very quickly (just like was the case for the 2014 nourishment). And the method for the safety assessment was changed. See chapter 2.

B.2. Conclusion of performed studies

The last nourishment is performed in 2018. Following from the latest study of PUMA (2018) the morphological behaviour of the transition zone is determined by the strength and direction of the storms. Nourishments in the transition zone are not as effective as planned, because the nourishment is spreading out quickly. On the other hand, nourishments on the shoreface works positively for the safety of the transition zone. Based on the analysis and tables B.1 and B.2, the following general conclusions are made:

- morphological behaviour:
  - Erosion rates are higher at the beach and lower at the shoreface. Large fluctuations are present in the average erosion/accretion rates.
- nourishments:
  - In total 3.1 million m^3 sand is placed. This is significantly lower than the planned 3.9 million m^3. This can be explained by a milder wave climate or through conservative assumptions during the prognoses.
  - The transition zone and the recreative beach at the southern part of Maasvlakte 2 are two areas with the most erosion.

jaar	dune	beach	shoreface	offshore	**total**
2014	0	0.57	0.99	0	**1.55**
2016	0	0.83	1.55	0	**2.38**
2018	0	0.83	1.55	0	**2.38**
total	**0**	**2.22**	**4.09**	**0**	**6.32**

Table B.1: Predicted nourishments during adaptation period (in million m3)

jaar	dune	beach	shoreface	offshore	total
2014	0	0.76	0	0.31	**1.7**
2014	0	0.35	0	0	
2014	0	0.3	0	0	
2016	0	0.35	0	0.58	**1.4**
2016	0	0.46	0	0	
total	**0**	**2.22**	**0**	**0.89**	**3.1**

Table B.2: Applied nourishments during adaptation period (in million m3)

The adaptation period is almost finished. During this period two nourishments are planned: 2020 and 2022. The nourishment of 2022 will be larger than usual, because this nourishment must hold for 2.35 years to finish the maintenance period. Looking at the prior nourishments, in general 1.55 million m^3 of sand is placed. Through the fact that the nourishment of 2022 is larger, the amount of sand is estimated by 2.5 x 1.55 = 3.9 million m^3 sand.

B.3. Compass with directions

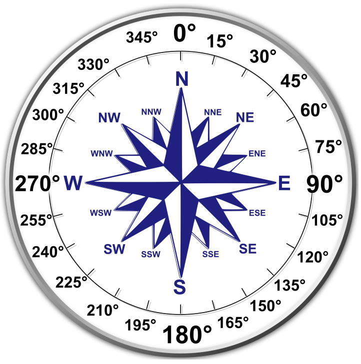

Figure B.5: Compass with directions for a better interpretation of tables 3.2 and 3.1 in Chapter 2

C

Wave climate analysis

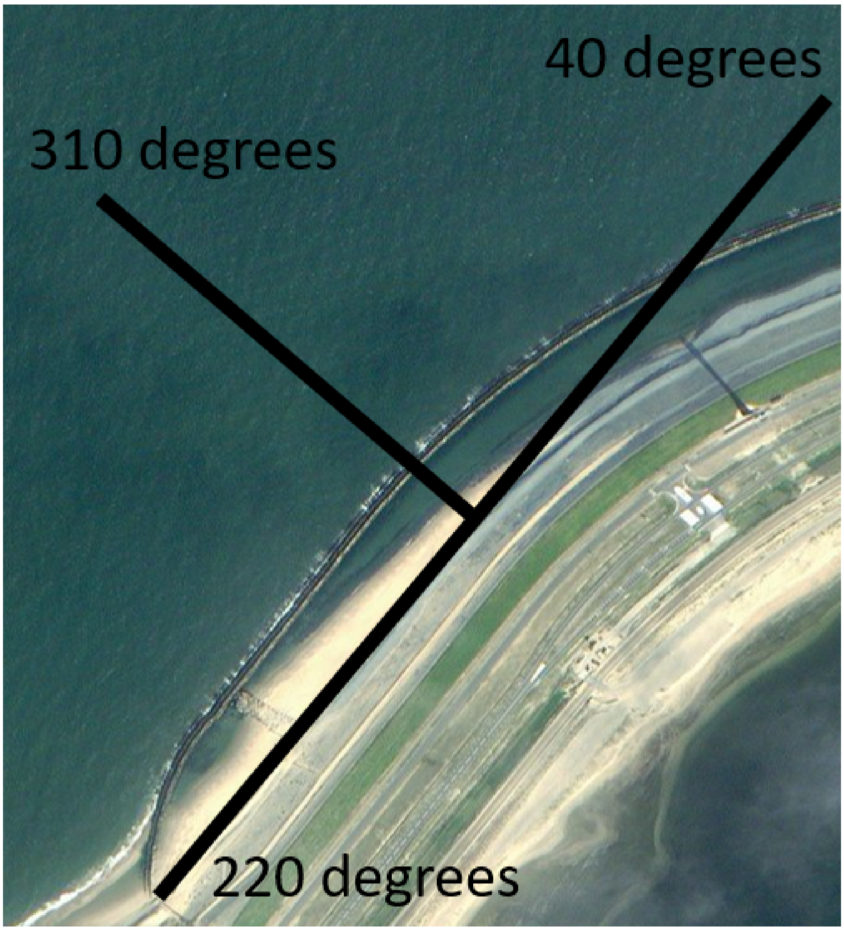

Figure C.1: Coastal orientation and the domain for the wave fluxes (between 220 and 40 degrees)

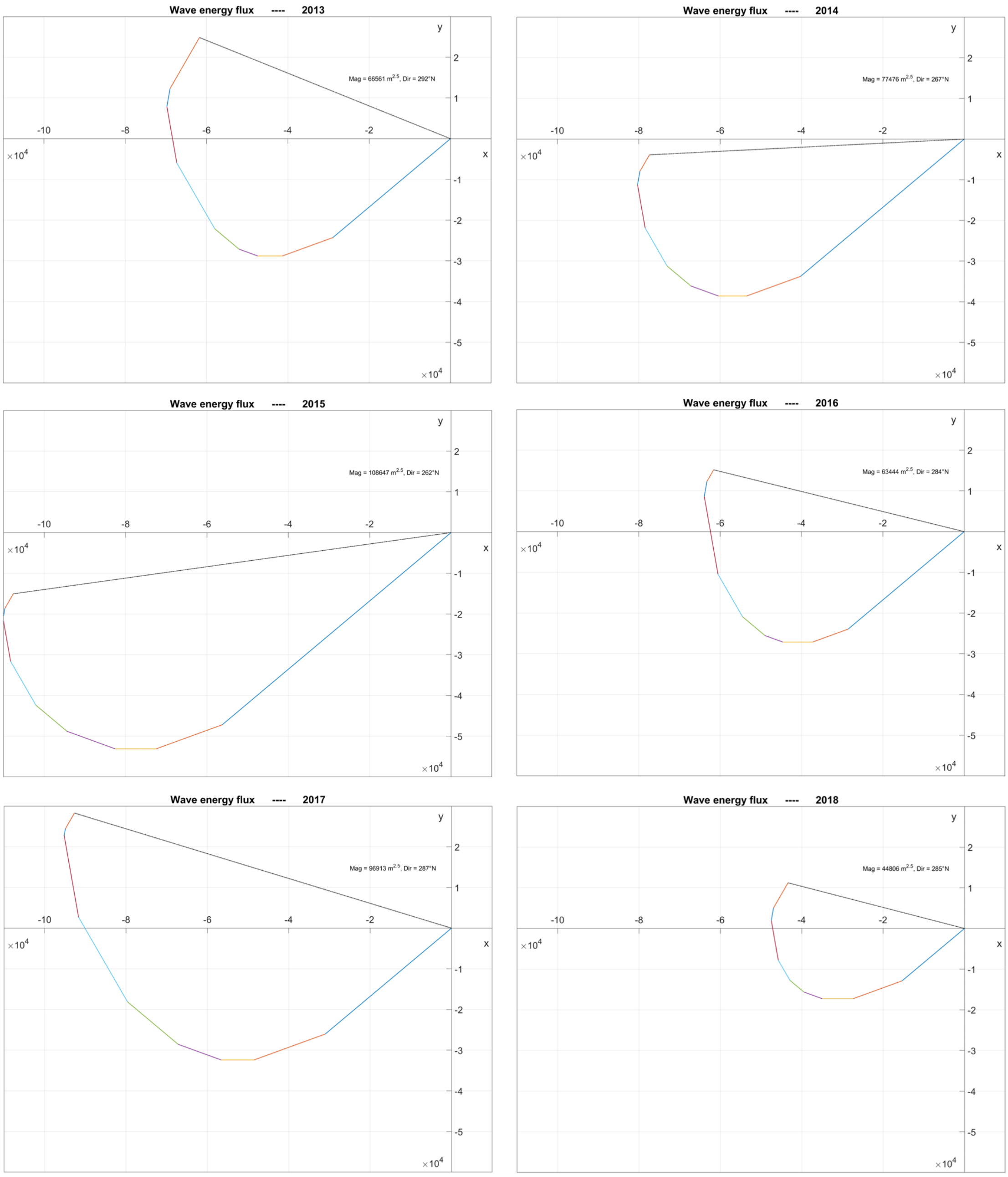

Figure C.2: Wave fluxes for the year round conditions of 2013 - 2018 from Europlatform

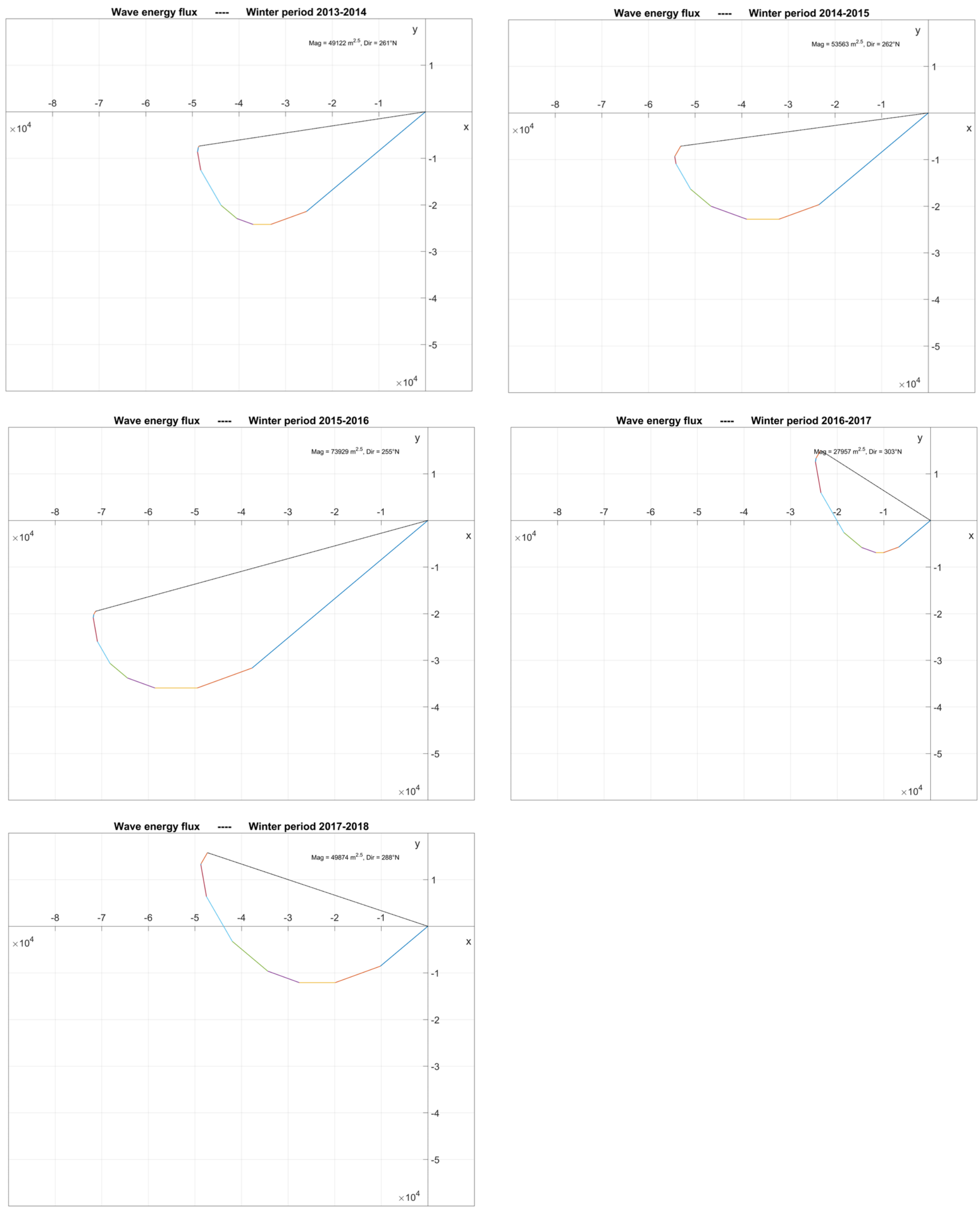

Figure C.3: Wave fluxes for the winter periods from 2013 until 2018 from Europlatform. The winter is defined from October 1st until April 15th.

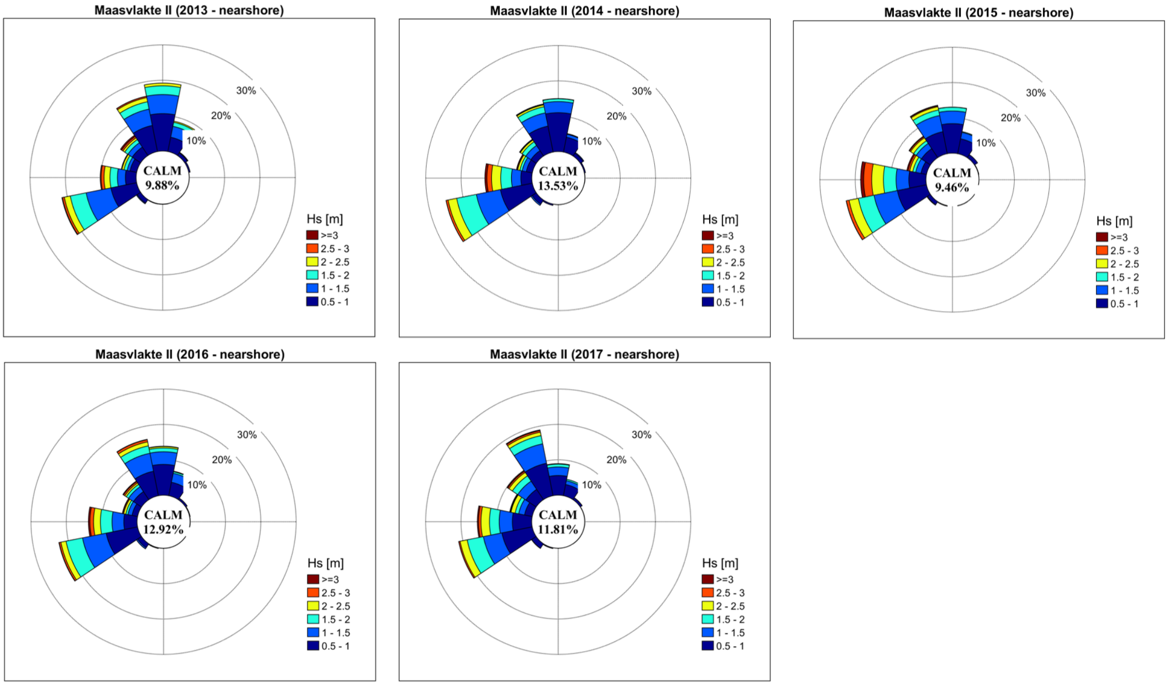

Figure C.4: Near-shore waves roses for the year round conditions of 2013 - 2018 from a point 500m offshore. The colors indicate the wave height and the length of the colorbar represents the percentage of waves from that direction.

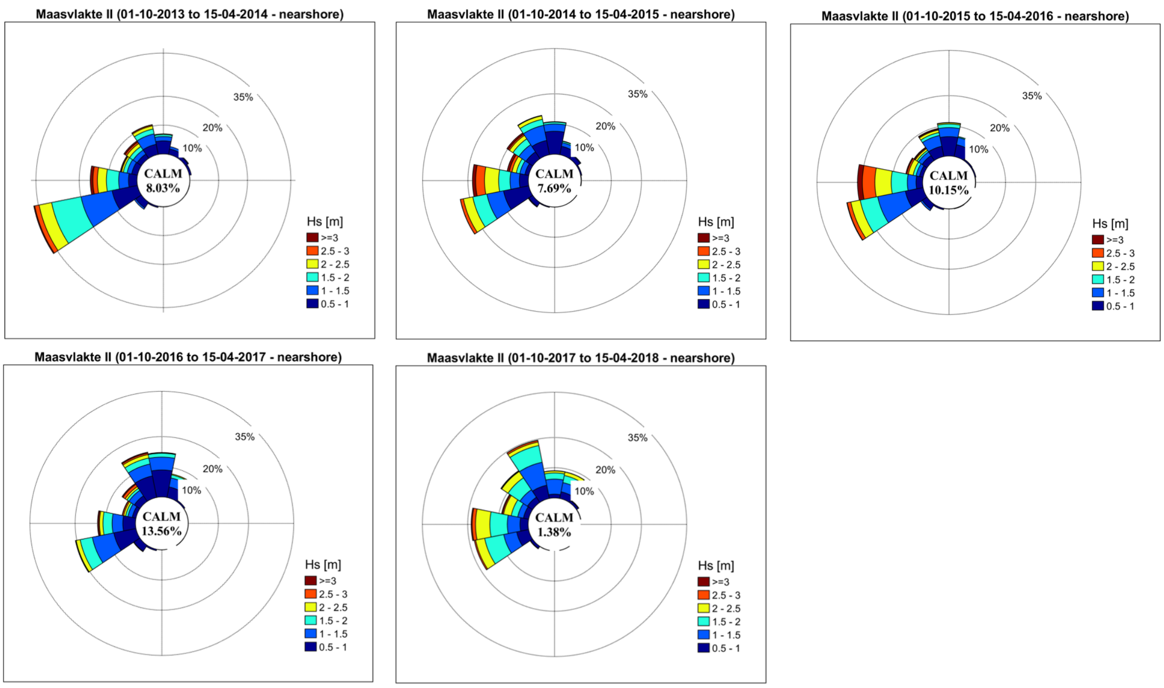

Figure C.5: Near-shore waves roses for the winters of 2013 - 2018 from a point 500m offshore. The colors indicate the wave height and the length of the colorbar represents the percentage of waves from that direction.

D

Sediment budget analysis

D.1. Storm impact

Cross-sections along the sand layer domain are shown in figures D.1 until D.5. In these figures the GPS measurement of November 5th (2018) and January 9th (2019) are plotted against the BIP-measurements of 2013 and 2018. The locations of the cross-sections are indicated with the black lines in figure 5.8b.

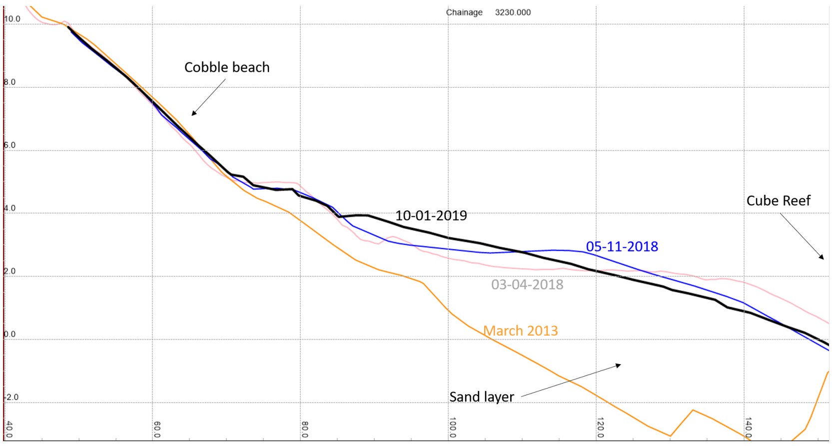

Figure D.1: KP3230

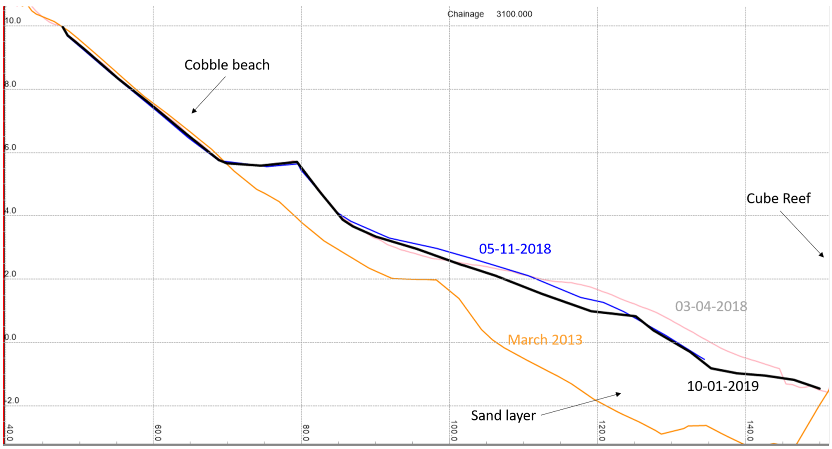

Figure D.2: KP3100

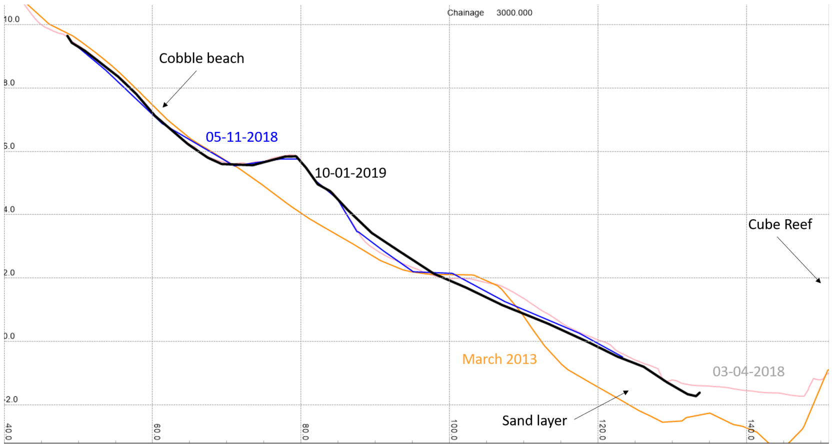

Figure D.3: KP3000

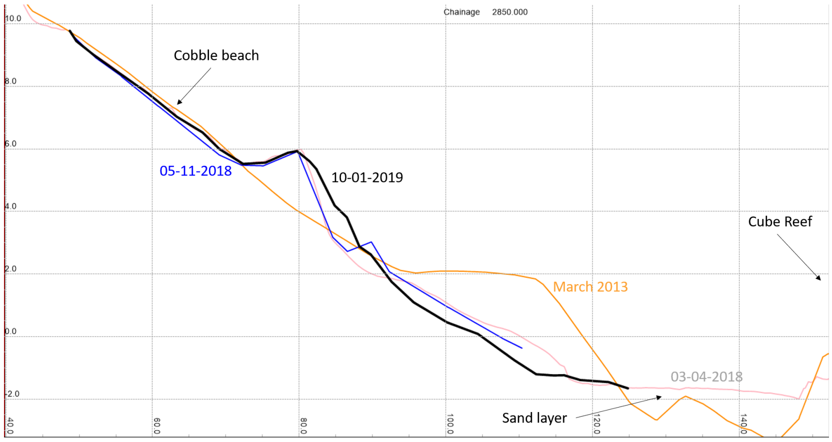

Figure D.4: KP2850

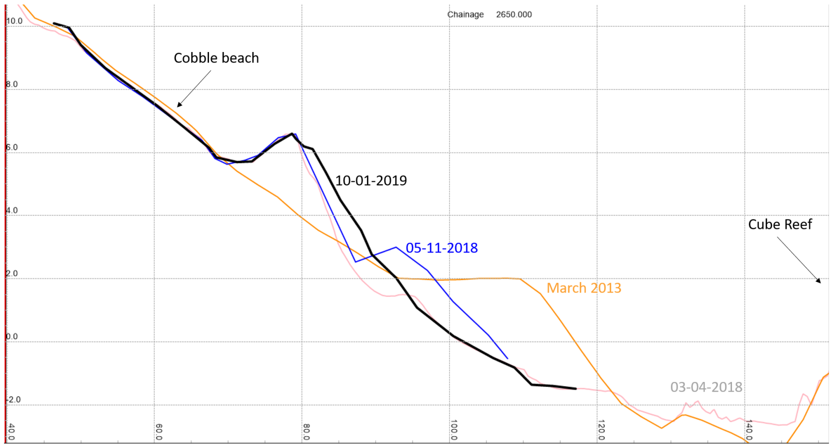

Figure D.5: KP2650

E

Hydrodynamic transport

E.1. Flow velocity measurements

Flow velocities are performed at Maasvlakte 2 to obtain more information about the processes. At December 12th (2019) the flow velocities are obtained with two devices:

- Valeport106 current meter
- GPS-drifters

See Chapter 6 figure 6.1 for an image of the two devices. During November 10th and November 20th oranges were dropped in the water and the flow velocity of those oranges is determined, these results are shown in chapter 6. In the following sections the method and results of the measurements at December 12th are described in more detail.

E.1.1. Tide directions

In the Netherlands there are two different tide directions. These directions are named a flood current and an ebb current. Two hours before high water the flood current is flowing in northern direction along the Dutch coast. This flood current is flowing until three to four hours after the highest water level. After that the current is in southern direction along the Dutch coast. This is called the ebb current. The ebb current is flowing from three to four hours after high water until two hours before high water. The change in flow direction is called the transition period. This will take about one hour. It will take approximately 12.25h from one high water to another high water (Bosboom and Stive, 2015). Wind velocity and direction could influence these the exact times that the flow is changing in direction. In figure E.1 all flow directions are schematically shown during the day of the measurements. The daily inequality is also visible in this figure.

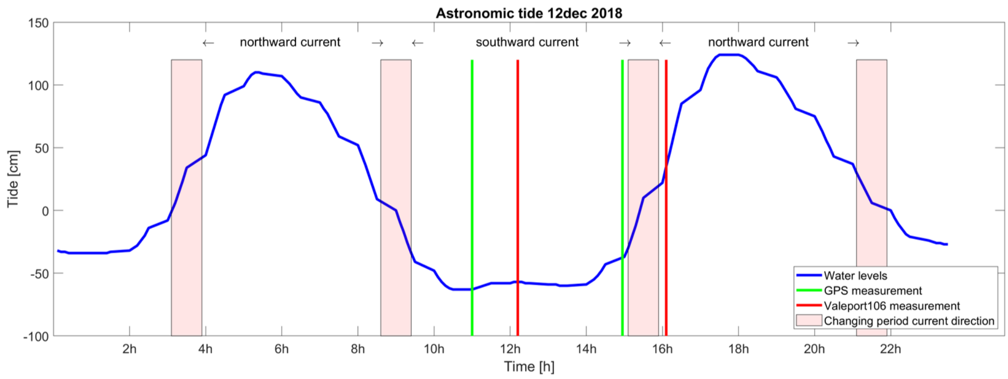

Figure E.1: Astronomic tides during the measurements at 12 December 2018

In figure E.1 all flow directions are schematically shown during December 12th. From this figure the following current directions are observed:
- during first GPS measurement: southern directed current
- during first Valeport measurement: southern directed current
- during second GPS measurement: in the changing period from south to north
- during second Valeport measurement: northern directed current

E.1.2. GPS-drifter results

The drifter devices consist of a constructed frame with a GPS device on top. The GPS is logging his location and velocities every second. The output of the drifters are NMEA-0183 messages, with the location given in degrees, minutes (dd° mm.mmm'). During the analysis of the results, the coordinate system is translated towards UTM (Universele transversale mercatorprojectie). In figure E.2a the drifters are located in the water in the canal in Delft to test the devices. In figure E.2b drifters are dropped into the water at Maasvlakte 2 during the measurement.

(a) GPS-drifters located in the canal in Delft

(b) Dropping the drifters in the lagoon at Maasvlakte 2

Figure E.2: The performed drifter measurements

E.1.3. Valeport106

In figure E.3 the locations of all Valeport measurements are shown. Three locations are performed during the first measurements (indicated with 1.x) and 7 locations during the second measurement (indicated with 2.x). Figures E.4 until E.13 are showing the measurement results from the Valeport106 current meter. For each location the measured velocity and direction are plotted. Some velocities are 0, this is probably due to the down/upward movement of the Valeport device during the measurements. Furthermore, it is visible that the velocities of the first measurements are in southern direction and the velocities of the second measurement in northern direction (this is due to the change in tidal direction, see figure E.1). At some locations during the first measurements, the velocities are higher in the top part of the water column. This is due to the wind influence. During the second measurement the tide and wind direction are against each other. The wind influence is not visible during these measurements.

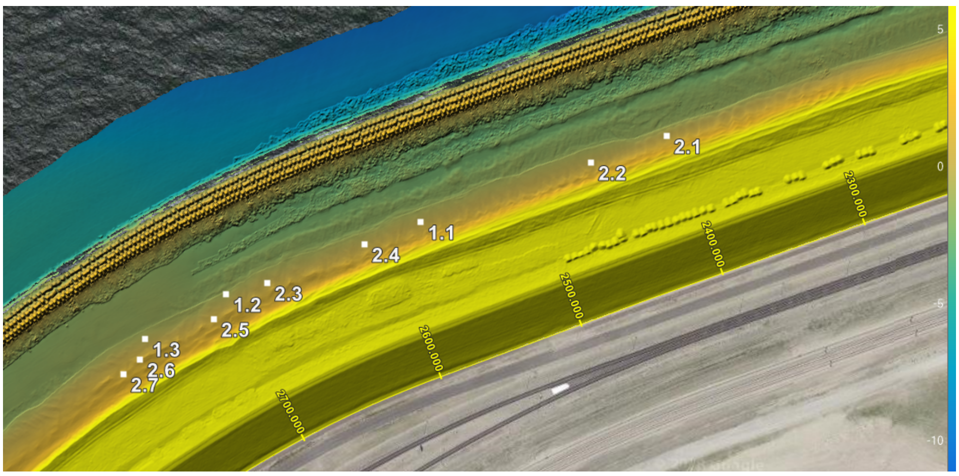

Figure E.3: All 10 locations of the Valeport measurements at December 12th, 2018

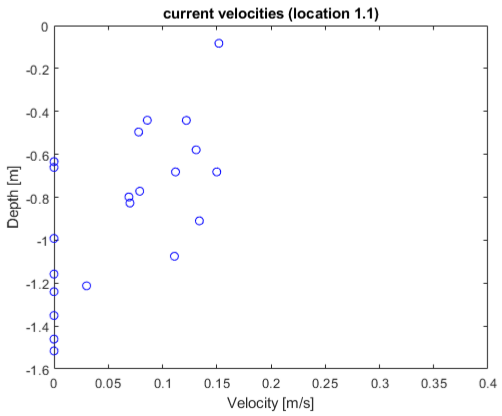

(a) Current velocities at location 1.1

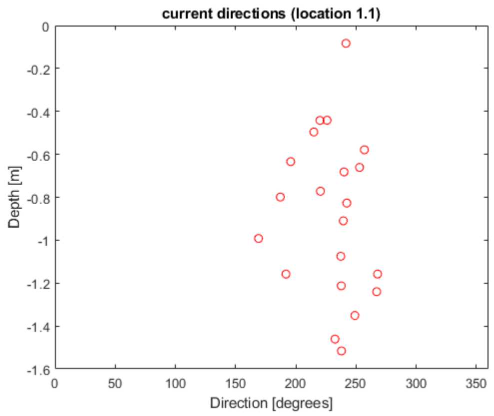

(b) Current directions at location 1.1

Figure E.4: Valeport measurements at location 1.1

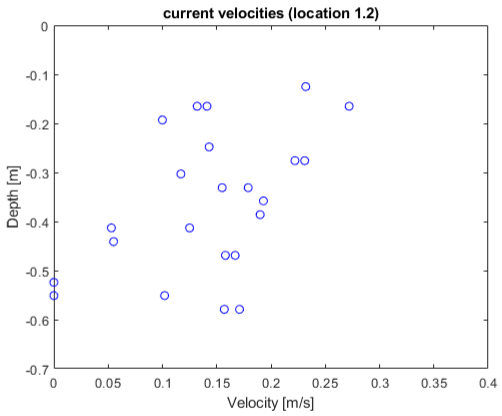

(a) Current velocities at location 1.2

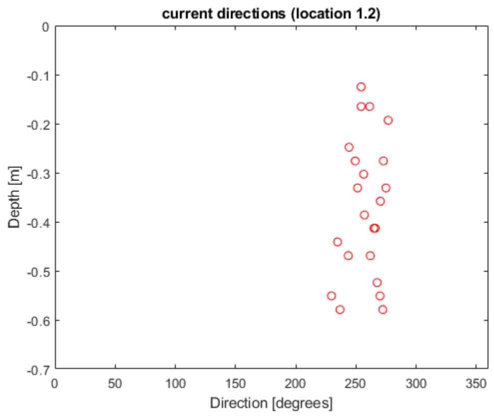

(b) Current directions at location 1.2

Figure E.5: Valeport measurements at location 1.2

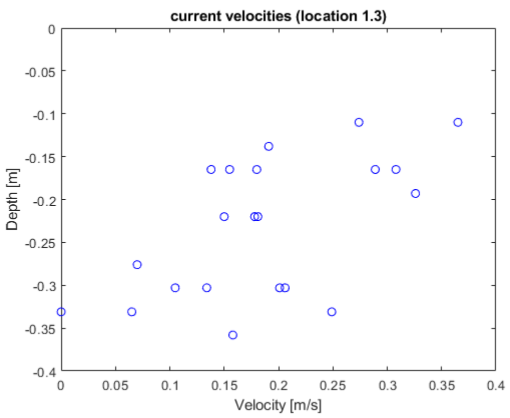

(a) Current velocities at location 1.3

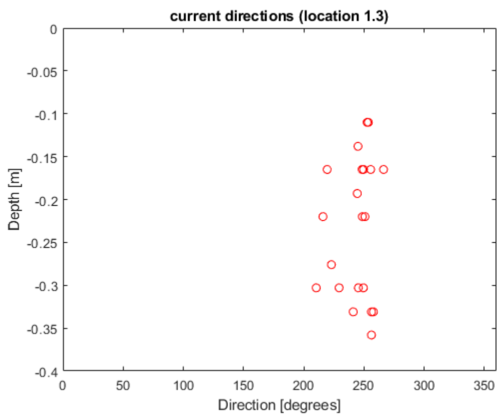

(b) Current directions at location 1.3

Figure E.6: Valeport measurements at location 1.3

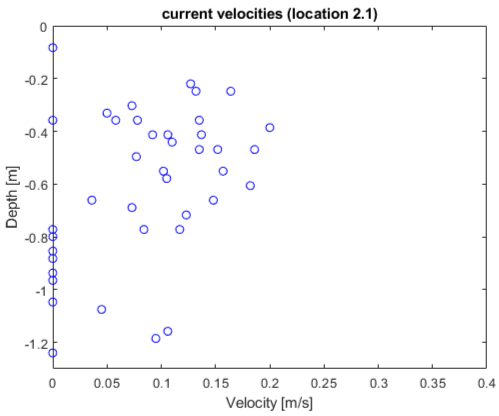

(a) Current velocities at location 2.1

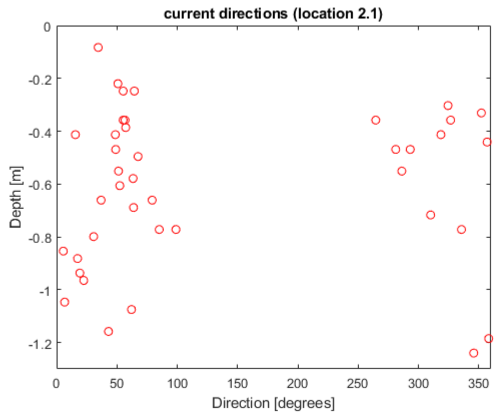

(b) Current directions at location 2.1

Figure E.7: Valeport measurements at location 2.1

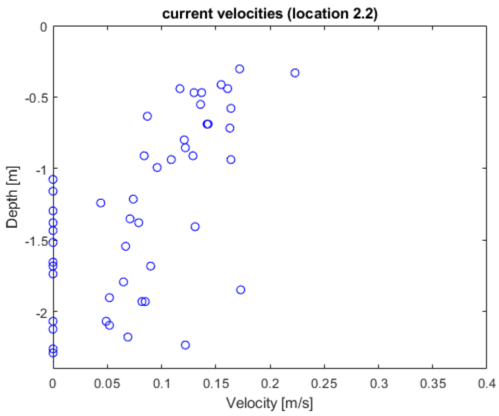

(a) Current velocities at location 2.2

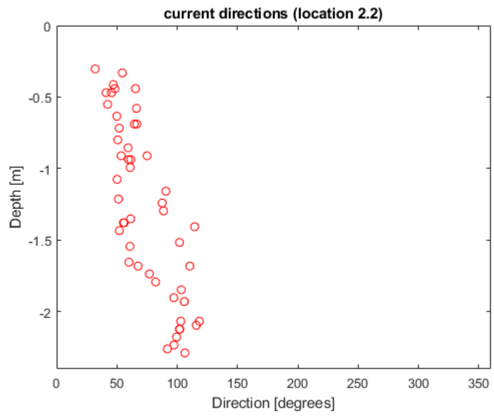

(b) Current direcitions at location 2.2

Figure E.8: Valeport measurements at location 2.2

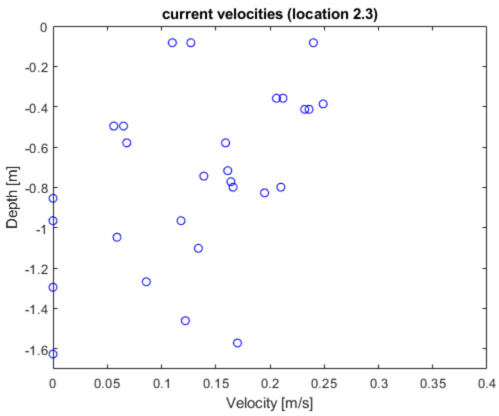

(a) Current velocities at location 2.3

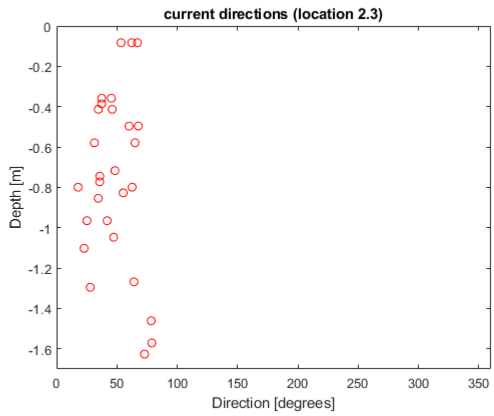

(b) Current directions at location 2.3

Figure E.9: Valeport measurements at location 2.3

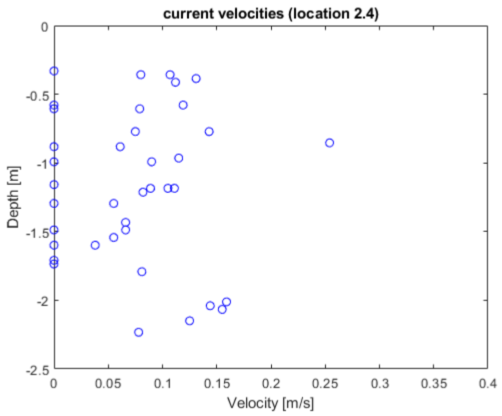

(a) Current velocities at location 2.4

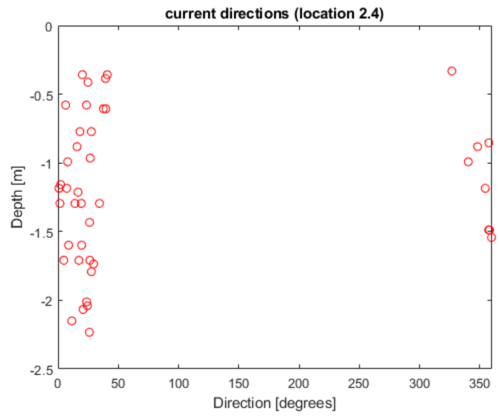

(b) Current directions at location 2.4

Figure E.10: Valeport measurements at location 2.4

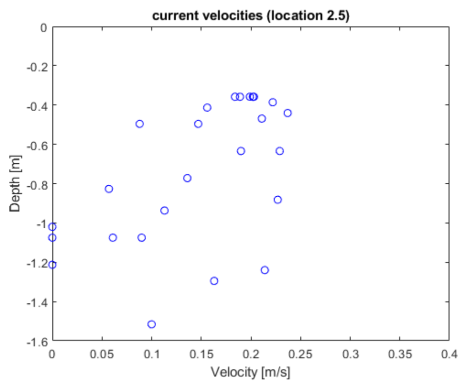

(a) Current velocities at location 2.5

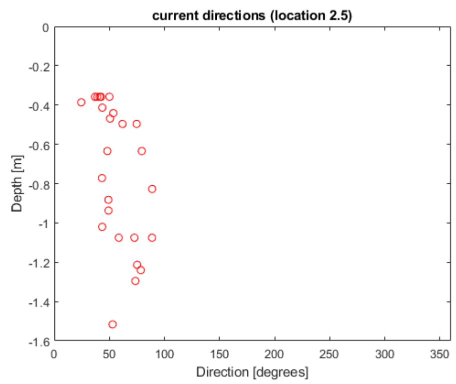

(b) Current directions at location 2.5

Figure E.11: Valeport measurements at location 2.5

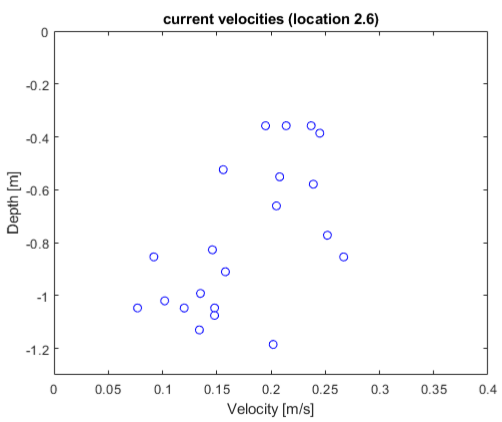

(a) Current velocities at location 2.6

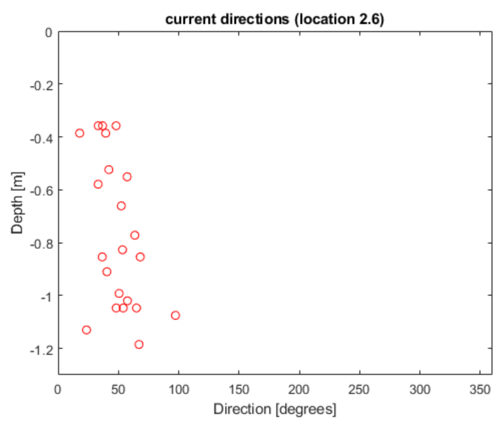

(b) Current directions at location 2.6

Figure E.12: Valeport measurements at location 2.6

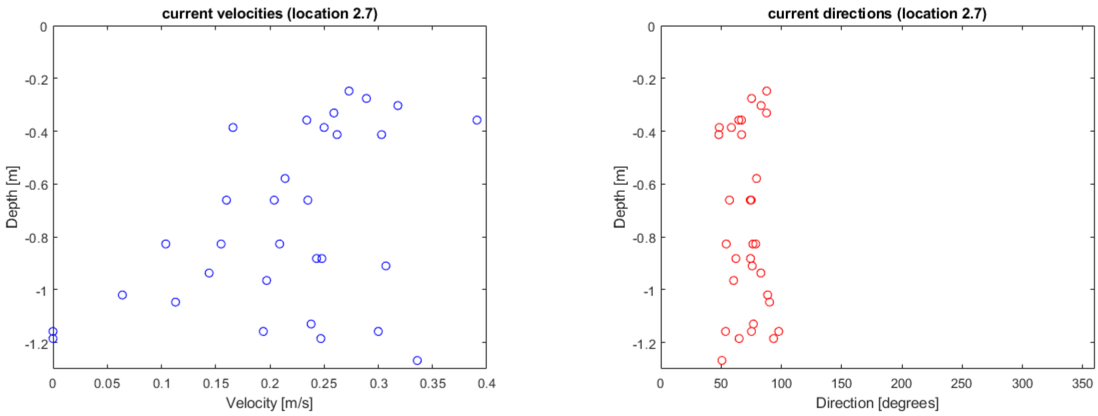

(a) Current velocities at location 2.7

(b) Current directions at location 2.7

Figure E.13: Valeport measurements at location 2.7

E.2. Sediment concentration as a function of depth

Equations E.1 until E.25 are used to calculate the reference concentration. The reference concentration is based on the bed shear stresses. The critical bed shear stress is obtained from Shields. The effective bed shear stress is based on the current and wave related bed shear stresses. All equations are obtained from the following sources: Van Rijn (1991), van Rijn et al. (2001), Van Rijn et al. (2004) and the Delft3D FLOW Manual (Deltares, 2014).

Reference concentration: $$c_a = 0.015 \times \rho_s \times \frac{d_{50}}{a} \times \frac{T^{1.5}}{D_*{}^{0.3}} \qquad [kg/m^3] \tag{E.1}$$

Dimensionless particle diameter: $$D_* = d_{50} \times (\frac{(\rho_s - \rho_w) \times g}{\rho_w \upsilon^2})^{1/3} \qquad [-] \tag{E.2}$$

Dimensionless bed-shear parameter: $$T = \frac{\tau'_{b,cw} - \tau_{b,cr}}{\tau_{b,cr}} \qquad [-] \tag{E.3}$$

Reference level for c_a: $$a = \delta_w, \quad \text{maximal } 0.01 \times \text{h} \qquad [m] \tag{E.4}$$

Time averaged critical bed-shear stress according to Shields:
$$\tau_{b,cr} = \theta_{cr} \times (\rho_s - \rho_w) \times g \times d_{50} \qquad [N/m^2] \tag{E.5}$$

Shields parameter: $$\theta_{cr} = 0.14 \times D_*{}^{-0.64}, \qquad 4 < D_* < 10 \qquad [-] \tag{E.6}$$

Time averaged effective bed-shear stress: $$\tau'_{b,cw} = \tau'_{b,c} + \tau'_{b,w} \qquad [N/m^2] \tag{E.7}$$

Current related effective bed-shear stress: $$\tau'_{b,c} = \mu_c \times \sigma_{cw} \times \tau_{b,c} \qquad [N/m^2] \tag{E.8}$$

Current-related bed shear stress: $$\tau_{b,c} = \rho \times g \times (\frac{U}{C_{ap}})^2 \qquad [N/m^2] \tag{E.9}$$

Current efficiency factor: $$\mu_c = (C/C')^2 \qquad [-] \tag{E.10}$$

Chezy coefficient: $$C = 18log(12h/k_{s,c}) \qquad [m^{0.5}/s] \tag{E.11}$$

Grain-related Chezy-coefficient: $$C' = 18log(12h/3 \times d_{90}) \qquad [m^{0.5}/s] \tag{E.12}$$

$$C_{ap} = 18log(12h/k_a) \qquad [m^{0.5}/s] \tag{E.13}$$

Wave-current interaction coeffient representing reduced velocity-effect near the bed:

$$\sigma_{cw} = \left(\frac{ln90(\frac{\delta_w}{k_a})}{ln90(\frac{\delta_w}{k_{s,c}})}\right)^2 \qquad [-] \tag{E.14}$$

Apparent current-related bed roughness height: $k_a = k_{s,c} \times exp(0.75 \times \frac{U_\delta}{U})$, max $10 \times k_{s,c}$ $[m]$ (E.15)

Physical current-related bed roughness height: $k_{s,c} = 150 \times d_{50}$ $[m]$ (E.16)

Wave related effective bed-shear stress: $\tau'_{b,w} = \mu_w \times \tau_{b,w}$ $[aa]$ (E.17)

Wave efficiency factor: $\mu_w = 1/8 \times (1.5 - \frac{Hm0}{h})^2$, minimal 0.14 $[-]$ (E.18)

Wave related bed-shear stress: $\tau_{b,w} = 1/4 \times \rho_w \times f_w \times (U_\delta)^2$ $[N/m^2]$ (E.19)

Wave related friction factor: $f_w = exp(-6 + 5.2 \times (\frac{A_\delta}{k_{s,w}})^{-0.19})$ $[-]$ (E.20)

Peak value of near bed orbital excursion: $A_\delta = \frac{H}{2sinh(kh)}$ $[m]$ (E.21)

Peak value of near bed orbital velocity: $U_\delta = \frac{\pi H}{Tsinh(kh)}$ $[m/s]$ (E.22)

Thickness of wave boundary layer: $\delta_w = 0.072 \times A_\delta \times (\frac{A_\delta}{k_{s,w}})^{-0.25}$ $[m]$ (E.23)

Wave related bed-roughness: $k_{s,w} = 150 \times d_{50}$ $[m]$ (E.24)

Bed-shear velocity: $u^* = \sqrt{(\frac{\tau'_{b,cw}}{\rho_w})}$ $[m]$ (E.25)

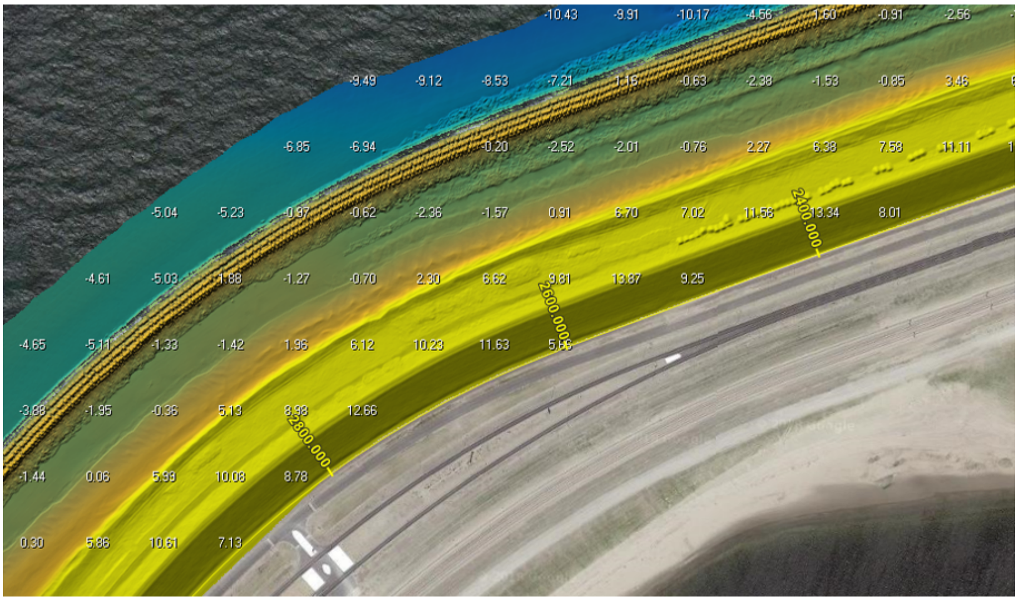

Figure E.14: Water depths around the sand layer domain at April 2018

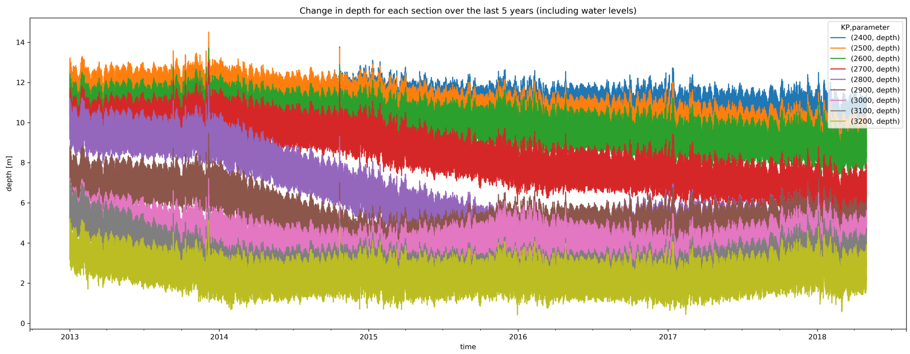

Figure E.15: Change in depth for each section over the last 5 years (including water levels)

KP number	Depth at toe	Sand volume $[m^3/m]$ (cube reef = 2m)	Sand volume $[m^3/m]$ (cube reef = 2.5m)
2400	4	437.9	253.6
2500	4	410.6	237.8
2600	4	370.5	211.7
2700	4	386.2	234.9
2800	4	187.5	104.4
2900	4	93.2	45.5
3000	4	33.2	13.4
3100	4	12.4	4.1
3200	4	6.0	1.5

Table E.1: Sand volumes for KP2400 until KP3200 caused by overtopping given in m^3/m. The water depths are kept equal for all locations. The larger volume at KP2400 compared with KP3200 is visible.

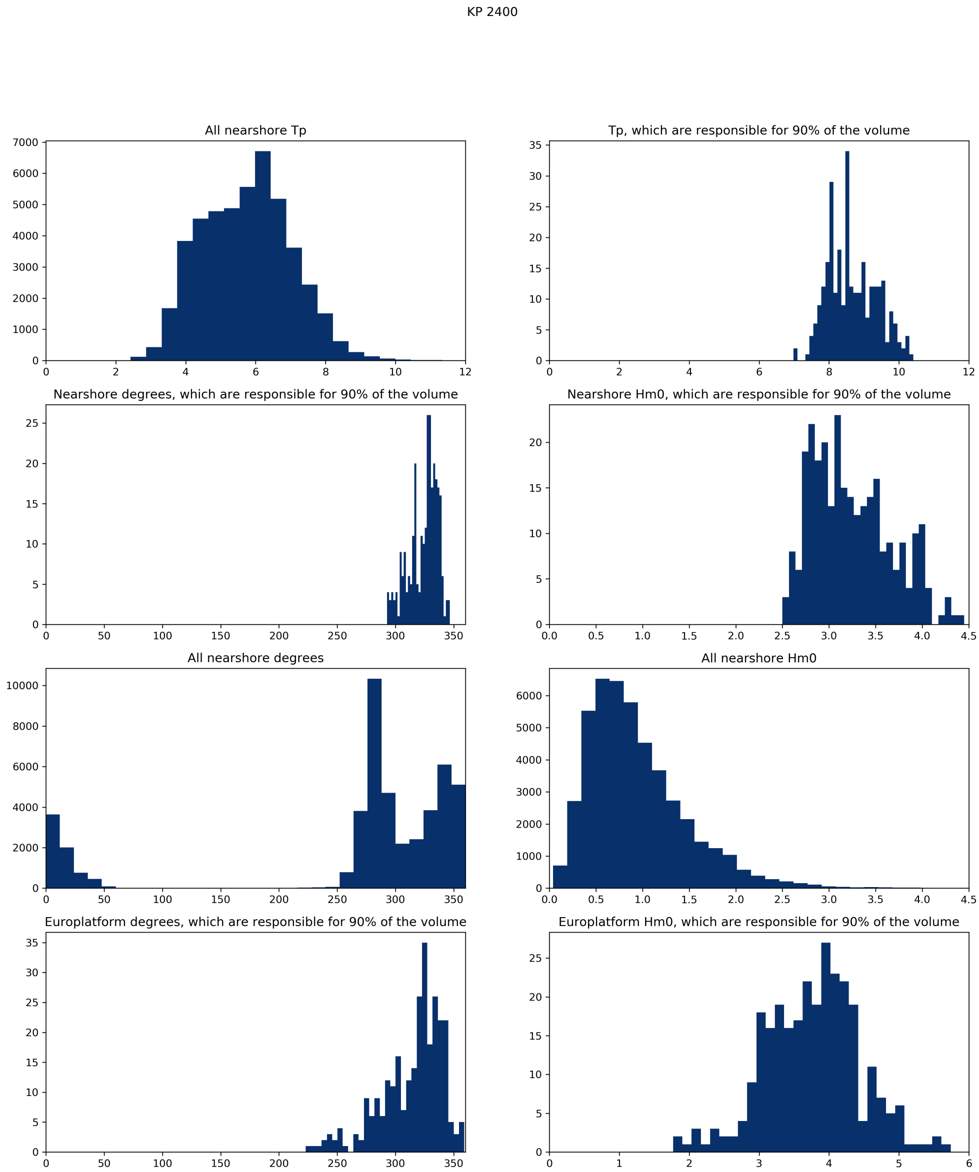

Figure E.16: Histograms for the overtopping volumes of KP2400

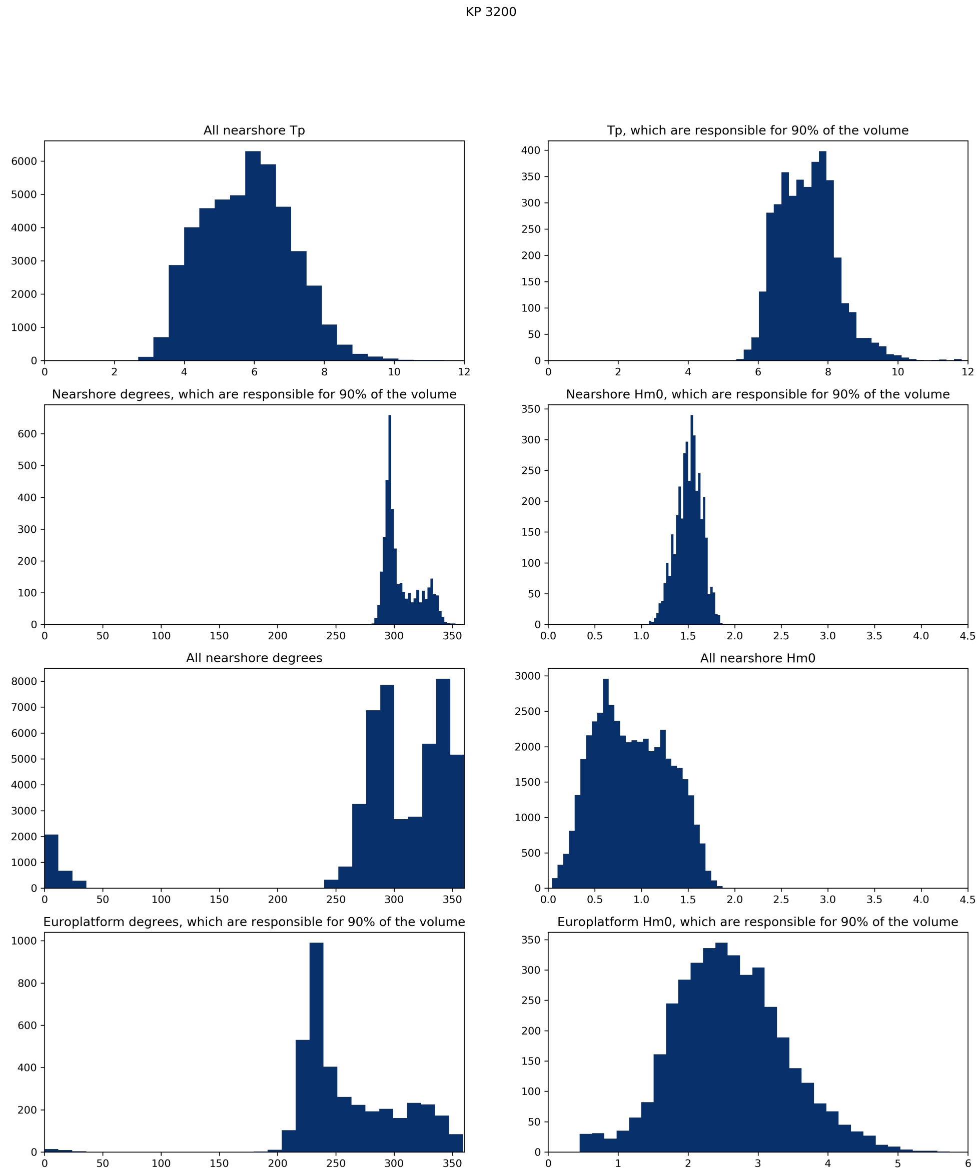

Figure E.17: Histograms for the overtopping volumes of KP3200

F
Aeolian transport

F.1. Bagnold formula

The Bagnold formula relates the amount of sand transported by the wind. The formula was derived by Bagnold (Bagnold, 1937). Wind tunnel and field experiments suggest that the formula is basically correct. Later on, the formula is changed a bit. Equation F.1 gives the Bagnold formula. The formula is valid in dry (desert) conditions (Bagnold, 1937). The effects of sand moisture, which is available in most coastal dunes, is not included in this version of the formula. The sediment transport Q [m^3] is estimated from hourly averaged wind speed u_{10} [m/s] and direction θ_u [$degrees$] measured at 10 meter height by (Rijkswaterstaat, 2018). To obtain the sediminent transport q [kg/m/s] the following equation is used:

$$\text{Bagnold formula:} \quad q_a = C \times \frac{\rho_{air}}{g} \times \sqrt{\frac{d}{D}} \times (u_* - u_{*th})^3 \qquad [kg/m/s] \tag{F.1}$$

Equation F.2: Bagnold formula (Bagnold, 1937)

Whereby the parameters:
- q: mass transport of sand across a lane of unit width in [kg/m/s]
- C: dimensionless constant of order unity that depends on the sand sorting = 1.8 (Hoonhout, 2017)
- ρ: density of air = 1.25 [kg/m^3]
- g: local gravitational acceleration = 9.81 [$m^3\ kg^{-1}\ s^{-2}$]
- d: reference grain size for the sand = 330 [μm]
- D: nearly uniform grain size originally used in Bagnold's experiments (250 [μm])
- u_*: friction velocity, proportional to the square root of the shear stress between the wind and the sheet of moving sand: m/s. This friction velocity is calculated by: $\alpha \times u_{10}$. Where α is the conversion factor from free-flow wind velocity to shear velocity = 0.058 (Hoonhout, 2017)
- u_{*th}: the shear velocity threshold = $\alpha \times 3.87$. Same α as for the friction velocity

To obtain the volumes per hour, the q must be multiplied with the corresponding alongshore length en translated to onshore or alongshore directions only. Moreover, q must be divided by the density of sand (=2650 kg/m3). And finally a porosity of p=0.4 is included to obtain the final volume in m^3, see equation F.3.

$$Q = \frac{q_a \times \Delta_y \times \Delta_t}{\rho_s \times (1-p)} \times f_\theta \qquad [m^3] \tag{F.3}$$

Equation F.4: Equation to obtain the hourly sand volumes

Whereby the parameters:
- Q: the hourly transported sand volumes by the wind = [m^3/h]
- Δ_y: length over which the wind has influence. See figure 7.2b
- ρ_s: density of sand = 2,650 [kg/m^3]
- p: porosity = 0.4
- Δ_t: 1 hour
- f_θ : factor to account for the onshore or the alongshore wind directions only

G

Cross-sections around Maasvlakte 2

In this chapter different cross-sections are shown with the measured data of 2014, 2015, 2016, 2017 and 2018. The black line corresponds with the way Maasvlakte 2 was designed. KP2900 is most northwards and KP3300 is at the soft-hard transition. From the figures it is visible that the sand volume is increasing in time.

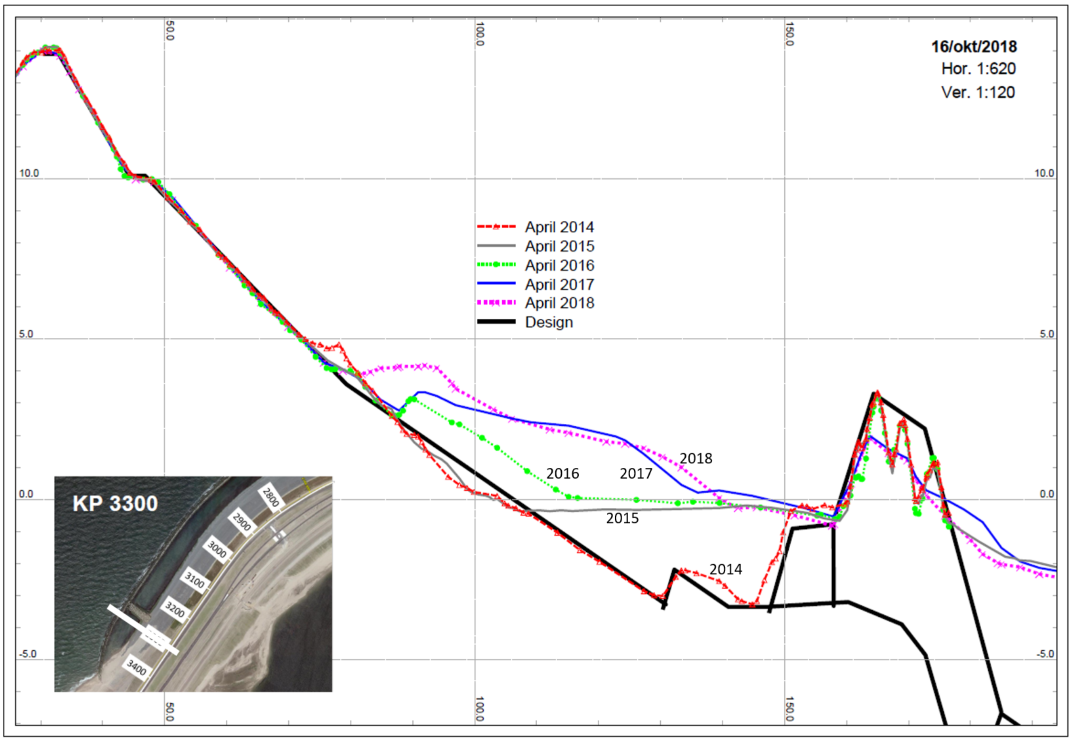

Figure G.1: Cross-section at Raai 3300

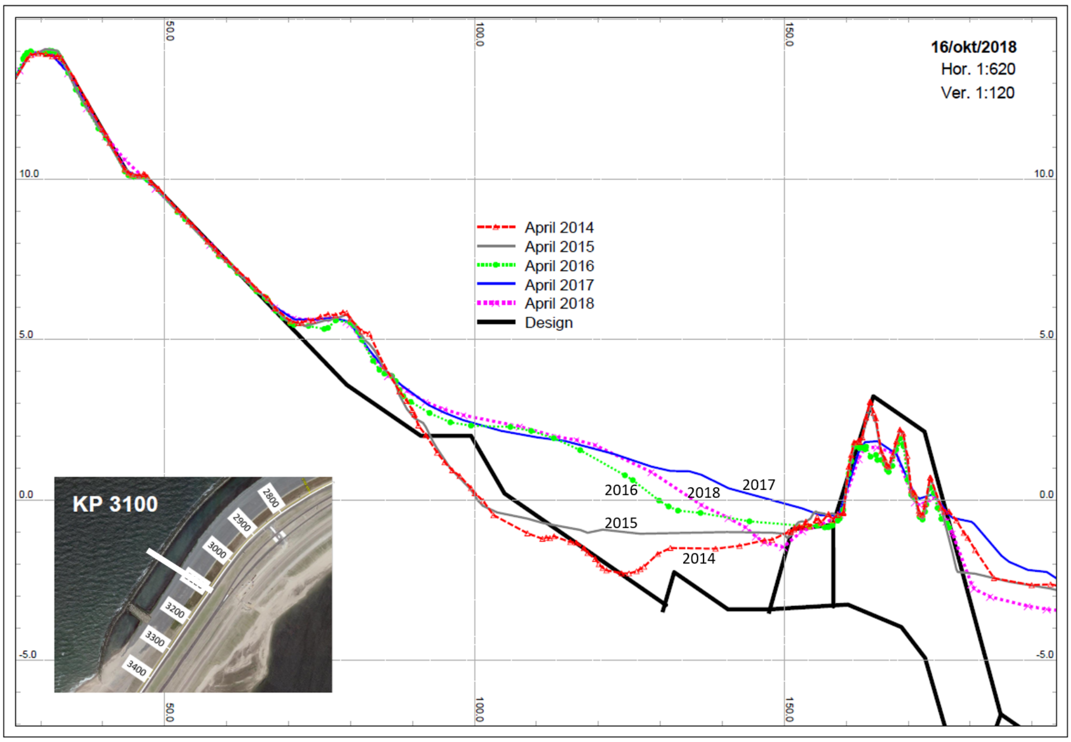

Figure G.2: Cross-section at Raai 3100

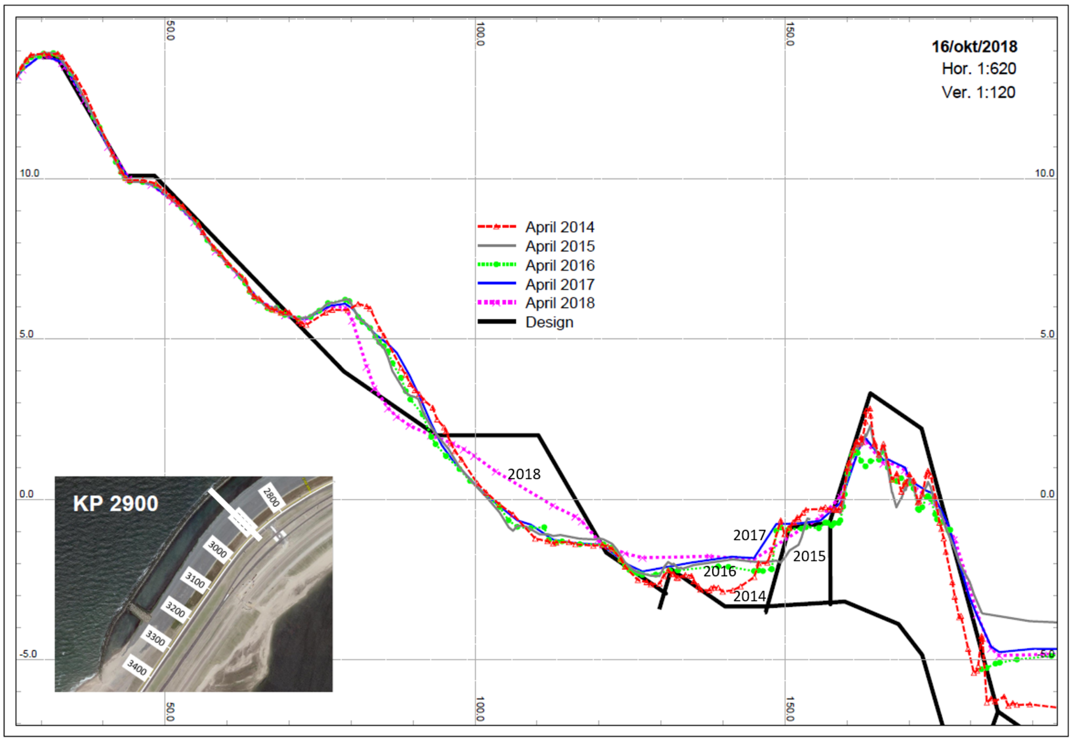

Figure G.3: Cross-section at Raai 2900